AN ABSTRACT OF THE THESIS OF

Heather Johnson Liburdy for the degree of Master of Science in Mechanical Engineering presented on May 29, 2014

Title: Microchannel Extraction of Te^{4+} from a Stream of CdTe via MIBK in Supported Liquid Membrane

Abstract approved:

A. Murty Kanury

A new technique is developed to recover elemental tellurium (Te) from cadmium telluride (CdTe) which is abundantly available in photovoltaic semiconductor waste. The method is based on microchannel fluid flow with the use of a supported liquid membrane (SLM) between the donor (feed) and acceptor (strip) channels. A predictive theoretical model is also developed based on diffusional transport. A comparison of the measured data with the theoretical predictions shows excellent agreement both in magnitudes and trends of dependency on the varied parameters. Areas for further required research in the development of the technique are identified.

The experiments were carried out in a three phase microchannel reactor with 0.5mm square channels. The flow geometry consisted of two counter-flowing hydrochloric acid streams of differing acidity, separated by a membrane saturated with the organic extractant methyl isobutyl ketone (MIBK). Separation funnel experiments were also conducted to characterize the extraction of Te in hydrochloric acid with MIBK. In the microreactor experiments, the Te mass transferred between the two streams was measured for two channel lengths, three feed volume flow rates, and two feed phase inlet CdTe concentrations.

Microchannel Extraction of Te^{4+} from a Stream of CdTe via MIBK in Supported Liquid Membrane

by
Heather Johnson Liburdy

A THESIS

submitted to

Oregon State University

in partial fulfillment of
the requirements for the
degree of

Master of Science

Presented May 29, 2014
Commencement June 2015

Master of Science thesis of Heather Johnson Liburdy presented on May 29, 2014.

APPROVED:

Major Professor, representing Mechanical Engineering

Head of the School of Mechanical, Industrial, & Manufacturing Engineering

Dean of the Graduate School

I understand that my thesis will become part of the permanent collection of Oregon State University libraries. My signature below authorizes the release of my thesis to any reader upon request.

Heather Johnson Liburdy, Author

ACKNOWLEDGEMENTS

I am grateful to my husband Jim and my children Leif, Marla, and Kohl for inspiration.

The interest and guidance of my advisor (and undergraduate thermodynamics teacher), Professor Murty Kanury, is very much appreciated.

Thanks are due to Intel for scholarship funds that assisted my education.

CONTRIBUTIONS

Based on a one page summary that I was given access to, Dr. Sudhir Ramprasad, at Pacific Northwest National Laboratory (PNNL), and Professor Kendra Sharp, at Oregon State University (OSU), co-authored the grant *Process development for separation of CdTE in a microfluidic device using liquid membranes: A pathway for efficient recycling of CdTe PV module*, which was reportedly funded by the U.S. Army, Tactical Exploration Program.

It is my understanding that these funds largely sponsored the graduate research assistanceship, which I received from Spring term 2011 through Fall term 2012. Additionally, it was reported to me that these funds were applied to the purchase of equipment and supplies required to collect the experimental data in this thesis.

Dr. Sudhir Ramprasad provided valuable insight into the envisioned project development and basic microreactor design during numerous meetings with me. He sought the expertise of a colleague at PNNL, Dr. Abhas Singh, to assist me with the development of the analytical chemistry method in the earliest stage, prior to collection of concentration data on experimental samples. Dr. Ramprasad provided daily guidance relating to: (1) laboratory access times, (2) relevant literature, (3) requesting a sample membrane, (4) specification of chemicals to be ordered, (5) specification of equipment to be ordered, (6) safety procedure and equipment, (7) separation funnel test plan, and (8) separation funnel data review. The separation funnel experiments were conducted by Dr. Ramprasad and me, by me, or by Dr. Ramprasad himself. I was responsible for all concentration measurements and data processing reported here. Dr. Ramprasad terminated his participation in the project on September 20, 2012.

Professor Kendra Sharp provided authorization and signatures as needed for: (1) the request for a sample membrane, (2) safety and hazard permits, (3) equipment and supply orders, (4) access to the fabrication lab at Microproducts Breakthrough Institute (MBI), (5) other permissions required for collaboration between PNNL and OSU, and (6) my payroll hours report. Professor Sharp prompted me to submit for her review: (1) ongoing project report materials, (2) the final project report, and (3) my graduate student seminar slides. Early in the microreactor design process, Professor Sharp specified that the microreactor should have a plenum at the channel inlet and provided leadership as to selection of appropriate pumps, requiring that two separate pumps be ordered to prevent cross-talk in the microreactor fluid channels. It was upon her insistence that Eppendorf® pipettes and pipette tips were purchased, to improve calibration of the analytical method. All the microreactor experiments were done by me. From September 20, 2012 to December 31, 2012 I informed (only) Professor Sharp of my daily progress in the lab on the microreactor experiments.

Winter term of 2014 Professor Murty Kanury became my advisor. Professor Kanury provided guidance in: (1) thesis writing and structure, (2) salient literature, (3) discussion of Stokes-Einstein equation, (4) model development, (5) derivations for the mass transfer rate correlations of the strip stream, (6) distribution ratio, (7) how to critically review my analysis, (8) data plots, and (9) defense preparation. The derivations contained in Appendix D were primarily authored by Professor Kanury based on discussions with me.

The data processing and analysis of separation funnel data presented in this thesis is my own. The data processing and analysis of microreactor data in this thesis is my own.

TABLE OF CONTENTS

Page

TABLE OF CONTENTS (Continued)

Page

TABLE OF CONTENTS (Continued)

Page

TABLE OF CONTENTS (Continued)

Page

LIST OF APPENDICES

Appendix Page

LIST OF FIGURES

Figure Page

LIST OF FIGURES (Continued)

Figure Page

LIST OF TABLES

Table Page

LIST OF APPENDIX FIGURES

Figure Page

LIST OF APPENDIX TABLES

Table Page

LIST OF CHEMICAL SYMBOLS, ACRONYMS, ABBREVIATIONS

Symbol, Acronym, Abbreviation

Cd	Cadmium
CdTe	Cadmium Telluride
HCl	Hydrochloric Acid
In	Indium
Te	Tellurium
EE	Extraction Efficiency
HDPE	High Density PolyEthylene
ICP	Inductively Coupled Plasma
ICP-OES	Inductively Coupled Plasma/Optical Emission Spectrometry
L	Liter, measure of volume = 1000 cm^3
LDPE	Low Density PolyEthylene
M	Molarity, a measure of concentration, in units of mol/Liter
MIBK	Methyl IsoButyl Ketone
nm	Nanometer, 1 x 10^{-9} meter
p	Pico, 1 x 10^{-12}
pm	Picometer, 1 x 10^{-12} meter
PP	PolyProlyene
PTFE	Teflon
ppb	Parts Per Billion, µg/L (for liquid) and µg/kg (for solid)
ppm	Parts Per Million µg/ml (for liquid) or µg/g (for solid)
PV	Photovoltaic
SLM	Supported Liquid Membrane

LIST OF NOMENCLATURE

Nomenclature

a	The width and height of the channel of square cross section, (cm).
b	Membrane thickness, (cm).
C_i	Concentration of species i in the fluid, (μg of i/ml, or g of i/cm^3).
C_{1F_B}	Concentration of species 1 (=Te^{4+}) in feed (=F) flow in bulk (=B).
C_{1S_E}	Concentration of species 1 (=Te^{4+}) in strip (=S) flow at exit (=E).
C_{1F_o}	Concentration of species 1 (=Te^{4+}) in feed (=F) flow at inlet (=o).
C_{1S_M}	Concentration of species 1 (=Te^{4+}) in strip (=S) flow at membrane (=M).
D_F	Diffusivity of species 1 in feed flow, (cm^2/s).
D_M	Diffusivity of species MIBK within the membrane, (cm^2/s).
E	Extraction efficiency, (fractional or %), (Eq. 5.1).
k_F	Rate coefficient for diffusion of species 1 in feed flow (=F). (cm/s), (Eq. 3.5). (Also known as the mass transfer coefficient, h_D), (cf. Appendix D).
k_M	Rate coefficient of diffusion of species 1 in membrane (=M), (cm/s), (Eq. 3.6).
L	Length of the microchannel, (cm).
M	Distribution constant, (no units), (Eq. 3.8).
Pe_a	Peclet number based on channel dimension a. ($Pe_a=au_o/D_F=Sc \cdot Re_a$), (no units).
Pe_L	Peclet number based on channel length L. ($Pe_L=Lu_o/D_F=Sc \cdot Re_L$), (no units).
R	Recovery efficiency, (fractional or %), (Eq. 3.10).
Re_a	Reynolds number based on channel dimension a. ($Re_a = au_o/ \nu_F$), (no units).
Re_L	Reynolds number based on channel length L. ($Re_L = Lu_o/ \nu_F$), (no units).
Sc	Schmidt Number, ($Sc = \nu_F/D_F$), (no units).
Sh_a	Sherwood number based on channel dimension a. ($Sh_a = ak_F/D_F$), (no units).
Sh_L	Sherwood number based on channel length L. ($Sh_L = Lk_F/D_F$), (no units).

LIST OF NOMENCLATURE

Nomenclature

t	Residence time, ($t = a^2 L/\dot{v}$) ,(s).
u_o	Bulk velocity of feed flow, ($u_o = \dot{v}/a^2$), (cm/s)
ν	Kinematic viscosity (cm^2/s)
$\dot{v}$	Volumetric rate of the feed flow, (cm^3/s).

LIST OF SUBSCRIPTS

Subscript	
M	Membrane
F	Feed flow
S	Strip flow
FEED	Feed flow inlet
RAFFINATE	Feed flow exit
STRIP	Strip flow exit

Microchannel Extraction of Te^{4+} from a Stream of CdTe via MIBK in Supported Liquid Membrane

CHAPTER 1 - INTRODUCTION

1.1 Motivation

The purpose of this project is to test a novel method of recycling cadmium telluride (CdTe) in which tellurium (Te) is separated from cadmium (Cd). The chosen approach to demonstrate separation of Te is a microchannel reactor by means of a supported liquid membrane (SLM) soaked in an organic extractant. This approach promises to someday provide an economical alternative process in the recovery of Te. The present research is based on concepts gleaned from literature supporting single ion extraction in microchannel two or three phase flows; separated by SLM supported liquid membrane.

It seems to bear out that a chemical reaction carried out in a barrel or batch process may be translated to the configuration of microchannel flow if there is an adequate means to allow separation of the fluid streams, such as by use of a membrane. The membrane may in principle be as simple as the interfacial contact area between two (or three) immiscible phases flowing concurrently. Or, it may be an extruded polymer membrane with small pores soaked in an organic extractant placed between two immiscible streams.

In the current era of semiconductor civilization, tellurium is a precious material. The concentration of CdTe selected for experimental conditions is representative of that found in an end-of-life-cycle solar cell material recycling environment. For the sake of simplicity, other

elements present in solar cells, such as copper, indium and silicon were excluded from the CdTe fluid stream. This research produced a demonstration model which may have promising potential to scale up to a practical commercial application for solar cell recycling, once refined by further work. At this early stage of development, the implications of scaling the research to design an economical production plant are considered premature.

1.2 Objectives

Publications in English on the topic of CdTe separation with MIBK are sparse at best, so the scope of this project is large by necessity. The objectives of the present project include:

(1) Identification and bench testing of appropriate separation chemistry;

(2) Design and fabrication of a microchannel device for performing the separation;

(3) Design and fabrication of a flow loop for device testing;

(4) Establishment of the testing protocol for material concentration with necessary accuracy and sensitivity; and

(5) Experimental demonstration of Te separation in the microchannel device.

1.3 Summary Outcome of This Study

Successful separation of Te from a stream laden with CdTe is demonstrated for both a straight and a serpentine microchannel of square cross section, 0.5 mm tall by 0.5 mm wide. The maximum Te recovery efficiency found in the 37 mm long straight channel is 6.5%. Similarly, the maximum Te recovery efficiency in the 129 mm long serpentine channel is 26.8%. The serpentine channel is 3.5 times longer than the straight channel, with the same ratio

increase in surface area. However, the serpentine channel performance of 26.8% is significantly better than the 15% that would be predicted by the proposed model in a straight channel of the same length (129 mm). This difference may be attributable to circulation in the flow due to channel wall curvature in the longer serpentine extractor.

1.4 Organization

This presentation follows the customary 'thesis' format. Chapter 2 is a summary of publications that 1) justify recovery of Te via recycling CdTe, and 2) discuss novel approaches to mass transfer of ions. Presented in Chapter 3 are: the problem statement, a hypothetical mechanism; relevant concepts; and a simple model. In Chapter 4 are descriptions of: the microchannel device; experimental setup; design and fabrication; and data collection. Experimental data are presented in Chapter 5. The most important results obtained from this research are given in Chapter 6 along with a salient discussion of the empirical findings. Finally, Chapter 7 deals with conclusions and further required research.

CHAPTER 2 – BACKGROUND LITERATURE FOR THE CADMIUM TELLURIDE PROJECT

2.1 Justification for Development of CdTe Recycling

There are three compelling reasons to develop technology for the recycling of CdTe solar cells; 1) predicted growth in demand for Te, 2) the extreme scarcity of Te in the earth's crust, and 3) environmental concerns.

2.1-1 Predicted Growth in Demand for Tellurium

Cadmium telluride semiconductors are one of a handful of thin film solar technologies. The high optical absorption of CdTe, CdS/$CuInSe_2$(CIS), and Cu(In,Ga)Se_2 (CIGS) solar cells have high optical absorption that require only a thin layer ($\leq$2 μm) of material to convert sunlight into electricity [1]. The efficiency of the CdTe solar cell is higher than 10% and is expected to grow to 13-14% by 2020 [2]. As efficiency increases in PV cells, the cost per kilowatt hour of solar power decreases, closing or reversing the gap in cost between solar power and other conventional sources of power. Thus, it is anticipated that if CdTe solar cells meet the expected improvements in efficiency, demand for both solar power cells and Te will increase. The growth of the demand for the tellurium market is also promising because of other novel applications for Te. Simon et al. [3] argue that tellurium's historical use as a metallurgical alloying element has expanded lately into myriad of applications such as; fireworks, catalysts, DVDs/BlueRayDiscs, Peltier units, and thermoelectric devices. There is some evidence that the Te market is already reacting to increased market pressure, as the price of Te escalated over a decade to a high of $220/kg in 2010 before settling down to $150/kg in 2013 [3].

2.1-2 Tellurium Scarcity

The cost of tellurium reflects its extreme scarcity. Tellurium is found less commonly in the earth's crust than platinum, gold, or silver. Much of the earth's tellurium content of 501 ppb (μg/kg) is thought to be locked in the core; the accessible Te found in the earth's continental crust is reported to be a mere 0.1 ppb [4]. The tellurium content of PV materials is plentiful in comparison. Berger et al. [5] report the Te content of ground and sieved CdTe solar material to contain 1201 ppm Te (or 2260 ppm CdTe). Some doomsday forecasters cite the limited supply of Te as reason to abandon research into CdTe solar cells altogether. However, the more pragmatic solution of developing solar cell recycling methods in parallel with refinement of PV cells ensures affordable tellurium remains available as solar efficiency increases demand.

2.1-3 Environmental Reasons to Recycle Tellurium

There are additional incentives to recycle solar cells for environmental reasons. Tellurium is mined primarily as a byproduct of copper, nickel, and zinc ores [4] [3] [5]. As one might expect, a scare element is expensive to mine and damaging to the earth's crust. Some other negative impacts of mining are contaminated wastewater, poisonous emissions, and solid waste slurries [6]. One estimate of the cost of environmental production, the Total Materials Requirement (TMR), is 270,000 tons for Te [5]. In comparison, the same source publishes a TMR for copper of 300 tons. As Berger et al. [5] note, "The purification steps in production of the elements or the respective chemical compounds are in principle the same as for the recycling of waste streams". The life of a PV module is projected to be 25 years [3]. At the end of a module's life disposal will likely be difficult, as the highly toxic metal cadmium is carefully

regulated in both the US and Europe. Dissolving CdTe deposits from the glass in solar panels for reapplication to the next generation of PV will keep cadmium deposits locked into a sandwich of glass where leaching into water is a low risk. Fthenakis [6] asserts the thin CdTe layer is encapsulated between sheets of glass or plastic from which dust cannot escape unless the module is ground. The exception of concern is a rare house fire; however, Fthenakis [6] found only 0.4%-0.6% of PV Cd content to be released upon exposure to temperatures ranging from 760-1100 ˚C because the CdTe was trapped in melted glass. Recycling CdTe for future application in solar cells or other technology is a preferred alternative to sending broken scrap to landfills at the end of solar panel's life.

2.2 Methods of PV Recycling

There are quite a few processes around the globe being implemented on a small scale to recycle PV materials according to Marwede et al. [1]. These programs target waste originating from customer returns (due to warranty or end-of-life) and manufacturing waste resulting from production plants (such as grindings or sputter targets) [1].

The method developed by Brookhaven National Laboratory (BNL) and the American company First Solar is a hydrometallurgical process for recycling of tellurium [7]. Fthenakis and Wang [8] report that First Solar PV is ground into small pieces by hammer mill (to open the laminate for removal of metals); it contains a weight distribution of 0.055% cadmium, 0.062% tellurium, and 0.010% copper. This metal is recovered when the ground glass is separated from metals with a leaching solutions followed by separation of tellurium from cadmium and copper with cation-exchange resins [8].

Many alternatives to this approach heat the PV modules to unseal the glass layers and expose the metals, or induce separation by some other means such as water jet cutting [1]. Once the PV module is open it can be scrubbed of metals by blasting or washed with an acid to dissolve the metals [5]. The PV industry requires metals to be very highly purified (99.9% and higher) [5]. And so the metals removed from the solar panel must then be separated into pure stock. This entails further processing methods such as evaporation, liquid-liquid extraction, precipitation and filtering, plating, electro-winning, or ion-exchange [1]. Research on a closed loop electrochemical approach to recycling by Menezes [9] is one such possibility.

2.3 Microchannel Applications and Advantages

Researchers around the world have been experimenting with transport of ions via fluid flows in microchannels since the late 1990's. The applications for this type of technology are both numerous and diverse. It has been suggested that microchannels might someday be models for biological membranes, purify water, yield miniature analytical chips in the environmental and biomedical fields, and manufacture pharmaceuticals.

The most frequently cited advantage of microchannels is the large surface area to fluid volume ratio which promotes the conduction of heat as well as diffusion of molecules in a stream. The low fluid volume requirement is especially an advantage over the traditional bench top laboratory where large volumes of chemicals are costly and often hazardous. A multiple step batch extraction can be combined into one step in a microreactor. The small scale of the microchannel promotes fast reactions, to such a degree that extraction requiring an hour in a batch reactor, may require only minutes to reach the same degree of completion in

microreactor. The microchannel provides the designer precise control of the variables that ultimately determine the outgoing stream properties and material composition. Some of the flow variables commonly noted and reported in the microchannel research are contact time, flow rate, velocity profile, fluid volume, temperature, surface area, and chemical content.

2.4 Overview of Microchannel Ion Transport Designs

Mass transfer of ions from one microchannel fluid stream to the adjacent stream occurs nearly instantaneously at the interface between two immiscible fluid phases. The interface between the immiscible fluids acts as a membrane permitting mass exchange. Many reactors consist of just two streams, an organic and an aqueous phase, flowing concurrently side by side. For example, Maruyama et al., 2004 [10] report parallel two phase extraction of metal ions (Y^{3+} and Zn^{2+}). And Priest et al., 2011 [11] published such a microchannel based copper extraction. If a counter-flow stream pattern is preferred (over concurrent flow), one or more supported liquid membranes (SLM) will be required to hold the flow in place. This alternative SLM utilizes a thin porous manufactured membrane to give integrity to the liquid interface thereby stabilizing a partition between phases. For example, Molinari et al. [12] report using various SLM configurations to extract copper(II). There are also other novel microchannel configurations for extraction. One design mimics the steps of a batch reactor by mixing the fluid streams on-chip then separating the streams via membrane downstream [13]. Some of the most relevant examples of ion transport are summarized in Table 2.3-1. The extensive array of design options and extraction efficiencies (EE) in these publications demonstrate that rapid CdTe separation via Te ion extraction in a SLM microchannel is theoretically possible.

Table 2.4-1 Examples of Mass Transfer in Microchannel

Author	Membrane Type	Flow Pattern	Extracted Ion	Channel D x W x L	Flow Rates	EE (%)
Hisamoto et al. [14]	Liquid interface	Parallel Flow Two Phase	Na^+ with dye	100 µm 250 µm 10 mm	1-10 µL/min	100
Hotokezaka et al. [15]	Liquid interface	Parallel Flow Two Phase	U(VI)	43.5 µm 100.5 µm 120 mm	2.2-4.3 µL/min	93.8
Kim et al. [16]	Liquid interface	Parallel Flow Two Phase	Al^{3+}	10 µm 200 µm 100 mm	0.46-1.8 µL/min	90-100
Kralj et al. [13]	Zefluor PTFE	Two phases mixed then separated	DMF	156 µm 300 µm 400 mm	10-2000 µL/min	~10
Kuban et al. [17]	Liquid interface	Parallel Flow Two Phase	Methyl Blue	150-380 µm ~2000 µm 45 mm	70-320 µL/min	2-80
Maruyama et al. [18]	Liquid interface	Parallel Flow Three Phase	Y^{3+} Zn^{2+}	25 µm 150 µm 30 mm	8.33- µL/min	22-36 4-10
Maruyama et al. [10]	Liquid interface	Parallel Flow Two Phase	Y^{2+} Zn^{2+}	20 µm 100 µm 30 mm	10-14.66 µL/min	50-80 6-80
Molinari et al. [12]	Accurel solid support	Parallel Flow Two Phase	Cu^{2+}	Continuous Circulation Loop	75 ml/min	85
Surmeian et al. [19]	Liquid interface	Parallel Flow Two Phase	Methyl Red	22 µm 120 µm 30 mm	0.5 µL/min	~46
Tokeshi et al. [20]	Liquid interface	Decaying (Pump Off) Parallel Flow Two Phase	Fe(II)	100 µm 250 µm 10 mm	30, 60, 100.5 µL/min then static	~47-100
Wang et al. [21]	Celgard 2400	Cross Flow Three Phase	Haloacetic Acid	100-750 µm 750 µm 11.1 cm	0.88-2.64 µL/min	35-50

2.5 Concurrent Two Phase and Three Phase Microreactors

The two phase immiscible flow microreactor is quite simple; one channel carries an aqueous donor directly in contact with an organic acceptor. In the case of a three phase reactor, the organic stream is flanked on either side by an aqueous phase. The membrane between the phases moves with the fluid streams. Streams are often set to flow at the same rate but this is not a requirement.

There are some inherent difficulties in this design. One such difficulty is in realizing a smooth laminar flow in each streambed to prevent the streams from overt mixing into an immersion. Parallel laminar flow of the phases is not guaranteed for any range of flow conditions or geometry but must be confirmed via inspection on a case by case basis, giving rise to need for at least one side of the channel plates needs to be transparent. Stable parallel flow with a liquid interface membrane requires circumscribed flow rates, meaning not too fast and not too slow. Counterintuitively, slower flow rates are not necessarily conducive to creating the conditions needed for a stable contact area or stream interface [17]. Surface forces at liquid-liquid interface and the flow rate dictate if two liquids are able to flow side by side with a stable interface suitable for ion extraction [22]. Each desired system of aqueous-organic liquid-liquid flow must be tested and observed at various flow rates to determine if the interface is stable or breaks down into uncontrolled segmented flow. For example, Kuban et al. [22] found that MIBK, ethyl acetate and 1-butanol all formed stable interfaces with an aqueous stream flowing in parallel (whereas hexane and xylene failed this test).

All authors review using this approach report concurrent streams flow. Cross flow without

a supported liquid membrane would tend to break down into uncontrolled mixing, which is a disaster, unless there is a plan to separate the phases downstream. Kuban et al. [17] note on parallel concurrent flowing streams, "flow of two parallel streams in a microchannel device will necessarily be concurrent, since attempts to establish countercurrent flow leads to a "short-circuit" between two adjacent inlet/outlets."

Some chips are fabricated with continuous small chamfered ridges between the two streams to guide the phases into maintaining the desired flow pattern [19], effectively decreasing the contact area between the phases but increasing stability of the flow. Ban et al. [23] find an asymmetric channel cross section is able to stabilize aqueous/organic two phase laminar flow. Hydrophobic/hydrophilic patterning on the microchannel surface has also been found to provide effective guides for concurrent dual phase flow even in complex circular microchannel patterns [24].

Channel shape is a factor in both establishing stable flow boundaries between the streams and extraction efficiency. Many micro extractors have a Y inlet with very simple straight channel geometry, although it is reported that channel partitions or other curvature promote extraction efficiency [10] [25]. A serpentine curvature of the channel also has an advantage of creating a longer channel in a smaller foot print. There are other channel arrangements of interest, such as Hibara et al. [26] findings that an extractant stream running with a feed stream on either side increases the rate of extraction of Co-DMAP.

2.6 Supported Liquid Membrane in Microreactors

Supported liquid membrane (SLM) technology sidesteps the difficulty of maintaining a stable flow at the liquid-liquid interface by imposing the restriction of a manufactured porous membrane on at least one phase in the system of exchange. This phase may be sandwiched between two membranes, as was at least one case reported by Molinari et al. [12]. Or the membrane may be soaked in the desired phase, until its pores are thoroughly saturated, then placed between two streams. Only a few microliters of liquid [21] are needed to saturate the pores thus creating the SLM, and the extractant in the pores, is free to retrieve ions over and over once the ion is relinquished to the acceptor stream. Additionally, there is no need to separate the phases after the extraction is complete, as the phases do not mix. There can be a problem over the long term, however, in retaining this small volume of chemical in the pores. If small particles of the extractant break off the SLM and leach into the adjacent flow, the duration of effectiveness of the membrane at extraction is compromised. It has been found that when the ratio of the volume of aqueous to organic liquid is very large, as it is for a thin sheet supported liquid membrane; the organic solvent must be highly hydrophobic to form membrane that is considered stable [27]. Molinari et al. [12] report literature supports the conclusion that metal ion transport via SLM is not proven practical on a large scale because of limited membrane stability, at least in part attributed to loss of the liquid phase from the pores of the membrane. The same authors report in their own research finding membrane stability to range from 22.3 hours to 311.8 hours; however, there are tradeoffs between membrane system stability and a high flux of metal ion (copper in this case). Perforations in the SLM, due

to mishandling or wear and tear, end the effectiveness of the phase separation and permit free mixing, potentially ending the process of separation, sometimes prematurely.

Theoretically, the SLM system structure is versatile and one sheet of SLM can be used to create a three phase mass transfer system. For three phase flow, the liquid membrane could be soaked in either the organic or aqueous phase, depending on the properties of the selected membrane. If the membrane is hydrophobic, the organic phase would be more likely to soak into the membrane pores. If the membrane is hydrophilic, the aqueous phase would be expected to fill the membrane pores. A membrane containing the organic phase would separate two aqueous streams. Or alternatively, a membrane containing the aqueous phase would separate two organic streams. The SLM pores must be on a larger scale than the ion associated with its carrier molecule complex in the solvent to facilitate mass transport through the membrane. A few examples of ion extraction using SLM are worthy of mention here. Wang et al. [21] report that several haloacetic acids were extracted through a supported liquid membrane soaked in trioctylphosphine oxide in microchannel. The results of copper ion flux across membrane systems using the extractant D2EHPA in microchannel was reported by Molinari et al. [12], who noted the membrane continued to transfer ions even after the concentration gradient was against the flow of diffusion, acting as a pump. This raises a question to be addressed in the next section, if the concentration gradient is such that diffusion is no longer driving mass transfer, what is the cause of continued mass transfer?

2.7 Microreactor Chemistry

The chemicals of choice for microreactor extraction are indicated by the proven chemistry of the larger scale batch reaction. Tokeshi et al. report experimental extraction of Fe(II) in the microchannel is very similar to that found in the separation funnel to such a degree that, "the specific interface area formed in our microchannel corresponds to that formed by a rather vigorous mechanical shaking". Tamagawa et al. [28] found an 80% extraction efficiency of Cs^+ via di(2-ethylhexyl) ester (D2EHPA) in their slug flow microreactor to be equivalent to their findings in a conventional batch extraction. However, the microreactor was shown to be 10X faster to extract Cs^+ then the batch reactor [28].

2.7-1 Extraction Dependence on pH

Metal extractions are known generally to be pH dependent. For example, Molinari et al. explain the mechanism of Cu(II) via the extractant D2EHPA (di-(20ethylhexyl) phosphoric acid with the statement "The functional group of this molecule is –OH that at high pH tends to release the H^+ ion substituting it with positive ions (in this study the Cu(II) ion)" [12]. Reports of metal ion transfer in the microchannel by Maruyama et al. [10] assert that at a pH of 2.0 almost no Zn^{2+} ions were extracted in the microreactor, while at a pH of 3.0 80% of the Zn^{2+} ions were extracted in the microreactor. They drew a direct correlation between these results and much earlier published pH selective extraction studies of Zn^{2+} ions done in a separation funnel [29] [30]. The same authors conclude pH adjustment allows selective extraction in the microchannel as predicted by preceding separation funnel experiments [10].

2.7-2 Distribution Ratio Dependence on pH

Extractions are frequently known to be dependent on pH because reactions are driven by equilibrium kinetics. The *distribution ratio* quantifies the proportion of a substance (in this case metal ion) to be found at equilibrium between two adjacent immiscible phases. A sterling discussion of the distribution ratio is provided by Glasstone [31], in that the distribution law applies,

> If to a system of two liquid layers, consisting of two immiscible or slightly miscible components, there is added a third substance which is soluble in both layers, this substance is found to distribute, or divide, itself between the two layers in a definite manner. It has been shown experimentally that at equilibrium, at constant temperature, the ratio of the concentrations in the two layers has a definite value, independent of the actual amount of the dissolved substance; thus if c_1 and c_2 are the concentrations of this substance in the two layers, then
>
> $$\frac{c_1}{c_2} = \text{constant} \qquad (40.10)$$
>
> In words, therefore, *the dissolved substance, irrespective of its total amount, distributes itself between the two layers in a constant concentration ratio, at constant temperature*. This may be regarded as the statement of the **distribution law**; the ratio, equal to the constant in equation (40.10), is referred to as the **distribution ratio**.

Unfortunately, the term *distribution ratio* is often found to be used interchangeably with the terms *distribution constant* and *partition coefficient* in literature. The distribution ratio is a function of proton concentration (or pH) and other variables such as temperature, concentration of extractant, concentration of secondary analytes, and the concentration of the analyte itself. Surmein et al. [19] report with respect to the microchannel extraction mechanism, “Molecular transport through the liquid/liquid interface is due not only to diffusion

but also to the analyte-solvent molecular interactions expressed by the partition coefficient." Marine et al. [32] note with respect to microfluidic extraction of dye, "The partition coefficient of fluorescein, a fluorescent dye, is measured as a function of pH". As Maruyama et al. [10] found to be the case for Zn^{2+}, the right pH is critical for a successful metal extraction because equilibrium kinetics drive the ion from one liquid to another via the pH dependent distribution ratio.

2.7-3 Extraction of Te with MIBK

To avoid redundancy, literature review on the chemistry of MIBK in Te extraction is developed first in Section 3.2, as part of the mechanism discussion, with additional details provided in the discussions found in Sections 6.1-6.3.

CHAPTER 3 – THREE PHASE MICROCHANNEL EXTRACTOR

3.1 Problem Statement with Proposed Mechanism

Ramprasad and Sharp [33] proposed an experimental microchannel device as an innovative alternative to the batch-reactor recycling method and other CdTe recycling approaches documented in literature, in order to separate CdTe found in solar manufacturing waste and PV recycling materials. The Ramprasad and Sharp proposal employs the use of a supported liquid membrane (SLM) process causing the desired separation. The microchannel promotes relatively rapid liquid diffusion by using the micro-scale advantages to effect, a short diffusion distance, and a high ratio of surface area to fluid volume. An additional benefit of the SLM is that only a few milliliters of the liquid extractant effects Te extraction in microchannel. The goals of the research reported in this thesis are: 1) to develop chemistry for separation of CdTe, 2) to design and fabricate a microchannel device with a membrane utilizing the said chemistry, and 3) to evaluate the performance of the chemical-membrane system in the microreactor.

3.2 The Membrane Mechanism

The central thrust of this research project is how to separate a single stream of dissolved cadmium telluride into two pure streams, one carrying tellurium ions, and the other carrying cadmium ions. The solution proposed here places a supported liquid membrane saturated with a *carrier* (or *extractant*) between two moving streams to essentially create a liquid pathway for the tellurium complex to be instantaneously transported from the cadmium telluride *feed* (or *donor)* stream to the *strip* (or *acceptor)* stream flowing on the other side of the membrane, as is

indicated in Fig. 3.2-1. A continuous separation of ions via SLM requires a sequence of physical events to repeat until extraction is complete.

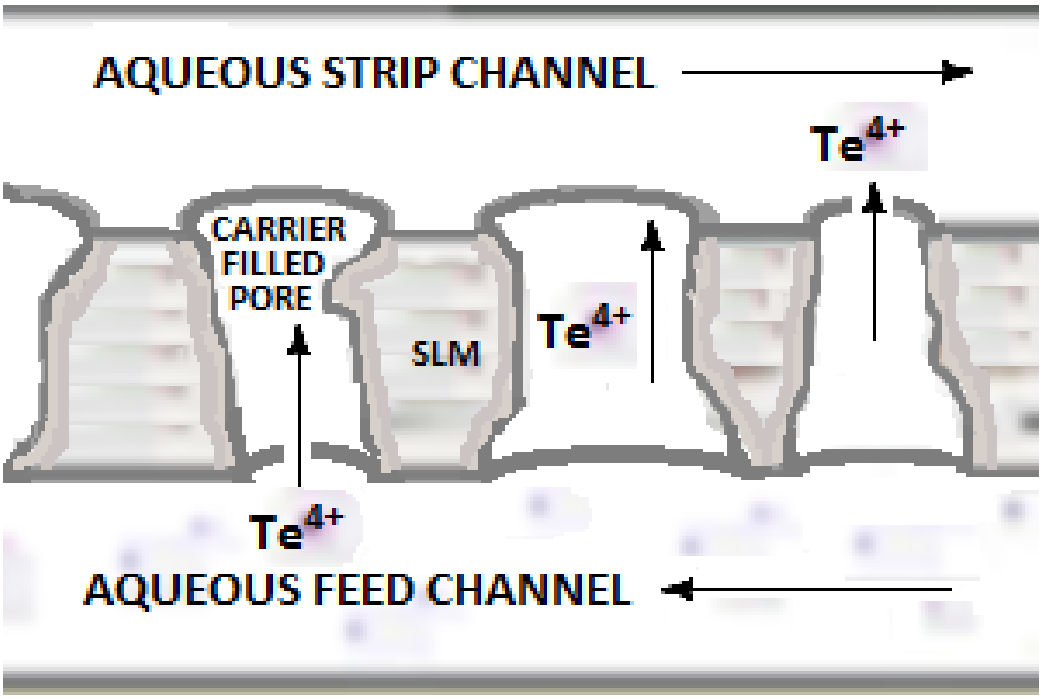

Fig. 3.2-1 Grand scheme mechanism depicting Te membrane transport via carrier

3.2-1 Mechanism of Extraction

The mechanism of extraction plausibly proceeds according to the following scenario. A Te^{4+} complex diffuses through the stream of cadmium telluride feed following the laws of diffusion until the Te^{4+} complex reaches the interface between the feed stream and extractant (i.e., the feed-side surface of the membrane). At the surface, the extractant attracts and captures the Te^{4+} complex, and pulls it across the fluid interface into the membrane pore. It is quickly surrounded (or solvated) by several molecules of extractant as shown in Fig. 3.2-2. Transport of the Te complex between streams may be reversed. However, the concentration of tellurium complex between the feed and extractant is determined by equilibrium kinetics

involving a “distribution constant (M)”. Once captured, overall equilibrium at the interface of the membrane with the feed solution drives the Te complex out of the feed into solvation by the carrier.

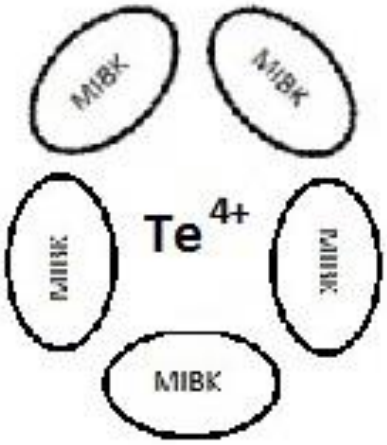

Fig. 3.2-2 Tellurium complex surrounded or solvated by MIBK

The Te^{4+} complex now solvated by the carrier fluid, moves through the stagnant liquid filled pore of the membrane again according to the laws of diffusion. As the Te^{4+} complex reaches the interface between the extractant and the strip stream, the strip stream attracts the tellurium complex again, as dictated by equilibrium, and pulls it across the interface, driving the Te complex to be unloaded from the carrier into the strip. The Te complex is free to follow the laws diffusion to be carried away from the membrane. The carrier MIBK remains in the SLM pore, renewed for the next cycle as long as the supply of Te^{4+} ions and H^+ ions permit continued mass transfer. Note that this model not only pumps the metal ion from one face to another but also gives cause for the H^+ ion to be pumped across the membrane.

The generality of how to extract Te shifts at this juncture into addressing the rationale used for choosing the specific chemistry presented herein. A basis for selecting a concentrated hydrochloric acid feed stream in conjunction with the extractant MIBK was made because MIBK is known to selectively extract Te^{4+} from Cd. As reported in a comprehensive review by Havezov and Jordanov [34]; extraction of tellurium (IV) into MIBK from 4-7M hydrochloric acid is an important method for the separation and purification of tellurium(IV) from Zn(II), Cu(II), Pb(II), Cd(II), and S(IV) due to low reagent price and high extraction capacity.

The most detailed publications on the topic of Te extraction in hydrochloric acid were written in German by Havezov & Jordanov in the sixties and seventies. It is possible through examination of publications across several decades to piece together the puzzle of how MIBK selectively extracts tellurium. The element tellurium is known to have 8 natural stable isotopes [35]. Three of these isotopes are known to form complexes: Te^{2+} ion, Te^{4+} ion, and Te^{6+} ion [34]. The Te^{4+} isotope is the most important of these in extraction chemistry as it is capable of forming stable halide-complexes in aqueous and organic solutions that are known to actively complex with oxygen containing solvating carriers like ethers, alcohols, ketones, and others [34]. More concisely, only Te^{4+} is known to actively complex with a solvating extractant such as MIBK, the ketone chosen for this project. For example, Hayashi et al. [36] report that Te^{6+} remains in the aqueous phase during extraction of the species Fe^{3+}, Cr^{6+}, and Mo^{6+} with MIBK; however, after boiling Te^{6+} to Te^{4+}, MIBK extracts the Te^{4+}, which was then back extracted with distilled water.

3.2-2 Extractant Synergetics

MIBK is used alone or synergistically with another extractant, such as TBP (tributyl phosphate). Venkateswarlu et al. [37] report extracting Te and other metals with 100% MIBK and a 50:50 ratio of MIBK:TBP. In this case, the 50:50 MIBK:TBP mixture is reported to enhance extraction of Te over that of MIBK alone. Te in 2-9M HCl solution is always extracted via MIBK with a Te:Cl ratio of 1:4 [34]. For HCl concentrations over 10M the ratio of Te:Cl is reported to be 1:6 [34]. Compounds containing ratios of Te:Cl lower than 1:4 are not considered to be active in extraction by any processes studied [38]. The tetrachloro species of tellurium are known to be extractable with MIBK polar extractants such as TBP [34], while the lower dichloro tellurium species have not been found to participate in MIBK extractions. Havezov & Jordanov [39] report Te to be extracted by MIBK with "solvent number of 5" and propose the formula $H_2Te^{4+}(OH)_2Cl_4\ MIBK_5(H_2O)_{4-8}$ is the carrier complex. The same authors indicate that for the experimental test condition of 6M HCl, the hydration number is eight and the distribution ratio between MIBK and the acid is 20.

3.2-3 Dissolution of Cadmium Telluride in Hydrochloric Acid

Modern kinetic studies done by Milne [40] and Milne & Mehadevan [41], have been modeled in detail by Laatikainen & Paatero [38], which predict that there are three dominant Te species in hydrochloric acid depending on the acidity. The species are $Te(OH)_2Cl_2(H_2O)_2$ in 0-6M HCl, $Te(OH)Cl_4^-$ in 2-10M HCl, and $TeCl_6^{2-}$ in 6-12M HCl.

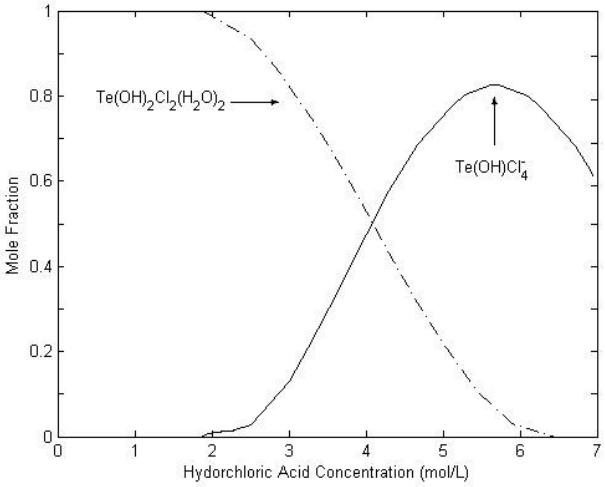

Fig. 3.2-3 Equilibrium species for adapted from Laatikainen & Paatero [38].

Fig. 3.2-3 shows the relationship between the dominant Te species and the molarity of the HCl solution, as characterized by Laatikainen & Paatero, 2005; the curves depict a model of the most prevalent Te species in HCl over the range of molarity shown. The species of Te most likely to be present is dependent upon the acidity of the solution.

For the case at hand, creation of the Te ion is accomplished by dissolving of cadmium telluride powder in 6M hydrochloric acid (with the aide of hydrogen peroxide). Milne [40] and Laatikainen & Paatero [38] predict that the Te complex in a 6M feed would be primarily of the tetrachloride form $[Te(OH)Cl_4]^-$. This Te complex is similar to the $[Te(OH)_2Cl_4]^{2-}$ complex which is reported by Havezov & Jordanov [39] to participate in extraction from HCl. Since these complexes are very similar, it may be that they are both present in aqueous solutions in a transitory equilibrium and participate in extraction, or one of the authors may be wrong on this point. The difficulty distinguishing between the signals of a double bonded oxygen versus a single bonded hydroxyl group in the proposed $[Te(OH)_2Cl_4]^{2-}$ is mentioned by Havezov &

Jordanov [39]. It is also pointed out by Laatikainen & Paatero [38], that the solution chemistry of tellurium is complicated by the co-existence of mixed oxo, hydroxo, and chloro complexes. On this topic, Milne et al. [41] determined the "square-pyramidal species" $Te(OH)Cl_4^-$ is the principal Te species in equilibrium (with other species) in 3M-9M HCl,

> No evidence for species suggested by other authors such as $TeCl_5^-$, $Te(OH)_2Cl_4^{2-}$, *or* $TeOCl_3^-$, among others, has been obtained although these may be present in very low concentration relative to the principal anions.

Havezov & Jordanov [39] find MIBK extracts Te via solvation only (without changing the bond structure) since the extraction energy is too low at 1.2 kcal/mol to be caused by the bonding of a reaction. This is consistent with assuming that the Te complex $Te(OH)Cl_4^-$ is unchanged after absorption by MIBK. It is most likely that the Te complex in feed and MIBK exists as the tetrachloro $[Te(OH)Cl_4]^-$. Extraction studies of cadmium in various HCl solutions [42] [43] indicate that $CdCl_3^-$ is probably the dominant species of cadmium formed in 6M HCl solution. Thus, creation of the Te complex in 6M HCl may proceed according to the following to create a precursor of Te extraction.

$$CdTe + 7HCl + H_2O_2 \rightleftharpoons H^+[Te^{4+}(OH)Cl_4]^- + H^+[Cd^{2+}Cl_3]^- + OH^- + 5H^+ \quad (3.1)$$

3.2-4 Transport of Te Complex in Carrier Solvation Ring

At the interface of the feed solution with MIBK at the membrane surface, the extractible Te^{4+} complex in equilibrium with MIBK may follow the equation, in which the symbolic carrier molecule MIBK is denoted by the letter X,

$$HTe(OH)Cl_4 + 8H_2O + 5X \rightleftharpoons HTe(OH)Cl_4\,X_5(H_2O)_8 \quad (3.2)$$

Assuming sufficiently high extractant to metal ion complex ratio, of the order suggested by Eq. 3.2 to be 5:1, the extraction starts when the Te^{4+} complex diffuses across the boundary layer in the aqueous feed solution where it is surrounded by hydrated carrier or solvated as envisioned in Fig. 3.2-4. The extractant MIBK has a polar oxygen bond, which likely gives sites for links with hydrogen in its associated water molecules, creating a crown around a central void where the square pyramid Te complex neatly fits. The Te complex thus lodged, moves in a large molecular complex during transit through the membrane.

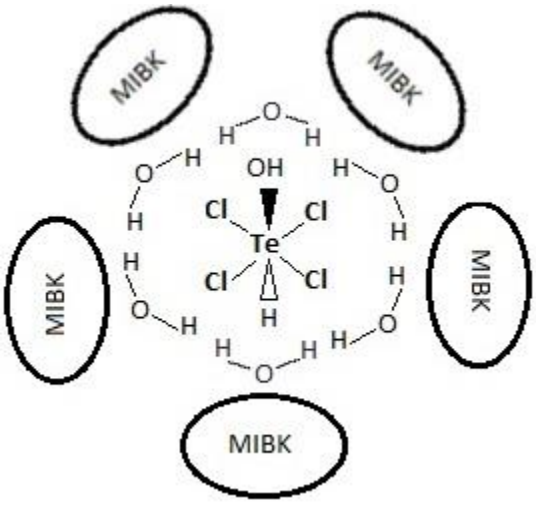

Fig. 3.2-4 Dual solvation ring of water and extractant (MIBK) in the Te carrier complex

The multi-molecular Te-MIBK complex then diffuses through the carrier as predicted by diffusion theory, drifting towards locations of lowest complex concentration. Because both the H^+ and Cl^- ions present in the Te complex are present in lower concentration in the 2% HCl strip solution than the 6M HCl strip solution, it is expected that the Te complex will move toward the strip stream.

3.2-5 Unloading of Carrier to Aqueous Strip Solution

When a Te complex comes into contact with the MIBK-strip solution interface, the complex instantaneously crosses from the organic extractant phase into the aqueous strip solution, as follows;

$$HTe(OH)Cl_4\,X_5(H_2O)_8 \rightleftharpoons\ 5X + 8H_2O + HTe(OH)Cl_4 \tag{3.3}$$

In the strip solution, the dominant Te molecule at equilibrium is expected to be of the form $Te(OH)_2Cl_2(H_2O)_2$ due to the lower acidity of the stream. The equilibrium reaction, very similar to that proposed by Milne [40], may proceed according to the equation;

$$HTe(OH)Cl_4 + 3H_2O \rightleftharpoons\ Te(OH)_2Cl_2(H_2O)_2 + 2HCl \tag{3.4}$$

The most important aspects of Te extraction chemistry are summarized in Fig. 3.2-5.

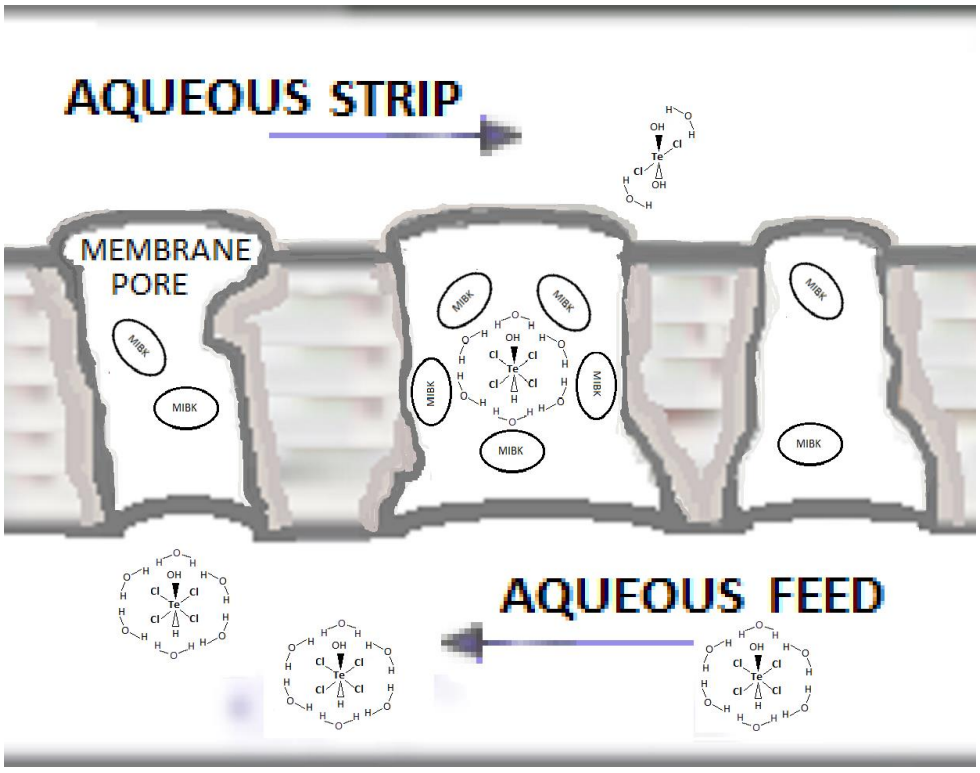

Fig. 3.2-5 Detailed grand scheme mechanism.

3.2-6 Reaction Kinetics Dependence on pH

According to the mechanism underlying Eqs. (3.2-4), it may be expected that Te exchange between the streams in channels of infinite length will cease when the pH of both streams is equalized by the extraction process. This reaction is theoretically reversible; however, because of the low acidity in the strip stream, reaction kinetics change the primary Te complex to a form with Te:Cl ratio to 1:2, creating a Te complex that is not extractable by MIBK, as only the tetrachloride species of Te molecules are extractable in 6M hydrochloric acid. It is proposed that the equilibrium reactions Eq. (3.3) and (3.4) do not offer a dominant resistance to diffusion of Te but proceed in sequence nearly instantaneously; creating a dichloro form of Te complex that is not extractable at the pH (2% HCl) of the strip solution. Once the MIBK releases the Te complex into the strip stream, it is instantaneously transformed into the dichloride complex which does not get taken up by MIBK, thus effectively creating an infinite sink for the tetrachloride species of Te coming from the highly acidic strip.

It is interesting that the mechanism permits extraction of Te to continue against the gradient of Te complex concentration, so long as the concentration of H^+ in the feed stream is greater than that of the strip stream. Initially it can be said that both the concentration gradients and the pH simultaneously drive tellurium transfer between the streams. As the concentration of Te in the strip stream increases, the pressure for Te^{4+} to move from the feed stream to the strip stream solely by Te concentration decreases. Te^{4+} might then continue to diffuse against the gradient if driven by pH, creating a stream of highly concentrated Te^{4+}. This

is because there is an exchange between the streams of both Te ions and HCl as illustrated in Fig. 3.2-6 and Fig. 3.2-7, as discussed below.

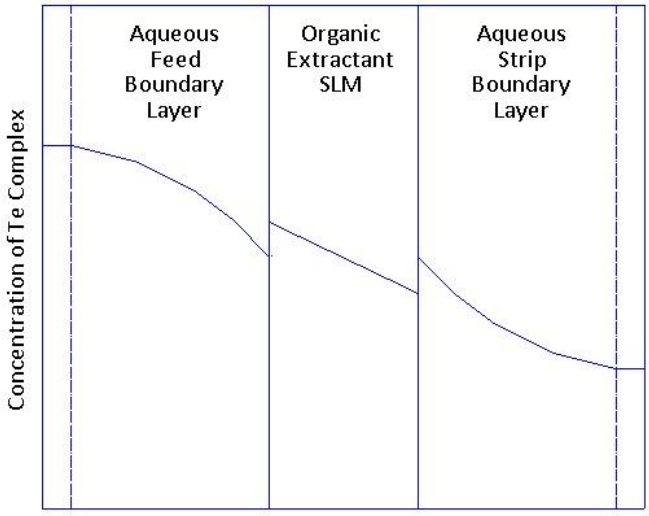

Fig. 3.2-6: The Te concentration profile during a extraction drops across the SLM. Concentration of H+ follows the same pattern as one hydrogen proton is extracted with each Te. The concentration gradient of Cl- is steeper as four Cl- ions are extracted with each Te.

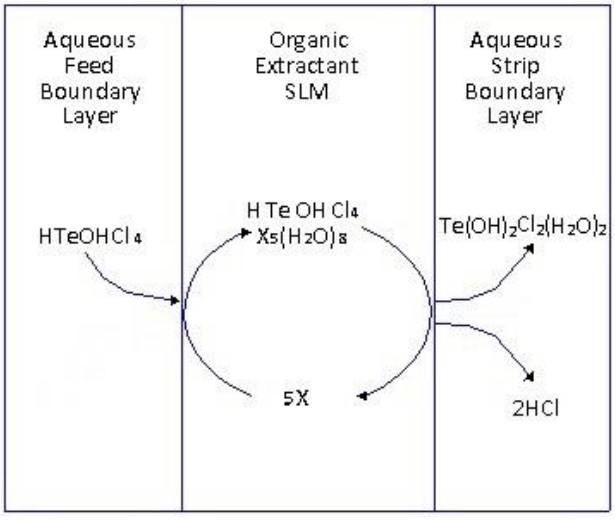

Fig. 3.2-7: Proposed MIBK carrier (X) cycle in SLM for Te complex (neglecting water exchange). The H+ and Cl- ions are pumped from the feed channel (left) to the strip channel (right) through the SLM carrier (middle).

The pH of both aqueous streams plays a role in the extraction dynamic, in the sense that pH plays a role in controlling the (constant) distribution ratio between the immiscible phases membrane interface on either side of the central organic SLM. The ultimate equilibrium distribution of the Te^{4+} ion between the phases is referred to as the "distribution constant", usually denoted by "M". This distribution ratio predicts how the concentration of Te^{4+} complex will distribute itself between the aqueous and organic phases at equilibrium.

For example, at any given (aqueous stream) pH flowing alongside the SLM soaked in organic extractant, there is some equilibrium point between the two phases, such that a Te ion will move from one of the phases to the other, until equilibrium is satisfied. And so, if at a given pH, there is equilibrium pressure for the Te^{4+} ion to move from the aqueous solution into the extractant MIBK, the Te^{4+} ion will continue to move from one stream to the other, even against the concentration gradient, until equilibrium is satisfied. In the same manner, it is expected, the equilibrium pressure for movement on the Te^{4+} ion is easily reversed, by adjusting the pH of the aqueous stream. Ideally, to efficiently extract the Te^{4+} ion from the aqueous CdTe stream to the blank stream, equilibrium pressure coupled with diffusion, create a pump to move the ion from the feed stream to the extractant in the SLM, then again from the extractant in the SLM to the second blank aqueous strip stream.

The optimum pH to obtain a pure stream would be one such that MIBK is highly selective of the Te^{4+} ion and has a very low affinity for the Cd^{2+} ion. There also must be enough MIBK in the SLM to permit the optimum ratio of extractant per Te^{4+} ion, and the pores in the SLM need to be large enough to permit migration of a large complex of extractant-ion. Once equilibrium is

established between all three phases, there should not be an accumulation of Te^{4+} ions in the SLM, because to effect extraction of Te^{4+} on the feed stream, a Te^{4+} ion must first be released to the strip stream, and the mass of Te^{4+} must be conserved overall. Theoretically if there is an excess of HCl in the feed stream it should be possible to extract 100% of the Te. The concept of the distribution constant is critical to a successful extraction and more material on this topic is presented Section 3.5.

3.3 Physical Properties of MIBK

The pores of the supported liquid membrane are soaked in the organic extractant MIBK, a metal extractant that favors selection of the metal tellurium over that of cadmium under the right conditions. Because this organic phase is immiscible in both the aqueous feed and the aqueous strip, the two aqueous streams flow on either side of the membrane without mixing, although over time it is likely that small molecules of MIBK break off and wick into the flowing aqueous streams due to shear stress. Comparison of boiling point (116.5 C) [44] and water solubility for MIBK with that of a few other solvents tested in a thin sheet supported liquid membrane, as listed by Araki & Tsukube [27], indicate that a thin sheet supported liquid membrane containing the carrier MIBK might be expected to endure a few minutes to hours and is not likely to be stable over days. MIBK has the chemical formula $C_6H_{12}O$ as visualized in Fig. 3.3-1. It has polarity due to the oxygen double bond and may accept one hydrogen bond [44]. MIBK is very slightly soluble in water, with a solubility of 1.8% by weight; similarly, water is only sparingly soluble in MIBK with a solubility of 1.9% by weight [45]. Translated to a molar

ratio; MIBK may contain 1 mole water in 10 moles MIBK versus to a solution of water may contain up to 3 moles MIBK in 1000 moles water.

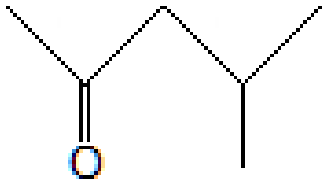

Fig. 3.3-1 Two-dimensional representation of a MIBK molecule

Development of the chemistry for Te extraction in microchannel requires discovery of the following: (1) a formula for the aqueous metal feed solution; (2) the proper ratio of MIBK to aqueous metal feed solution; and (3) an appropriate strip solution. Generalities found in other publications on microchannel metal extractions will be assumed to apply to the extraction of Te. As asserted by Maruyama et al. [18], the behavior of ions is predictable in the sense that an ion extraction demonstrated in a bulk reactor or separation funnel can be expected to be the same in microchannel. For example, Hotokezaka et al. [15] found for the U(VI) ion, the extraction in microchannel of 93.8% is comparable to the bulk liquid-liquid extraction of 96.1%. Further, Maruyama et al. [10] assert that metal ion extractions are dependent upon pH in the microchannel, just as they are in a separation funnel.

3.4 Physical Properties of Thin Sheet Membrane

The hydrophobic polypropylene membrane for both the model and experiments is the Celgard 2400. The manufacturer specifies it to be 25 µm thick with 0.043 µm diameter pores and 41% porosity. Arora & Zhang [46] report the single layer membrane is extruded in a dry

drawn process to create pore space. The role of the membrane in the mircroreactor design is to retain the organic agent MIBK in the hydrophobic membrane pores, while the aqueous solutions are repelled from the membrane, maintaining discrete phases on either side of the membrane. As long as the thin sheet membrane is free of perforations or other damage, mixing of the carrier solvent with the aqueous solution is ensured.

3.5 Model Development

A one-dimensional model based on diffusion theory is developed here to show that potential indeed exists for separation of Cd from Te in the microchannel device. This model will be useful in choosing the values of parameters in the experiment including flow rate(s), initial concentration, residence time, and channel dimensions, etc. This model is presented formally in Appendix D.

It consists of two microchannels separated by a very thin porous membrane. The square channels are symmetric with dimensions, *a* x *a* x *L*, where *a* denotes both width and height, and *L* is length. The membrane is of thickness denoted by *b* with pores of diameter *d*. Liquid streams will be pumped through each channel in a counter-flow pattern. One conveys an aqueous hydrochloric acid stream (i.e. *feed*) containing approximately equal amounts of Cd and Te. The Te concentration in the feed at the inlet is designated C_{1F_0} = 1145 ppm (1 = Te, F = feed, o = initial). The feed, upon exit from the microchannel will be referred to as *raffinate*. Flowing in the second channel is a stream of fluid which is a certified blank aqueous phase (i.e. *strip*) with an undetectably or zero small concentration of Te at the inlet, designated as C_{1S_0} = 0 ppm (1 = Te, S = strip, o = initial). The unknown concentrations of interest are that of the raffinate,

C_{1F_E} (1 = Te, F = feed, E = exit), and that of the strip at the outlet, C_{1S_E}(1 = Te, S = strip, E = exit). These concentrations are indicated in Fig. 3.5-1 for perspective.

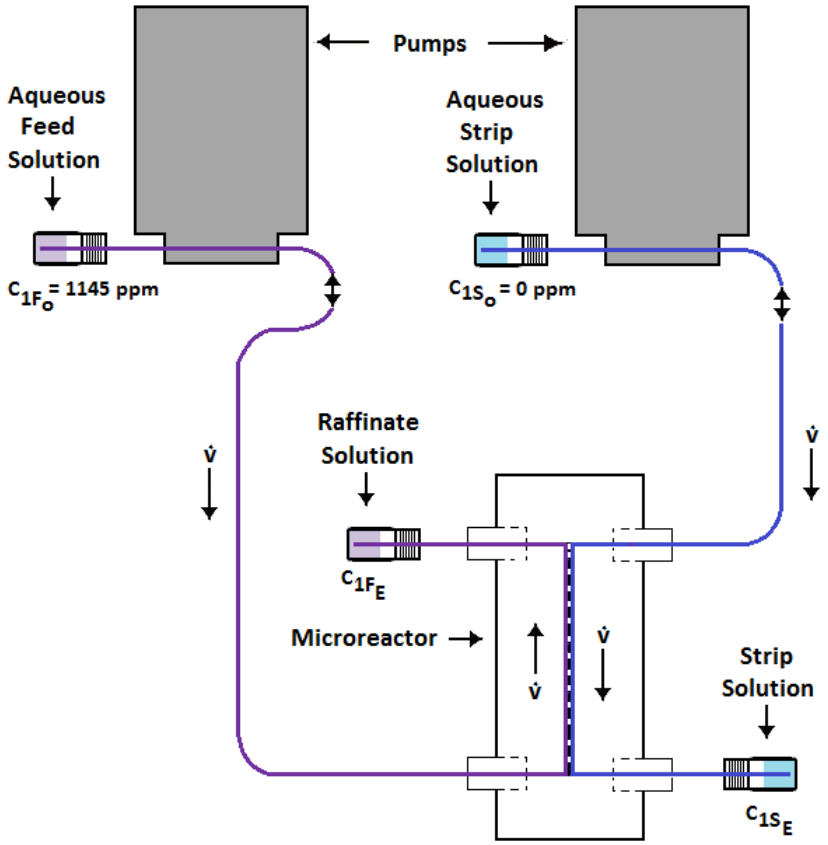

Fig. 3.5-1 Microreactor Te concentrations for the feed, raffinate, and strip solutions

A few drops of the extractant MIBK, or organic phase, will wet the pores of the membrane separating the two aqueous streams. An estimation of the tellurium mass transfer for various possible flow rates (and inlet concentrations) would be useful in the design of the experiment. A high mass transfer rate of Te to the aqueous strip phase (up to 100%) would be a desirable outcome of the experiment. The shape of the interface between the two immiscible phases is

likely to exhibit some curvature extending slightly beyond the surface of the membrane caused by forces of surface tension, not taken into account here.

This system ideally achieves mass transfer of tellurium both by diffusive convection in the pumped feed and strip streams in addition to pure diffusion within the stagnant membrane carrier. For insight into fluid dynamics, the Reynolds (Re), Schmidt (Sc), and Peclet (Pe) numbers for this system are calculated in Appendix E and Appendix F. The Reynolds number for internal flow through the square channel is close to one in the laminar regime. For the pumped aqueous streams, the Schmidt number ranges from 1800-2700, indicating that viscosity is larger than diffusivity by orders of magnitude. This basis justifies a model using thin film theory.

The hydrodynamic boundary layer is much thicker than the concentration boundary layer and flow is very slow. Due to the fluid-fluid contact it can be assumed that there is slip at the interface between the carrier in the SLM and the pumped streams. The diffusive mass transfer can be assumed as one-dimensional across the diffusive film, since the velocity gradient is considered to be absent at the point of phase interface. This makes a velocity profile one-dimensional in the direction normal to the flow across the channel that is nearly without curvature. The process of convection can be assumed to be one-dimensional in the stream direction. It is anticipated that the molar attention of solute(s) encountered in this experiment will be dilute in all solvents, and as such solute-solute interactions will be negligible. Only the diffusion of dilute Te is given consideration; the effect of diffusion Cd on that of Te is negligible. The organic extractant MIBK and the aqueous phases are immiscible fluids that maintain two separate phases. It was assumed that a hydrophobic membrane pore would permit itself to

wet and fill with molecules of the organic phase MIBK. On the feed side of the organic-aqueous interface, there is an equilibrium interaction between the Te^{4+} complex and extractant MIBK, but for the purpose of developing this model, the reaction was assumed to be a non-rate limiting step, as was found to be the case in at least one source in the literature, see [18].

On the strip side organic-aqueous interface, the equilibrium interaction between the Te^{4+} complex and the strip solution was determined to create an instantaneous and infinite sink for the Te complex due to effective irreversibility due to the pH of the strip in the experimental model. Fluid properties, such as viscosity and density, were assumed to be constant for a temperature of 25˚C at atmospheric pressure as given in Appendix A. The system can be modeled as a series of resistances across interfacing films: (1) a resistance in the convective feed stream of Te complex diffusion in the aqueous film; and (2) a resistance of Te complex diffusion in the static carrier saturated membrane. The third resistance for diffusion in the strip stream to carry the Te away to the exit is not necessary because C_{1S_0} = 0 ppm according to the membrane chemistry as pointed out at the start of this discussion.

3.6 Stokes-Einstein Diffusion Coefficient

The diffusion coefficients for the tellurium complex are calculated herein according to the Stokes-Einstein Equation in Appendix C (based on atomic radii in Appendix B). The diffusivity of the Te complex in the SLM carrier was adjusted slightly to account for the membrane pore size using the Hindered model as discussed in Appendix C. The diffusion constant(s), D, for Te in experimental media are shown in Table 3.6-1.

Table 3.6-1 Calculated Te Diffusion Constants

Solvent	D (cm^2/s)
Strip	5.44E-06
Feed	4.67E-06
SLM	6.15E-06

3.7 Series of Resistances

The model of the experimental conditions predicts the flux of the tetrachloro tellurium species from the feed, across the membrane, into the strip, where it is quickly transformed into the non-reactive dichloro-tellurium species. Labels are shown in Fig. 3.7-1 for Te concentration at edges of the boundary layer and at the phase interfaces. A control volume is designated inside the SLM as indicated by Fig. 3.7-2. It is assumed there is no accumulation in the membrane because experimental data are taken at steady state. Thus, the energy balance requires the flux into the control surface to equal the flux out of the control surface. A series of resistances is used to calculate this flux. The resistance of flux between the feed channel and the membrane surface; and the resistance of the membrane are deemed to be rate controlling. Other resistances, due to the fast reaction rates, are neglected.

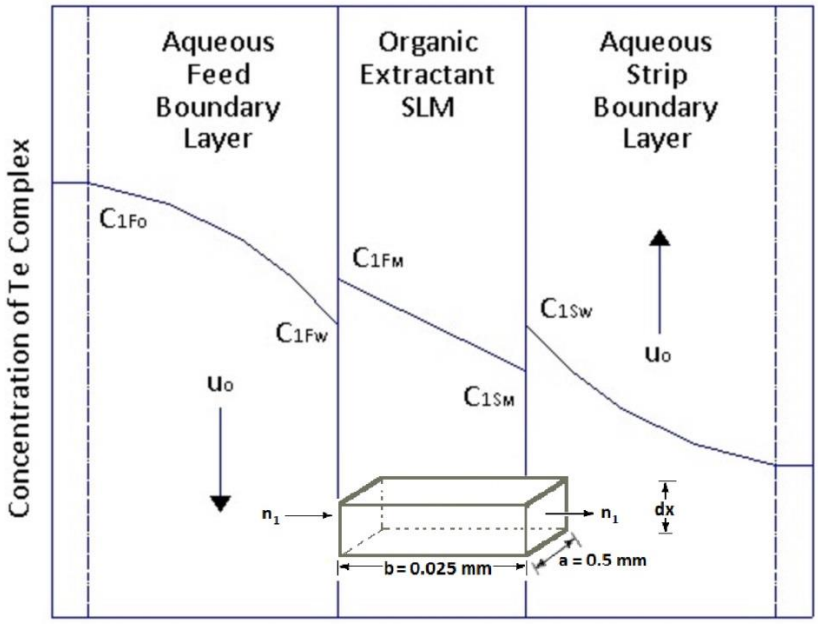

Fig. 3.7-1 Concentration of Te in the reactor around control volume in SLM

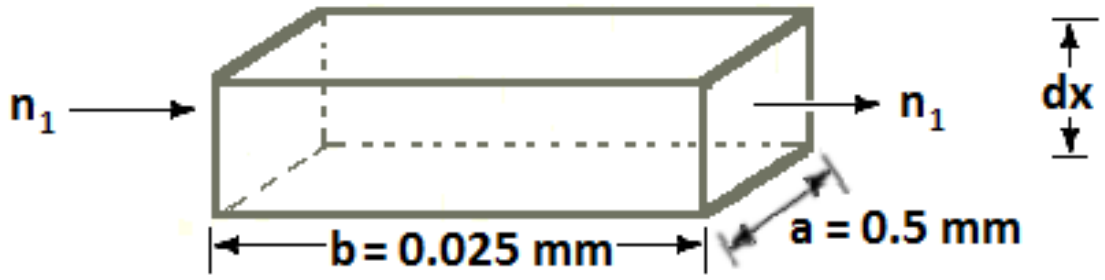

Fig. 3.7-2 Membrane control volume, zoomed closer

3.7-1 Feed Channel Resistance to Te Transfer

The resistance to mass transfer on the feed side is determined from a similarity solution for forced convection in a laminar boundary layer along a flat plate. The details of this approach, referred to as the 'Boundary Layer Model' in the results of Section 6.8, can be found in Appendix D. The solution obtained was integrated and normalized over the length of the

channel, to find an expression for the average mass transfer coefficient k_F for the feed flowing in the feed channel,

$$Sh = \frac{k_F L}{D_F} = 1.1284\sqrt{Re_L \cdot Sc} = 1.1284\sqrt{Pe_L} \tag{3.5}$$

where Sh is the Sherwood number, Pe_L is the Peclet number, and D_F is the diffusion coefficient for the feed solution (in Table 3.6-1 above). A local (x dependent) form of this solution, for a fluid-fluid interface, is found without details of derivation in Bird, Stewart, & Lightfoot [47]. Note that the Peclet number is a ratio of flow time to diffusion time.

An alternate approach to modeling the average mass transfer coefficient for the feed channel was developed and is referred to as the 'Internal Flow Model' in the results of Section 6.8. The complete details of this model are found near the end of Appendix D. This more complex model, is dependent upon the bulk concentration in the feed stream, C_{1F_B}, rather than the inlet concentration C_{1F_0}. In this case, the local mass transfer coefficient $k_F(x)$ is,

$$k_F(x) = \frac{au_o}{2x}\left[\frac{\mathrm{erf}(\eta_a)}{1-[B(\eta_a)-A(\eta_a)]} - 1\right] \tag{3.6}$$

where the similarity variable, η_a is defined to be,

$$\eta_a(x) = \frac{a}{2x}\sqrt{\frac{u_o x}{D_F}} = \frac{a}{2x}\sqrt{Pe_x} \tag{3.7}$$

in the context of $A(\eta_a)$ is defined as,

$$A(\eta_a) = \frac{\mathrm{ierfc}(\eta_a)}{\eta_a} \tag{3.8}$$

and $B(\eta_a)$ defined as,

$$B(\eta_a) = \frac{1}{\sqrt{\pi}} . \frac{1}{\eta_a} \tag{3.9}$$

For the internal flow model, the average mass transfer coefficient k_F, is found by numerically integrating and averaging Eq. 3.6 over the length of the channel,

$$k_F = \frac{1}{L} \int_0^L \frac{a u_o}{2x} \left[\frac{\text{erf}(\eta_a)}{1 - [B(\eta_a) - A(\eta_a)]} - 1 \right] dx \tag{3.10}$$

3.7-2 Membrane Resistance to Te Transfer

The resistance to mass transfer through the stagnant SLM is due to simple diffusion. The mass transfer coefficient may is expressed as,

$$k_M = \frac{D_M}{b} \tag{3.11}$$

where D_M is the species diffusivity in MIBK and *b* is the membrane thickness.

3.7-3 Strip Channel Resistance to Te Transfer

The resistance to mass transfer in the strip channel is considered negligible for three reasons: (1) equilibrium in strip channel prompts the Te species to form a non-reactive dichloro type upon release from the carrier at the interface; (2) transformation is considered to be instantaneous (i.e., the reaction time constant is zero); and (3) the reaction is essentially irreversible in the pH of the strip channel.

At the strip channel inlet, the concentration of Te in the blank solution is certified to be zero. Some distance down the channel, the strip solution has absorbed Te. However, the concentration of the tetrachloro species is zero due to the afore mentioned irreversible

instantaneous reaction. The interface between the SLM and the strip stream is considered to be an infinite sink for the tetrachloro Te species diffusing through the membrane.

3.7-4 Sum of Resistances

The total mass flux of the tetrachloro Te species, across the membrane is found by adding resistances in series, according to Eq. 3.7,

$$n_1 = \left[\frac{1}{k_F} + \frac{1}{Mk_M}\right]^{-1}\left[C_{1F_0} - \frac{C_{1S_M}}{M}\right] \tag{3.12}$$

C_{1F_0} is the inlet concentration of Te species in the feed at the inlet. C_{1S_M} is the concentration of the Te species in the carrier MIBK at the interface with strip. The distribution ratio, denoted here by M, determines the amount of analyte that distributes itself between the two immiscible phases at equilibrium. It is defined as,

$$M = \frac{[C_1]_M}{[C_1]_F} \tag{3.13}$$

where the analyte denoted by 1 is Te, the M subscript denotes the concentration in organic membrane, and the F subscript denotes the concentration in the aqueous feed solution.

The material balance on the Te mass in the SLM was evaluated, incorporating the flux as defined in Eq. 3.10, to estimate the total concentration of tellurium transferred to the strip stream at the exit C_{1S_E},

$$C_{1S_E} = \frac{a\,L}{\dot{v}}\left[\frac{1}{k_F} + \frac{1}{Mk_M}\right]^{-1}\left[C_{1F_0} - \frac{C_{1S_M}}{M}\right] \tag{3.14}$$

where L is the length of the channel, *a* is the width of the membrane (or channel), and $\dot{v}$ is the volumetric flow rate of the strip stream. The mass flow rates through the feed and strip

streams are kept equal, so there is no need to adjust for volume differences between the streams with respect to concentration in this case. Because C_{1S_M} is essentially zero, Eq. (3.12) reduces to the following,

$$C_{1S_E} = \frac{a\,L}{\dot{v}}\; C_{1F_0}\left[\frac{1}{k_F} + \frac{1}{Mk_M}\right]^{-1} \tag{3.15}$$

The recovery, R, in the mircroreactor model is simply Eq. 3.14.

$$R\,\% = \frac{C_{1S_E}}{C_{1F_0}}\,\text{x}\,100 \tag{3.16}$$

Rearranging Eq. 3.12 gives some insight into the extracted complex C_{1S_E} dependence on variables.

$$C_{1S_E} = \frac{a\,L}{\dot{v}}\;\left(MC_{1F_0} - C_{1S_M}\right)\left[\frac{k_M k_F}{Mk_M + k_F}\right] \tag{3.17}$$

If the distribution ratio M is very small, the dominant membrane resistance causes the amount of Te extracted to approach zero. If, on the other hand, the distribution ratio M becomes very large, the feed resistance becomes dominant, and the Te extracted is approximated by Eq. 3.16.

$$C_{1S_E} = \frac{a\,L\,k_F\,C_{1F_o}}{\dot{v}} \tag{3.18}$$

CHAPTER 4 – MATERIALS AND METHODS

4.1 Handling of Hazardous Materials

The safety protocols of both Oregon State University and PNNL were adhered to during experiments with the chemicals described herein. This entailed the frequent use of personal safety equipment such as a laboratory coat, an acid apron, two layers of eye shielding (safety glasses and goggles), and two layers of gloves (wrist length latex and chemical resistant elbow length gloves). All experiments were conducted in a PNNL hood with containment basins in place to catch spills. Contaminated solids, such as disposable pipette tips, were zip-lock bagged. The toxic waste, such as highly concentrated HCl contaminated with poisonous Cd, were stored in capped labeled jugs. All waste materials, liquid and solid, were disposed of in accordance with regulation.

4.2 Analytical Method and ICP Calibration Protocol

The foundation was laid for discovery, in that standard procedures for the chosen analytical chemistry method known as Inductively Coupled Plasma Optical Emission Spectrometry (ICP-OES) were developed and tested in coordination with Dr. Abhas Singh at PNNL. This facility can be used to detect trace metals.

The ICP-OES Thermo Jarrell Ash AtomScan16 shown in Fig. 4.2-1 was used as the analytical chemistry method for both chemistry development and microchannel experiments. The wavelengths for tellurium (Te) state I line 225.902 nm, cadmium (Cd) state I line 228.802 nm, and indium (In) state I line 325.609 nm were chosen for intensity measurements. Standard ICP

operation followed the procedure in Appendix H.

Fig. 4.2-1 Photo of Thermo Jarrell Ash AtomScan16

Standard solutions with known concentrations of cadmium, tellurium, and indium were diluted prior to measurement on the ICP to create an intensity calibration concentration expression. The element indium was selected as an internal standard in the calibration correlation to correct for errors that may occur due to transitory occlusions in the ICP peristaltic tubing or small system fluctuations in the ICP. Correction of small system fluctuations via this method requires a ratio of the measured intensity of a known concentration of the internal standard indium to the measured intensity of the unknown elements (Te and Cd) for every measurement taken on the ICP. This entails adding a 2000 ppb spike of indium to all calibration solutions and experimental samples (prior to measurement on the ICP). The ICP was configured to measure the intensity of each vial 10 times to report an average intensity measurement and standard deviation for each vial. Just prior to aspiration via the ICP, every vial solution was given five shakes in the operator's hand (with the vial cap on), to prevent sample density stratification. An example of ICP intensity data, calibration regression plots, and subsequent

sample concentration calculations with corresponding error may be found in Appendix G. ICP calibration data were measured on a daily basis, generally shortly after the experiments were started. Experimental sample data was measured on a daily basis, shortly after the experiment was completed. It was required that dilutions of samples be prepared to prevent oversaturation of the ICP (that might cause subsequent false high intensity readings) as documented in Appendix G. Occasionally, there was an overnight or weekend long delay between the preparation of ICP calibration solution tray and measurement on the ICP. Trays of standards and samples left to stand overnight or over the weekend were found to be stable and deemed suitable for testing at the next available time. The same can be said for time elapsed between sample collection, dilution preparation, and measurement on the ICP. Calibration data was processed into a regression in Excel and samples data concentrations are calculated as outlined in Appendix G.

4.3 Chemicals for the Analytical Method

Manufacturer certified chemicals were purchased specifically for ICP characterization of thesis experiments. Hydrochloric acid was chosen as the base chemical (for purchased chemicals, calibration dilutions and sample dilutions). Given that the project proposal named hydrochloric acid as the experimental chemical, it was reasoned that using the same acid in the ICP would reduce the matrix error. The certified chemical Cadmium ICP Standard Concentration 1000 ppm (µg/mL) Cd in 3% HCl came from Ricca Chemical. The certified chemical Tellurium Plasma Emission Standard (ICP) 1000 ppm (µg/mL) Te in 20% HCl came from Accu Trace Reference Standard. The certified chemical Indium 1000 ppm (µg/mL) in 2% HCl

came from High Purity Standards. A certified HCl 2% Reagent Blank solution from High-Purity Standards was used for the dilution of standards in calibration and sample dilutions. Nitric Acid 20% from Ricca Chemical Company, diluted to a concentration of 2%, was used for the purpose of rinsing dishes and flushing the ICP peristaltic tubing (prior to batch of samples, between batches of samples, and at the conclusion of sample runs). HCl 20% from Ricca Chemical, diluted to a concentration of 2%, was used to flush the ICP between samples. Water suitable for liquid chromatrography from the manufacturer Macron was purchased from the OSU Chemistry store to dilute the nitric and hydrochloric acids.

4.4 Analytical Method Equipment

Eppendorf pipets were used to measure chemicals as needed for both calibration and experiments. A Single-channel Eppendorf® Xplorer® electronic pipette 0.5-10 mL was purchased from Cole Palmer for measurement of small volumes of chemicals. This pipet was used with Eppendorf 500 to 2500µL epTIPS pipette tips purchased from Cole Palmer or Eppendorf epTIPS 1-10ML from PipetteSupplies.com. A Single-channel Eppendorf® Xplorer® electronic pipette 15-300 µL was purchased from Cole Palmer to dispense micro volumes of chemical. This pipet was fitted with Eppendorf 20 to 300µL epTIPS pipette tips from Cole Palmer. LDPE bottles with PP caps, washed twice with 2% nitric acid and rinsed with deionized water made in the purifier at MBI, were used to collect samples. Disposable polypropylene Griffin 15ml low-form beakers were purchased from Cole Palmer to use to clean pour ICP chemicals for pipetting. Sterile polypropylene centrifuge tubes purchased from the OSU Chemistry Store were used to hold calibration series and samples.

4.5 Feed Solution Chemicals and Formulation

The chemical cadmium telluride powder was ordered from Sigma-Aldrich preparation of a metal feed solution. HCl 20% from Ricca Chemical was used in all experimental feed solutions. Hydrogen Peroxide 30% solution made by Macron was purchased from the OSU Chemistry Store and diluted to the desired concentration after letting a small amount come to room temperature. Water suitable for liquid chromatrography from the manufacturer Macron was used for dilutions.

A metal feed solution to model a derivative of solar recycling material was developed. Throughout the experiments described herein, a dissolved cadmium telluride powder in aqueous solution, dubbed the *feed,* created a model for solar recycling material. The approximate desired concentration of Te in the feed solution is 1100 ppm as this has been reported to be the concentration in solar material that is ground up.

Some of initial feed solution formulas failed to effectively dissolve CdTe. These solutions with very weak hydrogen peroxide additions to 6M HCl (followed by sonification) resulted in cloudy black collusions of very low Cd and Te concentrations. The Cd and Te flakes remained in sediment on the bottom of the scintillation vial. Attempts with too much hydrogen peroxide yielded impressive smoky reactions that precipitated out in grayish white material on the bottom of the scintillation vial, once again yielding low concentrations of both Cd and Te in solution. The approach that ultimately succeeded, in creating several possibilities for a metal feed solution, was slow titration of 15% hydrogen peroxide solution into a scintillation vial containing cadmium telluride power. This approach was taken because there was only vague

indication in literature that CdTe is soluble in an acidic environment of at least 15% hydrochloric acid using two drops of 35% hydrogen peroxide [48]. Titration of hydrogen peroxide into the acid yields a few slightly different crystal clear feed solutions with the expected concentration of Cd and Te.

Several potential feed solutions were measured for concentration of Cd and Te. Clear solutions of satisfactory concentration could be made with 60 µl to 270 µl of 15% H_2O_2; however, the solutions with more hydrogen peroxide dissolved faster. A formula was settled upon that yielded roughly 1009 ppm Cd to 1145 ppm Te. The feed dubbed "2154" for the approximate concentration of Cd + Te concentration (ppm) consists of 0.0275 g of CdTe powder, 12.5 ml of 6M (20%) HCl, and 270 µl of 15% H_2O_2. The feed dubbed "4580" is made in the same manner as the 2154 feed with double the mass of CdTe powder.

The following procedure is used to mix feed solution. A clean glass scintillation vial is tare weighted on the PNNL scale (with all doors closed). A few black flakes of cadmium telluride powder are tapped from the end of a clean plastic measuring spoon into the scintillation vial until the desired weight of cadmium telluride powder is transferred. The actual weight varied slightly from batch to batch of feed and was recorded in the lab notebook. The scintillation vial is then capped and moved to a hood. A small volume of 20% HCl is poured into a clean bottle for the purpose of pipetting, measured with a clean Eppendorf pipet and tip, and then dispensed into the scintillation vial. A small volume of 30% hydrogen peroxide is poured into a disposable beaker and allowed to sit in the hood for approximately 30 minutes to come to room temperature before dilution. A second clean small disposable beaker is placed in the

hood in preparation for making a hydrogen peroxide dilution. An Eppendorf pipet is used to measure the 30% hydrogen peroxide and water needed to dilute the peroxide to 15%. Once the hydrogen peroxide is properly diluted, it is measured via Eppendorf pipet and dispensed into the open scintillation vial (already containing aqueous HCl and CdTe powder).

Shortly after contact, the CdTe powder begins the process of dissolution as demonstrated by the photographs in Fig. 4.5-1. This is facilitated by placing the capped scintillation vial in water-filled sonication bath for 60 minutes followed by five minutes on the degas cycle. At this point the feed is ready to use as the cadmium telluride power is dissolved. The solution appeared to be crystal clear and colorless. The feed solution is often prepared the day of an experiment or the afternoon before an experiment, but it remains stable capped in the hood and could be used for experiments weeks later. Just prior to measurement, it is given five shakes by hand, to redistribute any density stratification that might occur during storage.

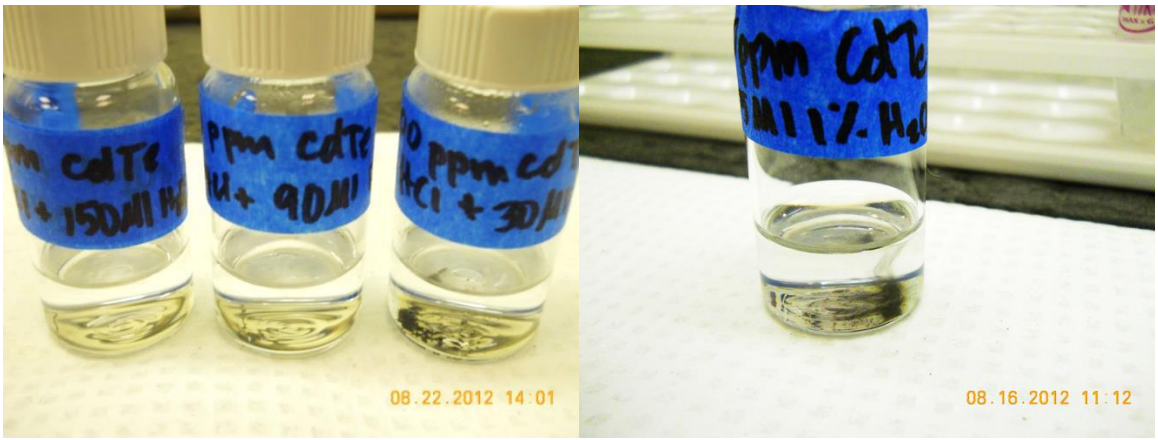

Fig. 4.5-1 Pictures of CdTe powder in various stages of dissolution.

4.6 Separation Funnel

4.6-1 Chemicals and Methods

The feed solution in separation funnel experiments is prepared as described in the preceding section. Reagent grade kerosene and 4-methyl-2-pentanone (MIBK) 99% were both ordered from Sigma-Aldrich for the purpose of testing in a separation funnel. Where indicated, a certified HCl 2% Reagent Blank solution from High-Purity Standards was implemented as an experimental strip solution. HCl 20% from Ricca Chemical was used in various concentrations for ACS grade test strip solutions. Hydrogen Peroxide 30% solution made by Macron was purchased from the OSU Chemistry Store and diluted to the desired concentration after letting a small amount come to room temperature for test strip solutions. Water suitable for liquid chromatrography from the manufacturer Macron was used for experiments calling for water or where dilution of other separation funnel chemicals was required.

The microchannel pilot chemistry was tested on the bench to determine optimum conditions. This entailed using a separatory funnel with a Teflon stopcock and valve purchased from the OSU Chemistry Store to separate cadmium from tellurium. The separation funnel is set in a ring stand as needed. A clean LDPE bottle or Pyrex beaker was placed below the separation funnel to catch the discharged liquid as it flowed out of the funnel. Eppendorf pipets with clean Eppendorf tips were used to measure ml and µl volumes of chemicals as needed for separation funnel experiments. Chemicals were poured in small clean bottles or disposable beakers prior to measurement with the pipette to avoid contamination of the source container.

4.6-2 Experiments

The separation funnel experiments proceed in two stages: (1) extraction of the Te from the aqueous feed into the extractant MIBK; and (2) back-extraction of the Te from the extractant MIBK into the aqueous strip. For most experiments the volume of the aqueous solution was 10 ml and the volume of organic solution was 10 ml. However, some of the final experiments required variable volumes of aqueous to organic solutions, as is indicated in Section 6.3. The variables considered during separation funnel testing include: phase contact time, addition of kerosene to the extractant (diluent), the ratio of organic phase to aqueous phase (OP:AP), and acidity (of the test aqueous strip solution).

The first stage, extraction of Te from the aqueous feed into the extractant MIBK was initiated by placing the separation funnel upright in a ring stand. The stopcock was turned to the closed position. The chemicals were added to the separation funnel in two additions, the organic phase, and the aqueous phase. The top plug was firmly set in place at the mouth of the separation funnel. Then the separation funnel was carefully lifted from the stand and shook by hand for a total of five minutes, with momentary breaks to open the stopcock for the purpose of venting every 30 seconds. At this point the organic and aqueous phases appeared to be mixed and the funnel was returned to the ring stand to rest for five additional minutes. After resting, the two phases separated, with the lower density organic (extractant) layer rising above the aqueous layer. A photograph of the first stage of extraction resting is shown in Fig. 4.6-1. A clean bottle labeled ‘raffinate’ with a test number was placed under the separation funnel. The stopcock was then opened and flow was permitted out of the funnel until the phase separation

meniscus nearly reached the stopcock, when the valve was quickly closed. The raffinate was capped for evaluation on the ICP. The organic phase, remaining in the separation funnel, was left in place for the second stage of Te back-extraction.

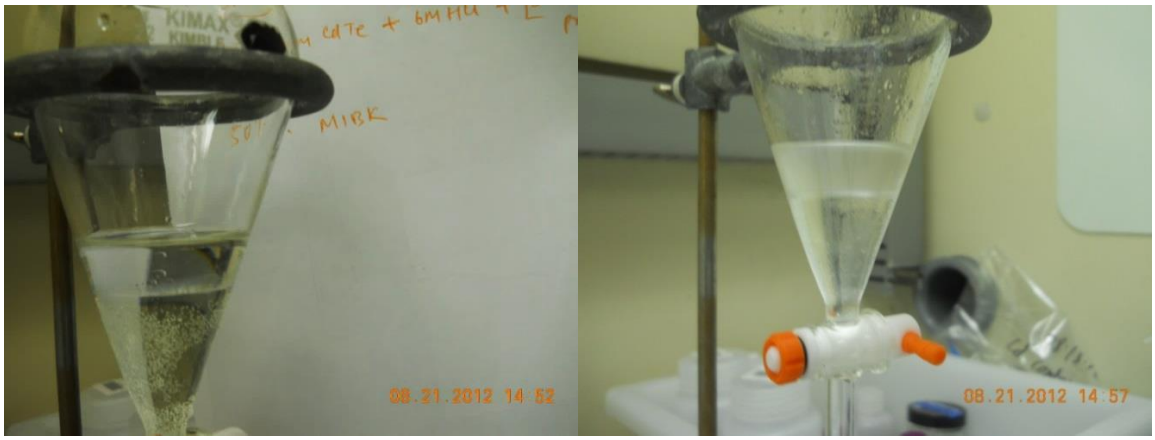

Fig. 4.6-1 A photograph of extraction in progress. The organic extractant is the top liquid layer. Left photo: The extractant is initially clear. Right photo: It turns opaque after absorbing Te.

At this point the stage was set to start the back-extraction of Te. Aqueous test strip solution was added to the separation funnel, forming a distinct layer (under) the organic phase left over from the first phase. The top plug was firmly set in place at the mouth of the separation funnel. Then the separation funnel was carefully lifted from the stand and shook by hand for a total of five minutes, with momentary breaks to open the stopcock for the purpose of venting every 30 seconds. At this point the organic and aqueous phases appeared to be mixed and the funnel was returned to the ring stand to rest for five additional minutes. After resting, the two phases separate, with the lighter organic (extractant) layer rising above the higher density aqueous layer.

A photograph of the separation funnel during this point of the back-extraction is shown in Fig. 4.6-2. A clean bottle labeled ‘strip’ with a test number was placed under the separation

funnel spout. The stopcock was then opened and the strip solution flow was permitted out of the funnel until the phase separation meniscus nearly reached the stopcock, at which point the valve was quickly closed. The strip solution was capped for later evaluation on the ICP. The organic phase, remaining in the separation funnel, was drained into another clean labeled bottle but was generally discarded as waste material as the metal concentration of the organic phase was not evaluated on the ICP.

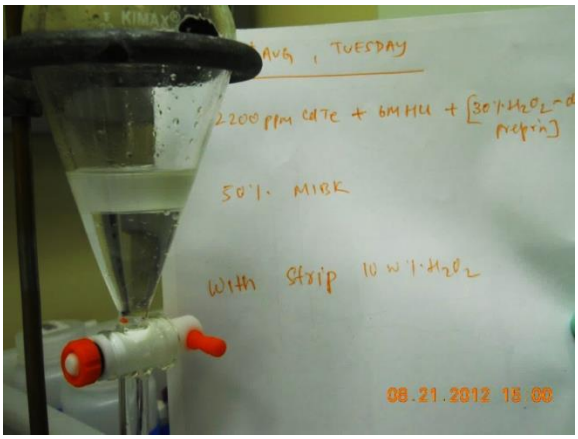

Fig. 4.6-2 A photograph of the back-extraction in progress.

4.7 Microreactor Chemicals and MIBK Stability

The chemistry which is found to be most successful in separation funnel testing was selected for experiments in the microchannel. The preparation of the aqueous feed solution in microchannel experiments is described in section 4.4 above (for both the 2154 and 4308 feed solutions). The organic extractant for microchannel experiments was reagent grade 4-methyl-2-pentanone (MIBK) 99% ordered from Sigma-Aldrich. A certified HCl 2% Reagent Blank solution from High-Purity Standards was the sole experimental strip solution.

A simple test was devised to determine the stability of MIBK in the membrane. A small volume of hydrochloric acid was poured into a glass dish, a square of membrane was set on the acid, and then 12 microliters of MIBK was dispensed on to the membrane. The membrane immediately wet with MIBK (became transparent so the MIBK flowed into the pores). The same sequence was repeated with another membrane except the ends of the second membrane was weighted to force the wetted membrane to stay immersed in acid (which it tends to repel). The dishes were closed with caps. Both membranes stayed transparent over a 45 minute observation period and remained clear several weeks later. This gave indication that the membrane can retain MIBK if it's sandwiched in acid. However, in this static test, there is no flow past the membrane to carry molecules of MIBK away in the aqueous stream.

4.8 Design of Microchannel Reactor

A simple two stream microchannel reactor was designed to continuously extract a stream of Te from a stream of CdTe. The three phase reactor consists of two aqueous phases separated by an organic phase. The highly acidic aqueous phase carrying the cadmium telluride feed material flows in one channel. A weakly acidic aqueous acceptor or blank solution flows in the second channel, counter in direction to the feed flow. A barrier between the two flowing streams was created by a small strip of hydrophobic Celgard 2400 membrane soaked with a few drops of essentially pure MIBK creating the organic phase. This supported liquid membrane (SLM) imposed structure on the flow that prevented free mixing between the streams and facilitated selective uptake and diffusion of Te through the pores of the membrane. The

membrane partition between the streams permitted the reactor to be configured in a counter flow pattern. The critical design components are illustrated in Fig. 4.8-1.

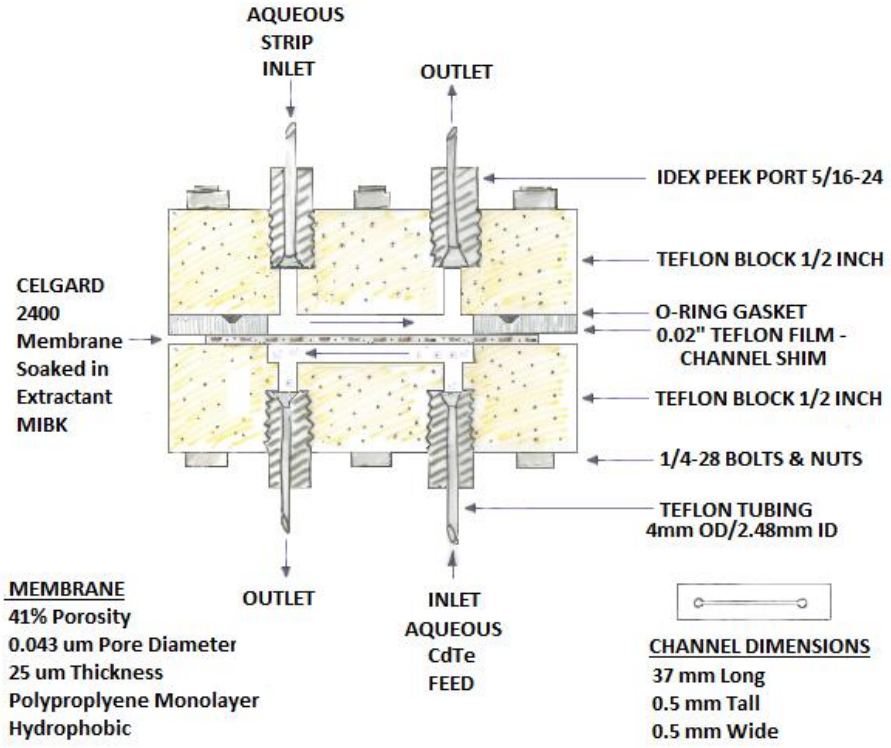

Fig. 4.8-1 Microchannel reactor configuration (straight channel shown). The aqueous streams are separated with a supported liquid membrane (SLM) soaked in an organic extractant MIBK, which selectively uptakes Te from the feed boundary interface, carries Te across the membrane, and releases Te to the strip boundary interface. Flow of the strip and feed solutions is arranged in a counter-flow pattern.

Three components are fabricated. The first is a smooth faced Teflon block with inlet/outlet port threads and 1/4" through holes (lacking the channel feature). The second is a similar block with the feed channel cut into the face 500 microns deep in the first generation and 450 microns deep in the second generation (the limits of available tooling). The third is a 500 microns thick shim with a through cut channel. The blocks were cut from 0.5 inch thick Teflon

material. The 1/4" through holes were unthreaded to permit 1/4" threads to pass through without difficulty.

Two configurations of the square 0.5 mm wide by 0.5 mm tall channel were designed: (1) a 37 mm long straight channel; and (2) a 129 mm long serpentine channel. The first generation straight channel layout is shown in Fig. 4.8-2 alongside the second generation serpentine channel.

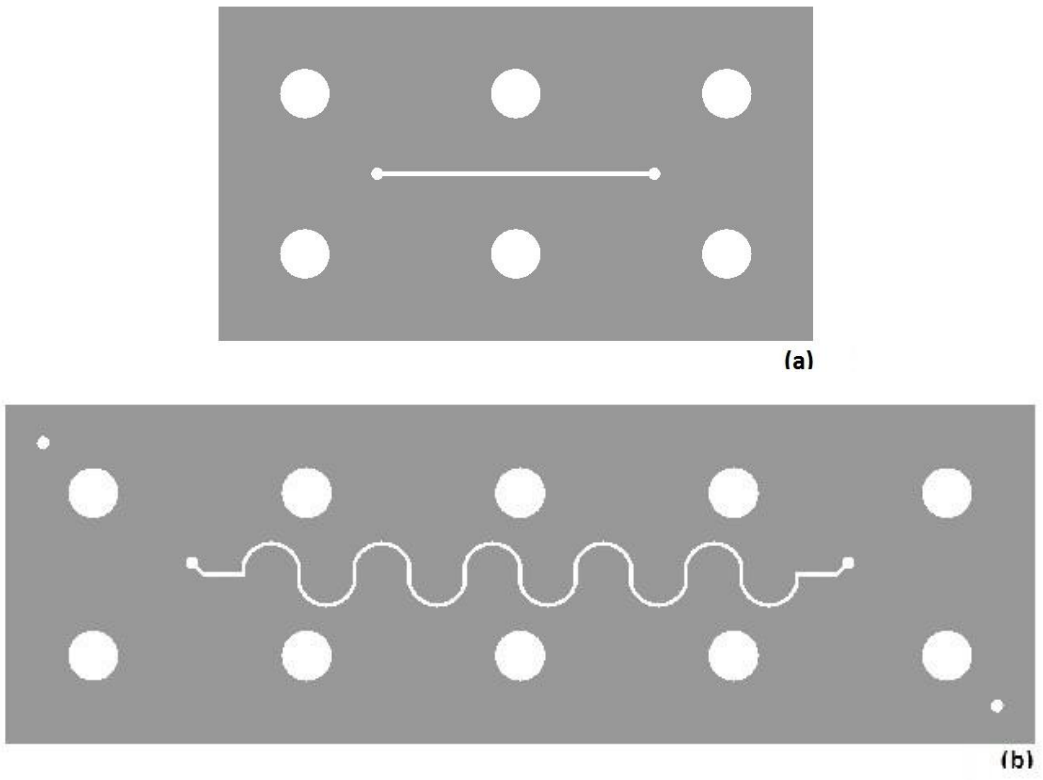

Fig. 4.8-2 A top view of the channel shims at 100% of actual size:
(a) The simple straight channel is the first-generation reactor.
(b) The serpentine channel is second-generation.

The serpentine channel of the second generation device yields roughly 3x the contact area of the first generation device. Both the first-generation and second-generation devices have a

small footprint as they are able to fit in an open hand. The plenums in both shims match to the same IDEX 5/16-24 threaded ports but the serpentine shim inlet and outlet are staggered off center to create a Y junction where the feed inlet (cut into the block) junctures with the strip outlet (cut into the shim). This is an improvement on the straight channel configuration where the feed and strip ports align over the plenums (wearing the membrane from both sides as fluid turned the corner from port to channel). The staggered ports improve membrane integrity. The second generation feed and strip ports do not align over the plenum but flow down a leg of the Y branch before flowing into the central channel. The central channels align in both reactors. An isometric view of the serpentine reactor is seen in Fig. 4.8-3.

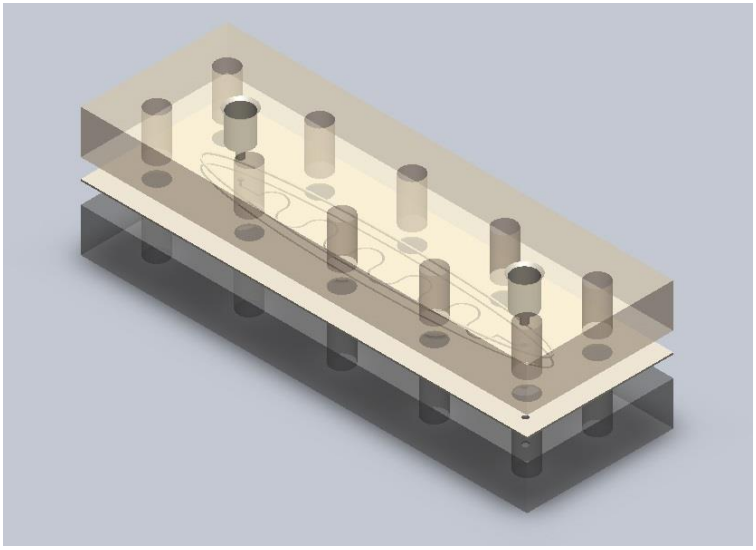

Fig. 4.8-3 Isometric view of the serpentine microreactor displays the blocks, shim, and gasket. Note that the channel cut into the feed block on its inward facing surface is not visible.

4.9 Material Compatibility

PTFE is the best choice of material for all parts contacting the acidic solutions because it is both durable and inexpensive. Delrin is found to be susceptible to the erosive effects of the

acidic feed. Metal was found to be easier to machine. However, a prototype reactor with stainless steel 316 channels is unable to withstand the experimental chemistry. Experiments in the stainless steel channel were not successful due to an unanticipated reaction between the metal in the feed solution and the stainless steel reactor. This became evident upon completion of the following compatibility test: a strip of SS316 was dropped into 1 ml of 6M 2154 pm CdTe feed solution. A few minutes later a blizzard of black “snow” flakes began peeling off the SS316 into solution. This reaction between the feed and SS316 appears to cause a color change in the raffinate, a dull black sediment (powder when dry), and gas bubbles. A similar test was done on several other steel alloys and it was determined that there is a need to use a non-metal material for construction of the microchannel and all surfaces that come into contact with the metal feed solution.

4.10 Sourcing of Materials and Parts

A few 1/2" thick by 3” wide Teflon® PTFE rectangular bars were ordered from McMaster-Carr to construct the reactor case. Film sheets made with Teflon®PTFE 0.020" thick by 12” wide were also ordered from McMaster-Carr for the purpose of cutting dozens of channel shims (as a new one was used for each experiment). Upchurch Scientific P-132 nut peek 5/16-132 flat bottom ports and P-139 ferrule kel-f (PCTFE) 5/16-24 flangeless ferrules of 4mm outer diameter were purchased from IDEX to connect the channels to the 4mm outer diameter PTFE tubing running through the peristaltic pump. The reactor was held in compression with ¼”-28 , 1-1/2” long 18-8 stainless steel hex socket head cap screws with zinc plated steel hex nuts with washers ¼”-28 ordered from Small Parts. A FEP-Encpsltd Viton Fluoroelastomer O-Ring AS568A

Dash Number 025 was purchased from McMaster-Carr to seal the first generation device. FEP-Encpsltd Viton® Fluoroelastomer O-Ring AS568A Dash Number 036 was purchased from the same source to seal the second generation serpentine channel. A sample of the Celgard 2400 hydrophobic monolayer polypropylene (PP) membrane was graciously provided by Celgard.

4.11 Microchannel Reactor Fabrication

The reactor external compression blocks (one with an internal facing microchannel and one with a smooth face) were cut from a 0.5" Teflon block with conventional machine shop tooling. The Idex ports were cut directly into the Teflon threads for the first generation (straight channel device). However, the brittle Teflon threads broke during fabrication of the second generation device. The machine shop improvised by substituting threaded Delrin plugs to fit into the Teflon block in the second generation device (serpentine channel). This improvising was only semi-successful, as the Delrin plugs did not react with feed during experiments but, as mentioned in Section 4.9, were susceptible to the erosive effects of the acidic feed, which eventually made it very difficult to seal the feed inlet and outlet ports.

The first generation internal shim with straight channel was cut from a McMaster-Carr 0.02" Teflon sheet using a template, exacto knife, and small bits of sandpaper. The second generation internal shim with serpentine channel was cut from the same material with conventional machine shop tooling. Drawings for the shims are given in Appendices I and J. Excess material was removed from the second generation bolt holes with an exacto knife. The machine shop cuts were "cleaned up" manually to minimize disturbances in the channel or

potential problems with sealing. Teflon fibers extending into the microchannel area were removed with bits of sandpaper. For each experiment, the device internally seals with one new 0.02” Teflon microchannel shim, and one new compressible ring type gasket, and one new piece of thin sheet membrane. The compressible ring gasket left an oval impression on the Teflon block after the first use, indicating that compression of the Teflon blocks contributed to sealing the device. The microchannel reactor assembly is shown in Fig. 4.11-1. Used gaskets, membranes, and shims are disregarded after one use.

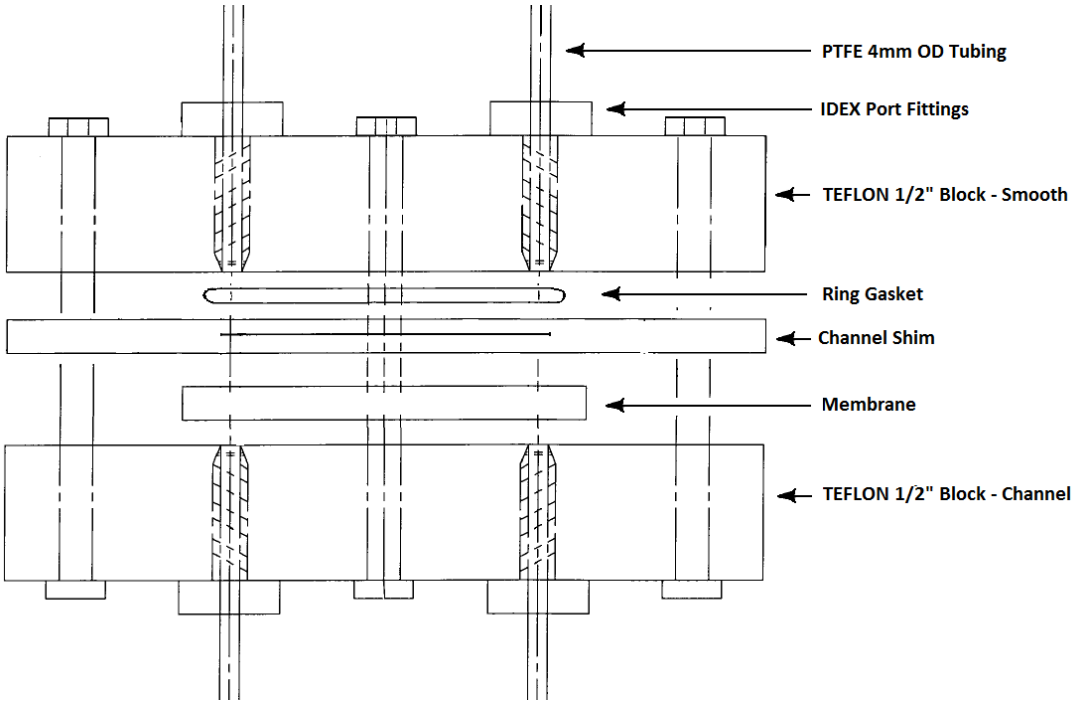

Fig. 4.11-1 Part assembly, with feed block and channel at top, and strip channel inside shim at center. The smooth bottom block applies compression to the gasket, holding the membrane in place, and seals the channels internally.

The Celgard 2400 membrane is handled with care, touching only on the edges to avoid creating microscopic tears, as it must be in good condition to seal the aqueous channels. Because the membrane has more tensile strength in the lateral direction then the lengthwise

direction, a small rectangular piece is cut with the long dimension of the membrane perpendicular to the direction the membrane unrolls from the bolt. The membrane is cut by gloved hands with scissors. A paper template for the shim is laid on the countertop. The rectangular strip of membrane is centered over the template, with care to place wrinkles or crimps in the membrane, outside the channel area. The desired membrane shape was traced directly onto the transparent membrane surface with a black sharpie marker. The membrane was finished by further trimming to the sharpie line, until the membrane fit just inside the bolt line but outside the sealing ring. The same membrane construction technique was used for both the straight and serpentine channel reactor. The cut pattern for bolt holes in the membrane is captured in the photograph shown in Fig. 4.11-2. Note in this frame that the membrane has slipped during the experiment slightly toward the top of the frame, out of the desired position, leaving a gap between the gasket and the bolt for a potential internal leak around the membrane.

Fig. 4.11-2 The membrane seen after an experiment.

The Idex flat bottom port/ferrule system purchased direct from Cole Palmer is shown in Fig. 4.11-3. This port mated with the peristaltic pump's 4mm OD Teflon tubing.

Teflon tubing was scored with a tubing vise as in Fig. 4.11-4. This was done to create a flat cut to seal against the reactor. The cut was finished by hand with an exacto knife and sanded with fine sandpaper until the tubing edges were smooth.

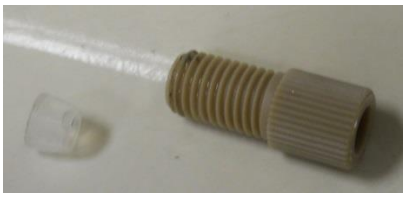

Fig. 4.11-3 IDEX port system and Teflon tubing

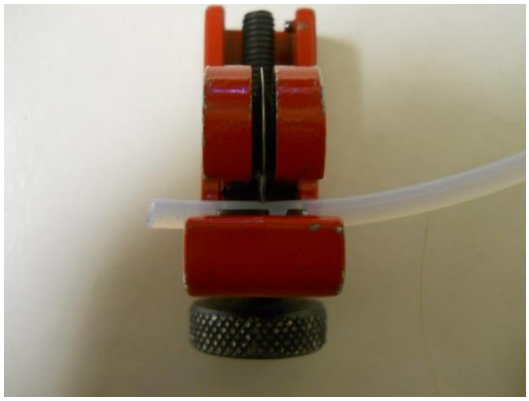

Fig. 4.11-4 Scoring Teflon tubing to get a smooth seal

The tubing was inserted into the IDEX port with a ferrule following manufacturer instruction. The IDEX port/tubing/ferrule assembly were locked together by pre-tightening with a wrench (over and above hand-tight) in a discarded SS316 threaded block cut as shown in Fig. 4.11-5. This was found to nearly eliminate leaks and prevent stripping of the brittle Teflon threads during assembly. The mating threads for the Idex ports (SS316/Teflon/Derlin) were cut according the manufacturer drawing. After the ferrule was locked onto the Teflon tubing it was

screwed into the Teflon reactor. If leaks presented upon starting flow, Teflon tape was wrapped around Idex port threads to fill gaps between the threads and maintain a tight seal. IDEX ports, tubing, and Teflon tape were replaced to repair leaks prior to achievement of steady state flow conditions.

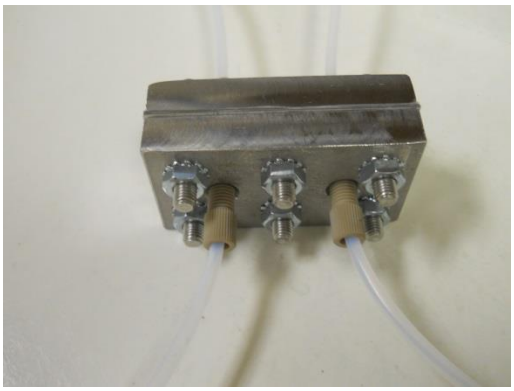

Fig. 4.11-5 Discarded SS316 block locks ferrule on port assembly

Assembly of the various components was performed by hand, paying attention to the precise bolt torque necessary to mitigate leakage but not to overstress the membrane, thus avoiding an internal tear.

The same procedure was used for both the straight channel and serpentine channel reactors. The feed side compression block was held with the microchannel side facing up and loose bolts extending upwards through the bolt holes. The membrane was then gently laid in place between the bolts in such a way that the edges fell between the first revealed threads on the bolts, holding the membrane in place without any puckers or wrinkles. The central area of the membrane was kept away from sharp bolt threads which if touched might cause damage. A channel/shim plate in the correct orientation was gently tapped down through the bolt threads, until it rested against the membrane, without shifting the membrane's position. A

round gasket was bent by hand into an oval shape and placed inside the bolt holes against the Teflon shim. The flat faced strip side compression block was then placed on the top of the stack and nuts were threaded onto the ends of the bolts until finger tight. The nuts were further tightened uniformly, in increments, until all the bolts received 2.5 to 3 turns of 360 degrees each.

Fluid leaks presented around the bolt holes (during experiments) if the bolt/nut system was left too loose. However, over tightening the bolt/nut clamp system caused the membrane to stretch too thin, permitting free mixing of the aqueous streams from the start of the experiment. Applying adequate compression to the block to ensure a successful seal without overstretching the membrane is the most important step of construction. Photographs of microchannel reactor assembly may be seen in Fig. 4.11-6 and Fig. 4.11-7.

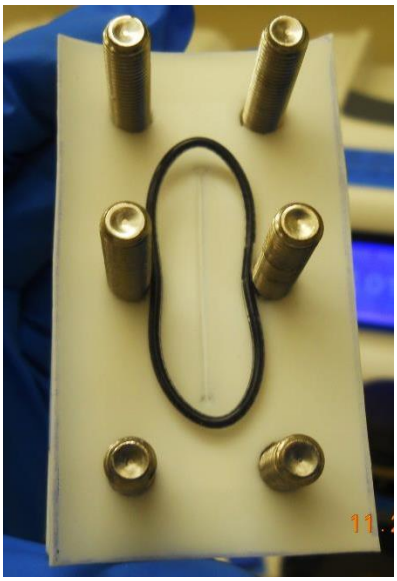

Fig. 4.11-6 Microreactor assembly (membrane in window)

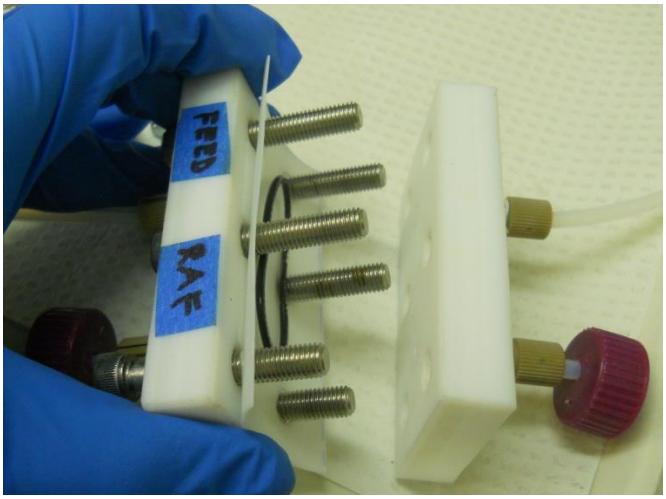

Fig. 4.11-7 Microreactor assembly (membrane not visible)

4.12 Test Loop and Assembly

4.12-1 Equipment

Two L/S Masterflex 600 RPM peristaltic pump systems were ordered from Cole-Palmer. Each independent pump system had its own L/S Standard Digital Drive, a L/S Rigid PTFE-tubing pump head, and a bowed 4mm OD rigid PFTE tube to run through the peristaltic pump. The high-precision peristaltic pumps are capable of delivering very low volumetric flow rates (0.005 to 17 mL/min). The PFTE tubing and pump head were selected in part due to the chemical resistance of the material since both concentrated HCL and MIBK are reactive agents. The two pumps operated independently to avoid cross-talk or feedback between the channels.

4.12-2 Test Loop Assembly

The test loop is shown in Fig. 4.12-1 consists of the reactor, two pumps, several lines of PTFE tubing, two bottles acting as fluid reservoirs, and two centrifuge vials. One pump was plumbed to the inlet of the IDEX port for the microreactor feed channel. The other pump was

plumbed to the inlet of the strip channel. The two inlets were staggered on opposite ends of the reactor, to create a counter-flow pattern of flow inside the device. The microreactor was set on side for all experiments, as shown in the photographs, to prevent buoyancy from displacing the extractant phase with fluid from either aqueous stream as was reported by Molinari et al. [12]. Small LDPE bottles with 4 mm OD holes punched in the caps (for PTFE tubing) acted as reservoirs for the feed and strip solutions in line with the pumps. The caps were left in place on the PTFE tubing between experiments. Clean centrifuge tubes with 4mm OD holes punched in the caps were placed on the PTFE tubing to capture raffinate and strip from the IDEX ports at the reactor channel exits. As samples were collected, the centrifuge vials were simultaneously removed from the exit lines, capped with new caps, and replaced with clean labeled vials. The vial caps with holes punched through the tops were left in place on the PTFE tubing from experiment to experiment. An additional small vent hole was drilled in the centrifuge vial cap (in addition to the hole for the PTFE tubing) to permit free flow into the sample collection vials without creating either vacuum in the device or pressure in the vial. The test loop was assembled inside a hood for experimental safety.

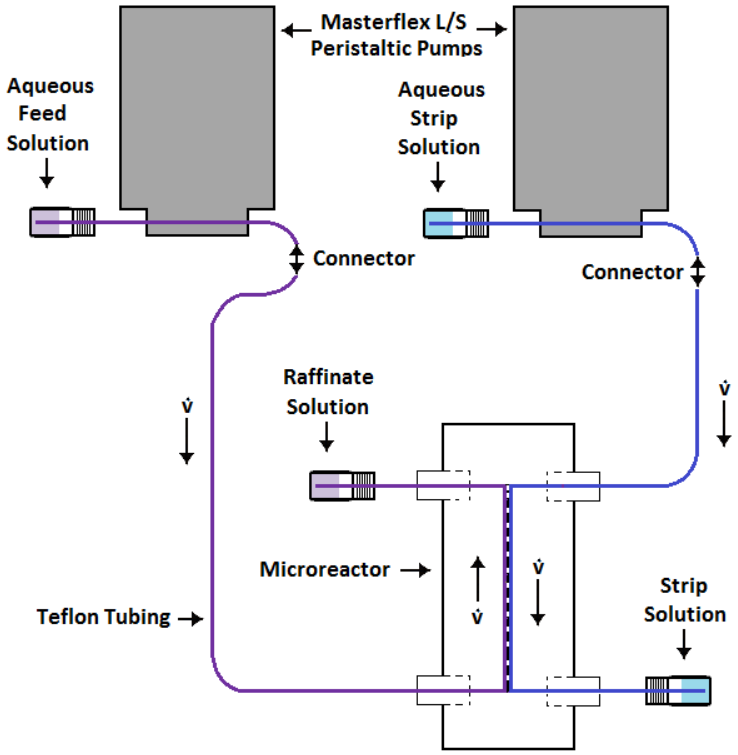

Fig. 4.12-1 Experimental test loop: measurements made are C_{STRIP}, $C_{RAFFINATE}$, and C_{FEED}

The photograph in Fig. 4.12-2 shows the experimental setup including: the two independent pumps, feed and strip reservoir bottles, Teflon tubing, labeled collection centrifuge vials, and microchannel reactor. A close up photograph of the microchannel reactor running during an experiment is shown in Fig. 4.12-3.

Fig. 4.12-2 Photo of experimental setup (first-generation)

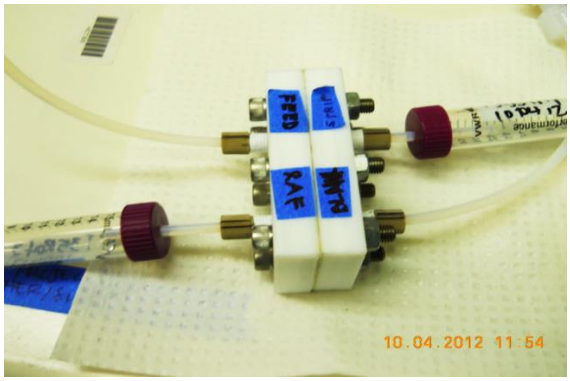

Fig. 4.12-3 Photo of microchannel reactor (first-generation)

4.13 The Microreactor Experiment

4.13-1 Overview

The strip side channel was primed with a small bolus of MIBK followed by a continuous stream of strip solution. The feed side channel was primed just behind the MIBK, at the same time as the strip channel was filled with a continuous stream of certified blank solution. When feed and strip were both visible at the outlet of the IDEX exit ports, a stopwatch was started, to count down the estimated time for the system to reach a steady state flow condition. The time needed to reach steady state depends on the channel volume (straight versus serpentine) and the experimental flow rate. A steady state flow condition was confirmed by measuring the concentration of Te and Cd on the ICP. Early concentration measurements on the ICP also gave an indication if the membrane was intact and the channel was effectively sealed. If ICP concentration measurements of exiting raffinate and strip solution ever showed free circulation of Cd in the strip stream, as indicated by 20%-60% Cd contamination, the experiment was stopped. Occasionally, tightening the bolts on the reactor a bit more could correct this

problem. However, generally in this event experiments were delayed due to a microchannel reactor seal failure, and the device had to be reassembled with a newly cut membrane.

4.13-2 Priming the Microreactor for Experiments

Because MIBK evaporates quickly in open air, MIBK was pumped through the tightly closed microchannel reactor after assembly of the device (immediately prior to each experiment). This process saturates the pores of the membrane with MIBK to create the needed SLM. A few milliliters of MIBK were placed in a small clean LDPE bottle. The bottle was screwed into the cap on the strip line pump where a small amount of MIBK was aspired into the Teflon line: the volume of MIBK pumped through the microreactor was 0.25 ml and 1 ml, for the straight channel and serpentine channel, respectively. In early experiments, a 1 ml bubble was aspirated into the line behind the MIBK, but later it was decided that it was better not to aspirate a bubble as this probably contributed to bubble accumulation in the device. The MIBK bottle was removed from the strip pump line and replaced with a clean LDPE bottle of certified blank 2% hydrochloric acid solution. The MIBK bolus was moved through the lines at a flow rate of 0.5 ml/min-1.0 ml/min until the bolus came close to entering the channel (as observed by eyesight through the clear tubing). At this point, to avoid damaging the membrane, the flow was slowed down to a very low flow rate. In the straight channel, the flow rate was set to 0.03 ml/min, and it was roughly 31 minutes later that the first drips of MIBK began to fall into the sample collection vial at the strip channel exit. For the serpentine channel, set at the flow rate of 0.1 ml/min, it was roughly 9 minutes later that the first drips of MIBK began to fall into the sample collection vial at the strip channel exit. Excess MIBK was purged from the device by

filling the strip channel with blank solution (moving into the channel right behind the MIBK). It is estimated that only a few drops of MIBK were retained by the membrane in the SLM. The first drips of MIBK at the exits were indication that the strip channel was full of fluid, and at this time the feed line flow was initiated at a rate of 0.03 ml/min. When it was observed that both the exits of the channel were dripping fluid into the collection vials, the channels were considered primed, and both pumps were reset to the desired flow rate for the experiment.

Bubbles were dislodged during priming by gentle tapping of the reactor or sometimes turning the device on end (to encourage the air to rise through the channel ahead of the liquid). At times, turning the device on end increased pressure at one of the ports, causing a drop to drip around the inlet or exit port. These were remediated by rewrapping the port or plug with Teflon tape. Sometimes the bolts on the device were tightened a bit more, to ensure sealing, or dislodge bubbles. A stopwatch was started to measure time.

4.13-3 Collection of Aqueous Samples from Outlet Ports

About 30 minutes after both exits exhibited a drip, new centrifuge vials were placed at both the raffinate and feed lines. Liquid samples were collected from the microchannel outlets in new labeled weighed centrifuge vials. As soon as enough fluid accumulated in the new vials to sample, the non-steady state strip solution was tested for Te and Cd concentration on the ICP. The time staggered between samples at or near steady state depended on the flow rate. There had to be enough fluid volume collected at the bottom of the vial to reliably pipette a measured amount of raffinate/strip (roughly 0.5 ml). At the lowest flow rate, samples were staggered further apart, as it took longer to collect the needed volume. After removal from the

outlet, these liquid samples were weighed and stored in a hood. While waiting for test vials to fill in experimental down time, collected test solutions were prepared at several dilutions for analysis on the inductively-coupled plasma mass spectrometer (ICP) instrument. High Cd contamination in the strip solution gave cause to tighten the block a bit more before testing a strip on the ICP again, to see if a better seal was achieved. A failed seal might exhibit a strip Cd contamination approaching 50% due to free mixing between the feed and strip steams. A successful seal is demonstrated by strip stream Cd contamination of less than 5 ppm in the straight channel and 16 ppm in the serpentine channel. If initial checks on the ICP indicate a successful seal and there were no visible leaks, the experiment proceeded as planned. The vials were stored upright and capped in the hood until such time it was deemed appropriate to discard them as waste.

4.13-4 Leak Mitigation

Leaks around the compressible seal were reasonably well-managed through careful attention to the torque applied to the bolts during tightening, and the use of IDEX ports. Teflon tape was applied to the treads of the IDEX ports or wrapped around the Delrin plugs to achieve a seal if drips arose. If a leak persisted beyond remedy, the experiment was aborted.

4.13-5 Steady State Experimental Test Condition

The time required to reach steady state is variable and dependent upon the channel volume and volumetric flow rate chosen for the experiment. It might take anywhere from 40 minutes to 120 minutes or longer to reach steady state test conditions in the microreactor. As

the experiment proceeded, clean labeled collection vials were placed at both the raffinate and strip exits. After 0.5 ml – 2 ml of fluid accumulated in the vials, they were replaced. Steady state was confirmed by two consecutive concentration measurements on the ICP spaced anywhere from 20-30 minutes apart without much change in Te concentration (the slope of the curve of Te concentration vs. time approached zero). Experiments that did not reach the steady state condition with an intact seal are not reported. Generally it was only possible to do one flow condition per day. However, in the rare event that several steady state measurements were successfully recorded at the first desired experimental test condition, the experimental flow rate might be adjusted to a new flow rate, in an attempt to record another data point. However, usually the second experiment for the same reactor assembly did not work out presumably because the membrane buckled under continuous flow of the acidic feed. Typically experiments did not endure for more than 5 hours before Cd concentration in the strip stream began to increase dramatically in tandem with the Te concentration. At this point, the experiment would be discontinued and the Teflon lines/channels were flushed with distilled water.

4.13-6 Experiment Breakdown and Fault Analysis

The microreactor is disassembled, and a diagnosis for failure was determined if possible. Indications of membrane stress in the form of ripples are sometimes seen around the outline of the feed plenum at the inlet ports. The membrane soaked in MIBK is clear because the pores are wetted (as compared to the dry white membrane). After the device is broken down, the clear MIBK soaked membrane in the best sealing tests did not extend beyond the ring of the

seal. This scenario is demonstrated by a picture taken at the end of an experiment as in Fig. 4.13-1. The membrane is clear on the inside of the seal imprint where it was primed with MIBK and white on the outside of the seal where MIBK was not allowed to wick. At top of Fig. 4.13-1, there is some visible rippling of the membrane around the plenum on the feed inlet (left side).

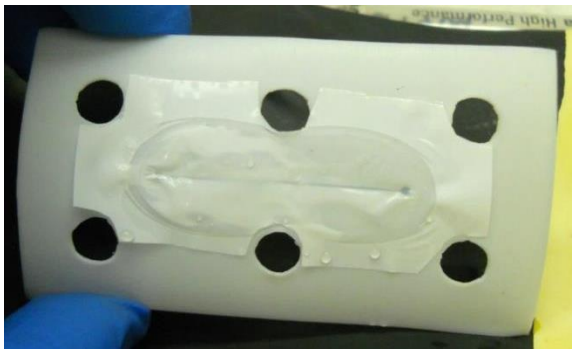

Fig. 4.13-1 Photograph of membrane after an experiment

CHAPTER 5 – DATA AND DATA PROCESSING

5.1 Raw Data Measurements

As discussed in the previous chapter, raw data from all experiments was collected in terms of ICP intensity and converted to concentration via regression analysis for each procedure in Appendix G. The concentration of analyte (both Cd and Te) in the aqueous phases was measured before the experiment and after the experiment. The initial concentration of the strip solution is always zero as it was a certified blank solution for the ICP tested by the manufacturer High Purity Standards. The other three measurements were made on the ICP and are designated as follows: C_{FEED} is the initial (or inlet) concentration of the feed solution; $C_{RAFFINATE}$ is the final (or outlet) concentration of the feed solution or raffinate; and C_{STRIP} is the final (or exit) concentration of the strip solution. The initial (or inlet) concentration of the strip solution is zero because it is a 'blank' solution. The organic phase concentration of analyte was not measured because metals are usually run through the ICP in an acid matrix.

5.2 Separation Funnel Extraction and Recovery Calculations

In the separation funnel, measured concentration data for the individual analyte of interest is used to calculate the fraction (or percentage) of the metal extracted from the feed into the organic phase. Based only on the feed solution and denoted by E, this fraction is calculated as,

$$E\ \% = \frac{C_{FEED} - C_{RAFFINATE}}{C_{FEED}} \cdot 100 \tag{5.1}$$

where C_{FEED} represents the initial (or inlet) analyte concentration in the feed phase and $C_{RAFFINATE}$is the final (or exit) analyte concentration in the feed phase.

The total recovery fraction (or percentage) of the combined extraction and back-extraction processes deals with the ratio of the quantity of the analyte in the final (or exit) strip solution to the quantity in the initial (or inlet) feed solution. The recovery or R, is

$$R\ \% = \frac{C_{STRIP} \cdot V_{STRIP}}{C_{FEED} \cdot V_{FEED}} \cdot 100 \tag{5.2}$$

where C_{STRIP} represents the final (or exit) analyte concentration in the strip phase and C_{FEED} represents the initial (or inlet) analyte concentration of the feed phase. V_{STRIP} and V_{FEED} denoting the volume (or volume flow rate) of the strip and feed solutions respectively.

If there were two strip stages, as observed in a few separation funnel experiments, the following expression displaces of Eq. (5.2),

$$R\ \% = \frac{(C_{STRIP_1} + C_{STRIP_2}) \cdot V_{STRIP}}{C_{FEED} \cdot V_{FEED}} \cdot 100 \tag{5.3}$$

where C_{STRIP_1} represents the final analyte concentration in the strip phase stage one and C_{STRIP_2} represents the final analyte concentration of the strip phase stage two.

5.3 Separation Funnel Distribution Ratio Calculation

The distribution law applies to a system of two immiscible liquid layers – one being aqueous and the other being organic – containing a third dilute substance that is soluble in both liquids. In this case, it is appropriate to conclude that the distribution of the dissolved substance Te maintains a constant concentration ratio, at a constant temperature. Both the extraction and the back-extraction steps have a constant distribution ratio; however, it is the

extraction that is of primary interest. Neglecting small residuals left on the glassware, it is possible to use conservation of mass, in conjunction with the known phase volumes, to calculate the distribution ratio between the aqueous feed and the organic phase according to the following expression,

$$M = \frac{C_{ORGANIC\ PHASE}}{C_{AQUEOUS\ FEED}} = \frac{\left[(C_{FEED} - C_{RAFFINATE}) \cdot \frac{V_{FEED}}{V_{ORGANIC\ PHASE}}\right]}{C_{RAFFINATE}} \tag{5.4}$$

where M is called the distribution ratio between the phases for the extraction only, V_{FEED} is the feed volume, $V_{ORGANIC\ PHASE}$ is the volume of the organic phase, and the other variables remain unchanged from those in the proceeding section. The concept of distribution ratio also holds in the microreactor.

5.4 Separation Funnel Experimental Data

A summary of the separation funnel experimental work is presented in Appendix K. Data are listed in Table K-1 and calculations are given in Table K-2.

5.5 Microreactor Steady State Averaging of Data Points

Reported data are for microreactor experiments at steady state. The steady state condition is confirmed by reviewing the recorded microreactor data. Each data point in an experiment is compared with the previous data points to determine if the reactor is approaching steady state operating conditions. When the data taken at regular time intervals stopped changing dramatically over time, it was determined the data was approaching steady state, and more frequent data points were taken, until the seal or the membrane on the reactor

failed, at which point the experiment is aborted. If the seal held up beyond establishment of the steady state condition, the steady state data points are averaged together at the conclusion of the experiment. If the data points taken after it appeared that the seal or membrane was into a failure mode, they were not included in the average. Sometimes there was only one steady state data point for an experiment but generally there were several data points to carry out the averaging, especially in the longer reactor.

5.6 Microreactor Recovery Efficiency Calculation

For microreactor experiments, concentration data measurements are used to calculate recovery (R) for the extraction and back-extraction coupled together. The experimental flow rates for the feed and strip channels were always equal, and so volume cancels out of Eq. 5.1 above to yield the following expression,

$$R\ \% = \frac{C_{STRIP}}{C_{FEED}} \cdot 100 \tag{5.5}$$

where C_{FEED} represents the initial (or inlet) concentration of the analyte in the aqueous feed phase and C_{STRIP} represents the final (or exit) concentration of the analyte in the aqueous strip phase.

5.7 Microreactor Residence Time Calculation

Residence time in the microchannel was determined by the equation:

$$t = \frac{V}{\dot{v}} = \frac{a^2 L}{\dot{v}} \tag{5.6}$$

where V is the volume of the fluid in the feed channel (with mass transfer contact area) and $\dot{v}$ is the volumetric flow rate of the feed solution. The channel volume is simply width, a, times height, a, times length, L. Estimated channel dimensions are based on drawings (and did not account for dead space due to gasket compression or other factors that might cause small variations in channel volume between experiments).

5.8 Microreactor Experimental Data and Calculations

A summary of the microreactor experimental data and calculations is found in Table 5.8-1. Raffinate data are not included in the table because raffinate concentration measurements are used only to confirm the mass of metals in the reactor is conserved within error.

Table 5.8-1 Microreactor Experimental Data and Calculations with Error

	Test Variables			Resid-	Cadmium Data				Tellurium Data				Recovery Calculation			
2012 Test Date	Feed Sol'n Cd+Te ppm	L cm	Flow Rate ml/min	ence Time t s	Strip Cd ppm	Error Strip Cd ppm	Feed Cd ppm	Error Feed Cd ppm	Strip Te ppm	Error Strip Te ppm	Feed Te ppm	Error Feed Te ppm	R% Cd %	Error R% Cd %	R% Te %	Error R% Te %
10/16	2154	3.7	0.01	56	4.3	0.10	1006	21.3	74.5	1.9	1150	29.1	0.4	0.013	6.5	0.2
10/19	2154	3.7	0.01	56	1.9	0.10	980	24.0	54.9	1.7	1143	37.3	0.2	0.011	4.8	0.2
10/29	2154	3.7	0.03	19	0.9	0.03	954	17.5	14.8	0.1	1150	29.9	0.1	0.004	1.3	0.0
11/20	2154	3.7	0.02	28	1.5	0.04	1143	25.1	25.1	0.6	1244	37.0	0.1	0.005	2.0	0.1
11/26	4308	3.7	0.02	28	1.4	0.03	1753	34.7	24.2	0.7	2353	58.2	0.1	0.002	1.0	0.0
11/27	4308	3.7	0.02	28	1.4	0.04	1871	38.7	25.8	1.0	2154	58.9	0.1	0.003	1.2	0.1
11/28	4308	3.7	0.01	56	4.7	0.01	1871	41.6	109.6	3.0	2148	59.5	0.3	0.006	5.1	0.2
11/30	4308	3.7	0.03	19	1.0	0.03	1902	49.7	23.1	0.9	2234	66.5	0.1	0.002	1.0	0.1
12/5	4308	3.7	0.02	28	1.2	0.03	1924	38.7	25.1	0.9	2326	59.3	0.1	0.002	1.1	0.0
12/5	4308	3.7	0.01	56	2.7	0.10	1924	38.7	71.7	2.0	2326	59.3	0.1	0.006	3.1	0.1
12/7	4308	3.7	0.02	28	1.1	0.03	1910	44.1	23.2	0.9	2252	64.9	0.1	0.002	1.0	0.0
12/12	2154	12.9	0.01	174	9.7	0.20	966	20.8	310.2	6.2	1159	27.3	1.0	0.030	26.8	0.8
12/17	2154	12.9	0.02	87	7.0	0.20	962	23.8	201.2	5.7	1113	34.5	0.7	0.028	18.1	0.8
12/20	2154	12.9	0.01	174	5.8	0.20	992	19.8	206.8	5.4	1150	31.3	0.6	0.023	18.0	0.7
12/21	2154	12.9	0.03	58	14.1	0.30	989	21.8	156.1	3.9	1133	29.6	1.4	0.044	13.8	0.5
12/28	2154	12.9	0.03	58	8.4	0.30	993	16.7	162.6	4.1	1122	26.1	0.8	0.033	14.5	0.5

CHAPTER 6 – RESULTS AND DISCUSSION

6.1 Separation Funnel Results with Kerosene

The concentration of the extractant(s) is reported to sometimes enhance and sometimes be detrimental to performance. Mixing increasing volumes of CCl_4 with MIBK decreases the distribution ratio of MIBK [39]. The same result is found to be the case here for extraction of Te with MIBK mixed with various proportions of kerosene, as is demonstrated by results presented in Fig. 6.1-1. The best extractant concentration tested is 100% MIBK. Increasing concentrations of kerosene cause an inverse result in the distribution ratio. And so, the findings of Chakraborty and Datta [49] extracting Te(IV) in a batch reactor with di-(2 ethyl hexyl) phosphoric acid (D2EHPA) using kerosene as a diluent for the carrier to stabilize the emulsion do not carry over to MIBK. Kerosene is not a good choice of diluent for the extractant MIBK. The extractant MIBK did not need this diluent to stabilize emulsion in the separation funnel, and indeed the concept of transferring this aspect of chemistry from the batch reactor to separation funnel may have been flawed. In the separation funnel, it was found that kerosene inhibited the uptake of Te^{4+} by MIBK to a large degree. This suggests that there is likely a strong interaction between the extractant MIBK and kerosene, effectively reducing the MIBK available to complex with Te^{4+}.

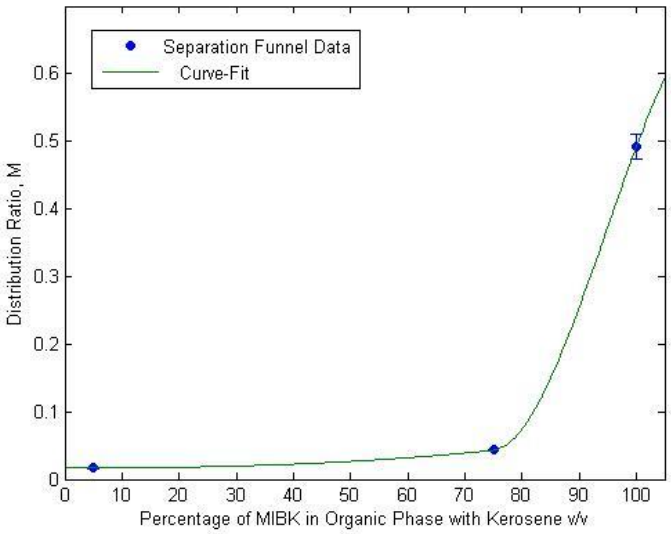

Fig. 6.1-1 The distribution ratio for Te increases with increasing volume of MIBK in the organic phase. [Organic phase is a mixture of MIBK and Kerosene of 10 ml volume. Aqueous phase is 6M HCl of 10 ml volume.]

6.2 Separation Funnel Results for Contact Time

A plot of the distribution constant M as a function of time is found in Fig. 6.2-1. The distribution ratio of Te extracted is not improved much by extended contact time. The extraction in separation funnel reaches equilibrium in 10 minutes. This is consistent with the results of extraction (of Te with MIBK in HCl) published by Havezov & Jordanov [39], who report that contact time between the phases for their experiments is less than 5 minutes. It is also interesting that Hayashi et al. [36] published a plot showing extended extraction time did not improve the mass of Te extracted from 6N HCl with MIBK . The lowest contact time tested, ten minutes split evenly between shaking and resting, is sufficient phase contact time in a separation funnel.

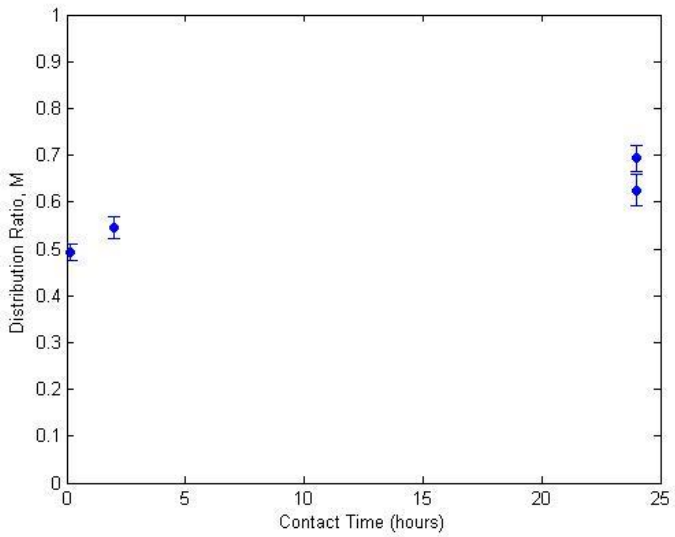

Fig. 6.2-1 The distribution ratio of Te is not significantly impacted by contact time in separation funnel. [Organic phase is 10 ml of 100% MIBK. Aqueous phase is 10 ml of 6M HCl].

6.3 Separation Funnel Results for Varied Volumes of MIBK

The distribution ratio of Te is dependent upon the ratio of organic phase to aqueous phase, as it evident in Fig. 6.3-1. A high distribution ratio, like 99, indicates that the analyte will proportion 99 parts in the membrane while leaving 1 part in the feed. The low distribution ratios found here, ranging from 0.5-4, are out of line with those in publication [50] [51] [36]. A 6M HCl feed solution should be expected to yield a very high fraction of Te to 100% MIBK, with only one or two extractions of a 1:1 ratio of organic phase to aqueous phase. Havezov & Jordanov [39] report the distribution ratio for the equilibrium of Te^{4+} between MIBK and 3-6M HCl is as shown below in Table 6.3-1. Their results indicate that for a 6M HCl extraction one would expect a distribution ratio of 20 at 23 ˚C. A previous publication by Jordanov & Havezov [50] found the distribution ratio for Te^{4+} extracted with MIBK in 4 M HCl to be 81 (for a 10 ppm

concentration of Te). The distribution ratio of Te in the experiments presented here is being suppressed by an unknown factor.

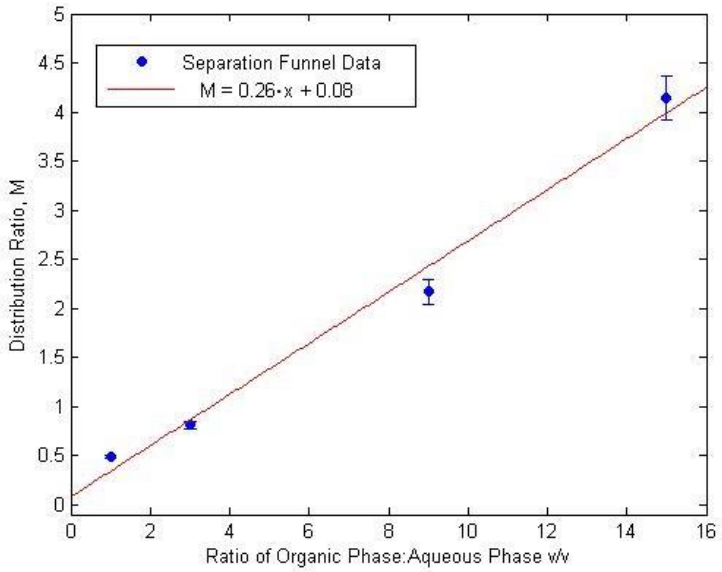

Fig. 6.3-1 The distribution ratio of Te as function of the ratio of organic phase volume to aqueous phase volume. [Organic phase is 100% MIBK. Aqueous phase is 6M HCl.]

Table 6.3-1 Distribution Ratio for Te^{4+} in HCl [39]

	Extractant MIBK			
HCl Molarity (M)	3	4	5	6
Distribution Ratio Te*	3.1	23	25	20
*For Te^{4+} starting concentration of $1X10^{-2}$ M (1276 ppm)				

The cause of the low distribution ratio needs to be investigated with further experiments in the separation funnel. It could be an unanticipated reaction decreased the acidity of the feed solution outside the targeted window (4-6M HCl) pushing the equilibrium species away from the extractible tetrachloro Te complex. The distribution ratio increases inversely with temperature [39]. This is probably because the extraction mechanism of solvation is more

likely to occur in a cold fluid. However, it's not likely that temperature is suppressing the distribution ratio because the experiments were carried out at a lower temperature than that for the reported higher distribution ratios. The distribution ratio of Te is known to be dependent upon the concentrations of Te, HCl, Cl^-, H^+, H_2O, and MIBK [51] [39]. The Te concentration tested here is very close to that prepared for derivation of Table 6.3-1, eliminating Te as a culprit.

Other ions, such as indium have been reported to suppress the uptake of Te by MIBK [52]. It is possible that the concentration of Cd^{2+} ions may suppresses the distribution ratio by competing for Cl^- or H^+ or water, shifting equilibrium of Te^{4+} away from the extractable tetrachloro species. Excess hydrogen peroxide may be impeding formation of the water solvation ring in the feed. All the MIBK came from a single container, and it is possible it was contaminated, or of a less than ideal grade.

The distribution ratio for extraction of Te in HCl using the extractant MIBK ranges from 0.02 (reported here in Fig. 6.1-1 and Appendix K) to 81 as reported by Jordanov & Havezov [50]. The distribution ratio varies over several orders of magnitude due to known dependencies upon seven or more variables that may interact in a complex system. It is not clear what mechanism suppressed the distribution ratio of Te in MIBK. These interactions are not the focus of the present study but could be addressed in subsequent works.

However disappointing the distribution ratio results are, there is more to be learned from reviewing at the efficiencies in Fig. 6.3-2. The extraction reaches 98% at a ratio of 15. This indicates that around 98% of the tellurium in the feed solution is of the correct oxidation state

(IV) to be extracted; this is good news for an experimental feed. The increase in extraction efficiency with increasingly large volumes of MIBK may belie the most likely cause of the suppression of the distribution ratio. Excess hydrogen peroxide or another polar substance may be impeding formation of the MIBK solvation ring via polar interaction or reaction, effectively decreasing the concentration of MIBK available to complex with Te. The total recovery of Te using 2% HCl appears satisfactory.

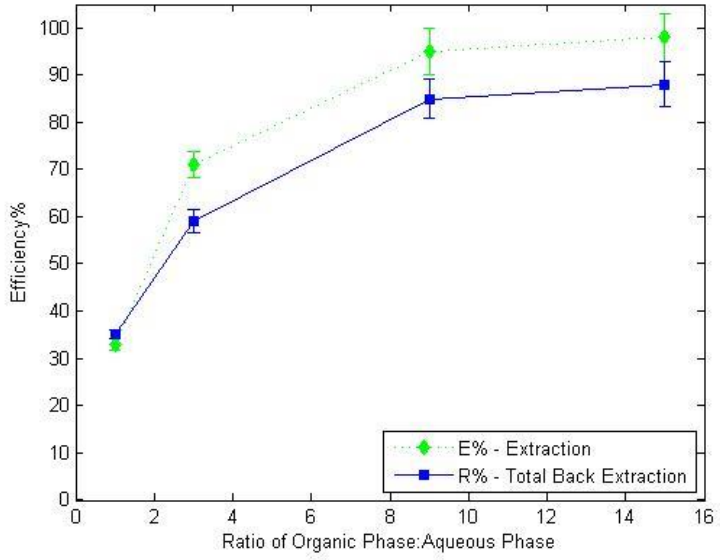

Fig. 6.3-2 The efficiency of Te extraction in microchannel is seen to be a function of the ratio of organic phase to aqueous feed phase. [Organic phase is 100% MIBK. Aqueous feed phase is 6M HCl. Aqueous strip phase is 2% HCl. Volumes of feed, extractant, and strip solution varied.]

6.4 Preliminary Microreactor Results in Straight Channel

6.4-1 Stainless Steel Channel

A few attempted experiments in the stainless steel block failed because the steel was reactive with the tellurium in the acid feed solution. The raffinate was greenish yellow with bubbles and the feed channel outlet shed some black sediment into the raffinate, all harbingers

of an uncontrolled reaction. The raffinate solution lost more than half of the Te in the microchannel and it did not show up in the strip solution. Plugs of sediment precipitated out of solution that periodically exited the reactor outlet. Upon examination of samples by the ICP, it was found that the mass balance for Te in solution did not match up with the difference between the feed and the raffinate; Te was “lost” during experiments!

A sample of the powder collected out of the feed manifold exit line (which comes into contact with the SS316) was placed in the bottom of a centrifuge vial to which 1 ml of 6M HCl was added. The powder did not dissolve within 24 hours. In order to dissolve the powder, hydrogen peroxide was periodically added in 15-30 microliter increments as long as black sediment appears to be still in the vial. The material dissolved into a slightly yellow solution. Testing on the ICP indicated that the sludge contained a Te concentration of 1480 ± 39 ppm without significant Cd. This is evidence that the "lost" Te in the stainless steel device was indeed coming out of solution into a solid precipitate. Stainless steel is not compatible with the feed solution used in experiments.

6.4-2 Teflon Channel

The mass balance is found to be satisfied (within experimental error bounds) in the Teflon reactor experiments, thus indicating that the feed solution is stable in Teflon material. An example of typical mass balance results, indicating overall conservation of Te and Cd is shown in Table 6.4-1. The Cd and Te entering the reactor in the feed match within ± 1% the sum of the same metals (raffinate concentration plus strip concentration) in the solutions exiting the reactor. Note that the extraction of Te in this early test is less than the extraction of Cd, most

probably due to either failure to seal the streams from each other properly or to a ruptured membrane.

Table 6.4-1 Results in Teflon Indicate Conservation of Mass

	Concentration			
	ICP		Total	
Results for 10/04/2012	Cd (ppm)	Te (ppm)	Cd %	Te %
Test 35: Microchip Counter Flow Control 0.1 ml/min				
T35F(Feed2200-6M HCl 12.5ml-270 µl 15% H2O2)-333x	911	1109	100%	100%
T35R1 (Raffinate 100%MIBK Microchip) - 333x	827	1012	91%	91%
T35Strip1 (2% HCl Matrix Microchip)-50x	64	57	7%	5%
T35R2 (Raffinate 100%MIBK Microchip) - 333x	853	1040	94%	94%
T35Strip2 (2% HCl Matrix Microchip)-50x	57	45	6%	4%
T35R3 (Raffinate 100%MIBK Microchip) - 333x	868	1070	95%	97%
T35Strip3 (2% HCl Matrix Microchip)-50x	83	76	9%	7%
Raffinate Average	850	1041	93%	94%
Strip Average	68	60	7%	5%
Sum of Average Strip+Raffinate (for mass balance)	918	1100	101%	99%

Further Experiments in Teflon include a control test where the membrane did not contain the extractant, a two phases test (feed/MIBK), and three phase experiments in two reactor channel configurations – the short straight channel and the long serpentine channel. Results from these experiments are discussed below.

6.4-3 Control Experiment

A control test was run in the Teflon microchannel device in which the membrane lacked the critical extractant MIBK. The test results on 10/15/2012; at a flow rate of 0.02 ml/min, less than 1 ppm (0.01%) Te was found in the strip solution with less than 1 ppm (0.9%) Cd. The

control test proved several critical concepts as outlined below:

(a) The device as designed can seal internally and withstand the 6M acid stream;

(b) The extractant-free membrane does not permit free diffusion of either Cd or Te between the two aqueous streams; and

(c) The measured concentration of metal entering the microreactor reconciled quite well with the measured concentration of metal ions exiting the device. This demonstrated that the new Teflon reactor does not have an uncontrolled reaction with tellurium or cadmium metal ions in solution. Mass is conserved in the reactor.

6.4-4 Two Phase Extraction

A preliminary two phase experiment in the Teflon microchannel demonstrated that tellurium does indeed pass selectively through the membrane from the aqueous feed solution into an organic stream of MIBK. Plans for three phase experiments could quite plausibly work. Experimental results obtained on 10/05/2012 indicate that at a flow rate of 0.03 ml/min for both an aqueous and organic streams divided by the hydrophobic membrane, roughly 7% of the Te (81 ± 3.1 ppm) was extracted in the organic stream with 1% of the Cd (11 ± 0.3 ppm).

6.4-5 Stagnation Test

An attempted 19 hour stagnation test in straight channel is inconclusive due to internal failure to separate the streams over the extended period of stagnation. The test on 11/28/2012 did not show signs of external leaking.

6.5 Three Phase Extraction in Straight Channel

The chemistry was tested in a 3.7 cm long straight microchannel with a SLM soaked in MIBK for a small array of flow rates (0.01, 0.02, and 0.03 ml/min) with two inlet concentrations of feed solutions. The two metal feed solutions tested are a 2154 ppm feed (1009 ppm Cd + 1145 ppm Te) and a 4308 ppm feed (2018 ppm Cd + 2290 ppm Te). The results in Fig. 6.5-1 and Fig. 6.5-2 demonstrate clearly that the physics seen on the bench applies to a microchannel. The results are also consistent with the boundary layer model, as presented in Section 3.5, albeit with a low (M) distribution ratio, M ≈ 0.006. However, it is not surprising that the effective distribution ratio in the membrane is lower than found in the separation funnel, as the porosity of the membrane effectively reduces the volume of MIBK available to extract Te. The consistently very low level of Cd in the strip solution in both of these figures verifies that the membrane is, as designed, serving as an effective barrier to cadmium transport.

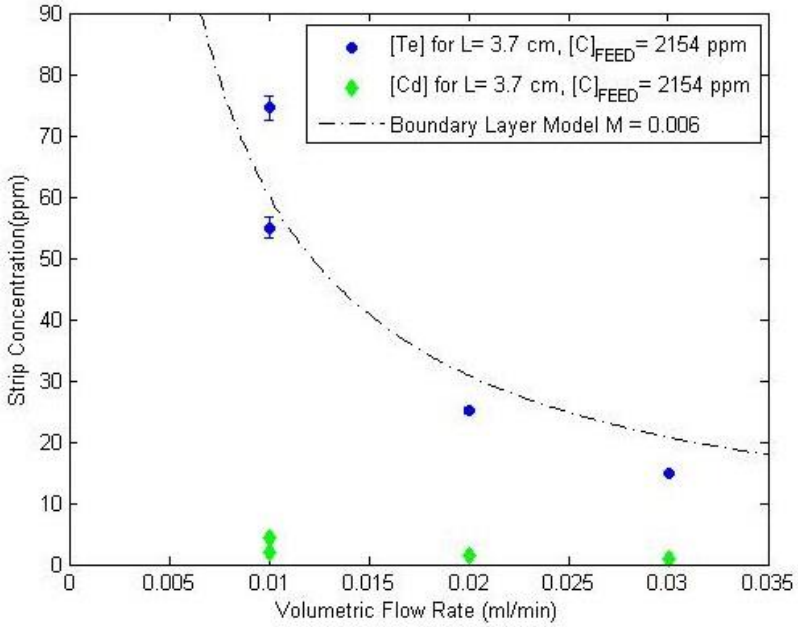

Fig. 6.5-1 Strip concentration at outlet of straight channel with 2154 ppm feed.

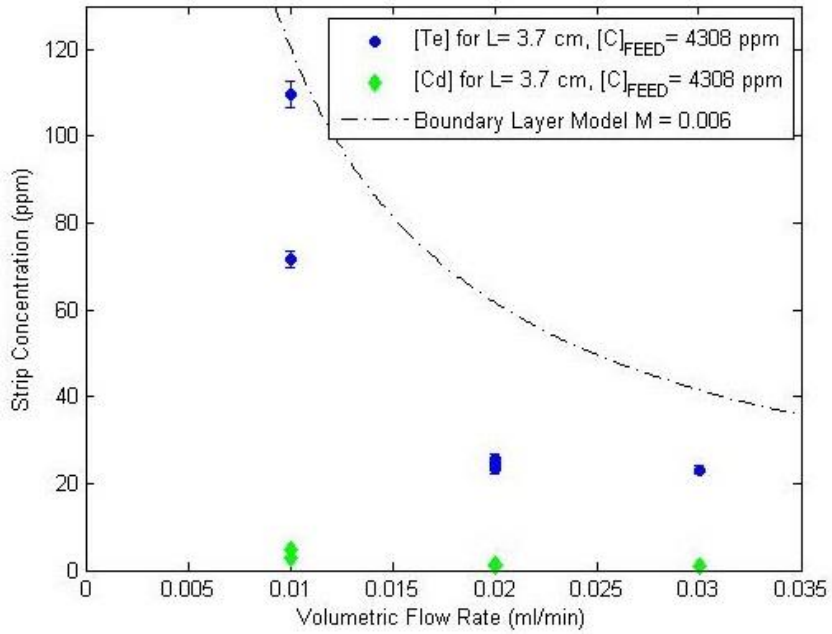

Fig. 6.5-2 Strip concentration at outlet of straight channel with 4308 ppm feed.

6.6 Three Phase Extraction in Serpentine Channel

The chemistry was also tested in a serpentine microchannel 12.9 cm long with a SLM soaked in MIBK for the same array of flow rates (0.01, 0.02, and 0.03 ml/min) with the 2154 ppm inlet metal feed solution (1009 ppm Cd + 1145 ppm Te). The results of tests in the serpentine channel are presented in Fig. 6.6-1. The longer serpentine channel reactor yields roughly 3.5 times the contact area of the straight channel. As predicted by the model, the concentration of Te in the strip solution increases significantly with the increased contact area over all the tested flow rates.

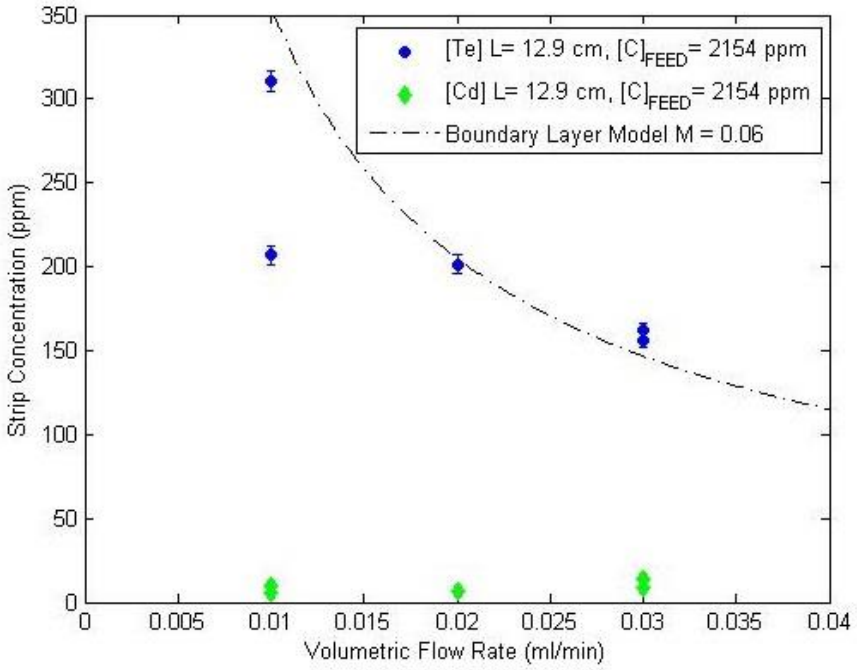

Fig. 6.6-1 Strip concentration at outlet of serpentine channel.

6.7 Modeling of Recovery in Microreactor

In the straight channel, the recovery of Te ranged from 1.3% to 6.5% for experiments using 2154 ppm feed. The extraction efficiencies of experiments using the more concentrated 4308 ppm feed solution were only slightly lower, ranging from 1.0% to 5.1%. In the serpentine channel, however, the recovery of Te ranged from 13.8% to 26.8%. Thus recovery improved nearly linearly with increased residence time in all configurations tested. These results are shown in Fig. 6.7-1. Comparison of experimental results with the boundary layer model shows that the increase in recovery of Te between the 3.7 cm reactor and the 12.9 cm reactor is equivalent to a 3X increase in the effective distribution ratio, more than would be predicted by residence time independently. It is likely that the geometry of the serpentine reactor enhanced mass transport in the longer channel by inducing small recirculating currents in the laminar

feed flow. Similar phenomena [10] [25] [24] have been reported in the study of other ion extractions.

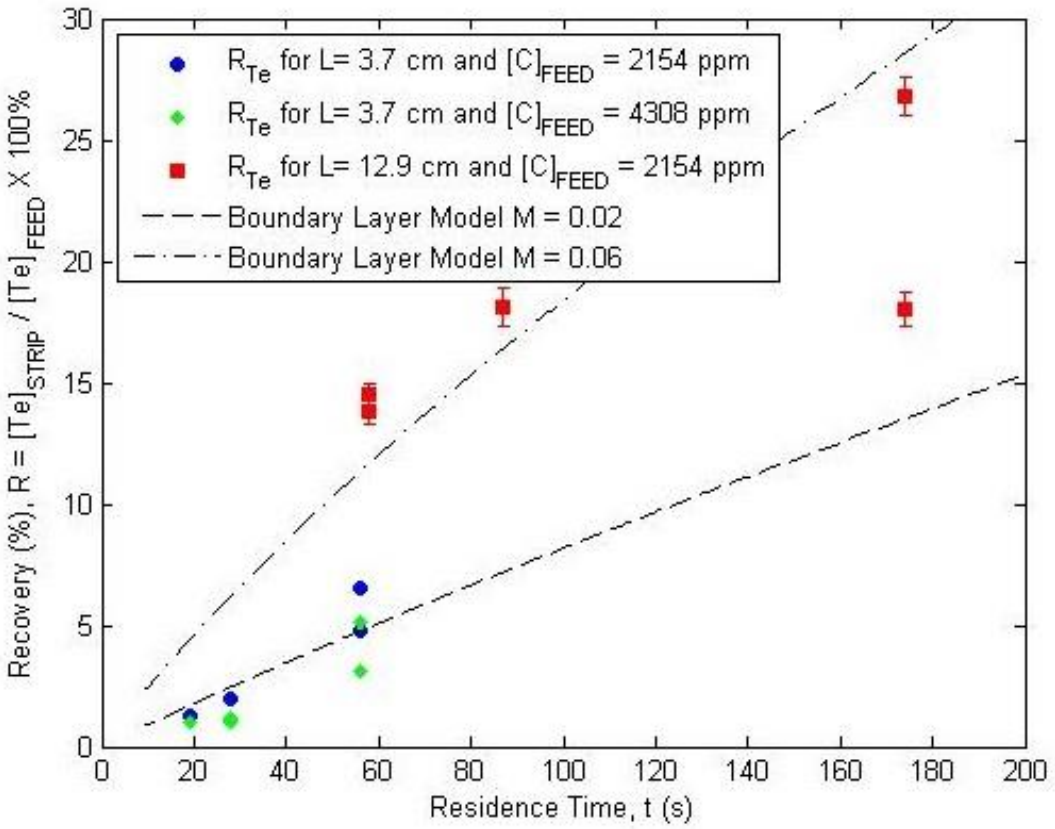

Fig. 6.7-1 Recovery of Te as a function of residence time for all reactor data.

The boundary layer model predicts that recovery is increased with longer residence time, which is effected by either a longer channel length or a smaller flow rate. Another approach to increasing recovery is to improve the chemistry. For example, in Fig. 6.7-2, the boundary layer model predicts that increasing the distribution ratio to 3 would more than double extraction at all flow rates tested.

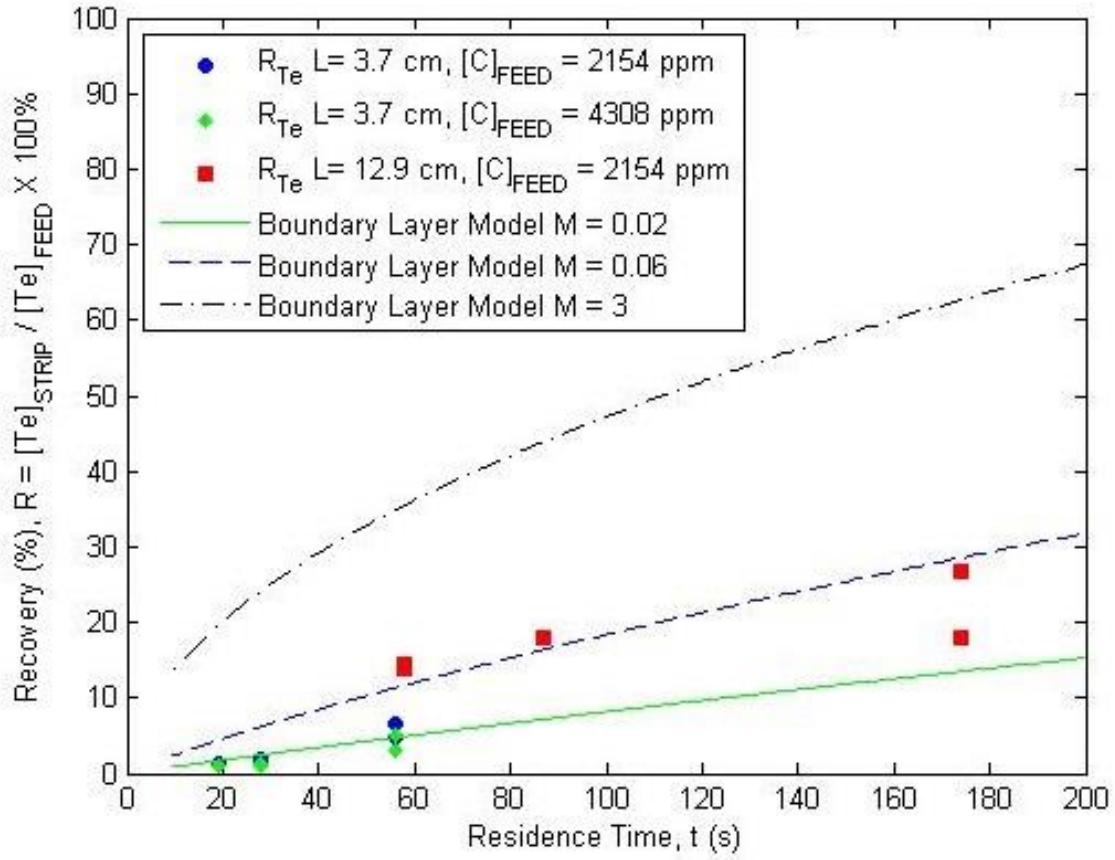

Fig. 6.7-2 Recovery of Te predicted by model for distribution ratio of 3.

The effective distribution ratio of the chemistry in the system reported here is suppressed below one, where small increases in the distribution ratio, such as an increase from 0.05 to 0.5, shift predicted extraction to 100% in half the residence time. This is evident in Fig. 6.7-3, where a new model for internal flow is introduced. The internal flow model matches well with existing boundary layer model and experimental data over the range of residence times. The difference between the two models bears out in systems with a fractional distribution ratio, where a decreasing concentration of analyte in the bulk flow may stretch the residence time required to effect 100% recovery. Additional data, at longer residence times, is required to validate the internal flow model.

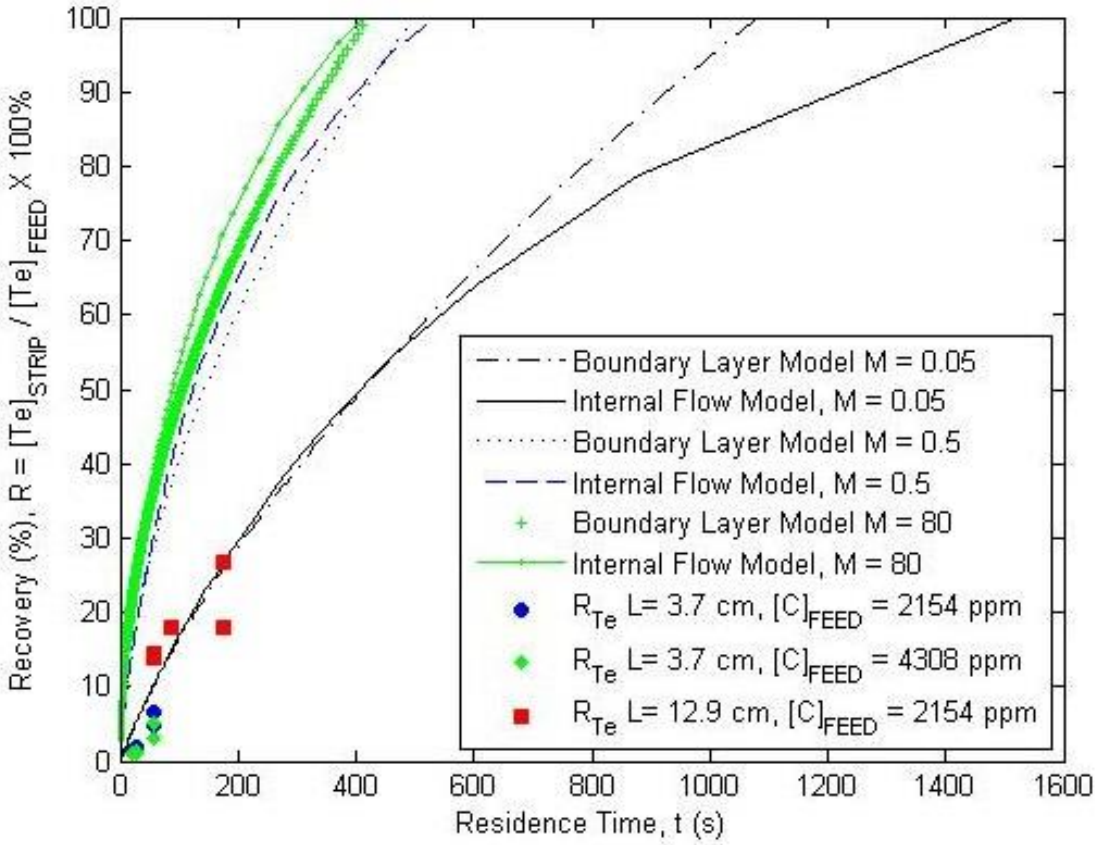

Fig. 6.7-3 Comparison of internal flow model with data and the boundary layer model

6.8 Discussion of Microreactor Results

The model and experimental data presented here for recovery of Te from a stream of CdTe are consistent with the experimental findings published in the literature on the topic of ion extraction. One device with a single serpentine 12.9 cm long channel recovered 13.8% - 26.8% of the Te over the flow rates tested. These measurements are comparable to those of Maruyama et al. [10] showing microchannel extraction ratios of yttrium ions ranging from approximately 20% to 80%, and zinc ions ranging from approximately 5%-10%.

The residence time of the feed stream in the microchannel is a predictor of the mass transferred to the SLM to the strip stream. This is demonstrated by excellent agreement

between the experimental data and model plots. A short discussion of the model may shed some light on this finding. The Peclet number is an independent parameter in these models, as shown in Eq. 3.5 to Eq. 3.7 in Section 3.7-1, per the development of Appendix D. It may useful to recall that the local Peclet number as defined at a location, x, along the lenth of the channel is,

$$Pe_L = \frac{u_o x}{D_F} \tag{6.1}$$

The Peclet number is dependent upon two time variables, the stream velocity u_o and the diffusion constant of the feed stream, D_F. Implicit in the velocity term, u_o, is a dependence on the dimension of the square channel, a, denoting both the width and thickness of the feed channel and a dependence on the flow rate, $\dot{v}$. The other time limiting step considered is diffusion through the membrane, as controlled by the membrane thickness, b, and the diffusion constant of the organic membrane D_M as seen in Eq. 3.9 of Section 3.7-2. For Te crossing the membrane, the time required for diffusion alone may be expressed in these terms as,

$$t = \frac{b^2}{D_F} \tag{6.2}$$

The time constants for chemical changes, such as the solvations and transformations, are considered to be non-rate-controlling. Agreement between the models presented and the experimental results give validation that this assumption is reasonable. Further, models with variants of feed channel resistance similar to that of the boundary layer model are published for application to microchannel extraction systems lacking a stagnant SLM [18], [53]. The model here is appropriate for systems where membrane resistance is not negligible. This may

be the case for a SLM with low porosity, substantial thickness, or for chemistry with low distribution ratios. However, the microreactor models given here are easily converted to that with a negligible membrane resistance by assuming a distribution ratio, M, of 1 or more.

The longer serpentine channel improved extraction efficiency by more than just the factor of residence time in the longer channel. The serpentine shape of the microchannel is found contribute to recovery of Te over that of a straight channel. This is consistent with other reports [10], [25], [24] of channel shape facilitating extraction in microchannel.

One explanation for the enhanced extraction observed in the serpentine channel is circulating flow. Kikutani et al. [24] report particle tracing in a microchannel of circular cross section revealed circulating flow induced by the pulling force acting at the liquid-liquid interface. The same authors postulate that the circulating flow may enhance extraction speed. The system of Kikutani et al., lacked a SLM, but this concept is likely part of the explanation for why Te extraction was increased by more than that expected on the basis of the residence time alone. The flow pattern in the serpentine channel may generate a more uniform Te concentration profile in the feed stream that facilitates extraction at the membrane surface.

In the separation funnel it was found that the distribution ratio for extraction of Te in HCl using the extractant MIBK varied over a wide range, and this is also case in the microreactor, where the effective distribution ratio for extraction ranged down as far as 0.006 for the experimental conditions tested. In addition to the variables known to play a factor in the distribution ratio in separation funnel mentioned in Section 6.3, there are additional considerations in the microreactor. A few factors that may contribute to suppression of the

distribution ratio in the microreactor are: 1) a reduced fluid-fluid contact area due to the membrane porosity; 2) a small volume of MIBK fluid (μL) captured in the pores relative to a large volume of aqueous fluid (ml) passing by in the channel flow; and 3) potential for the small volume of MIBK to be wicked away into the aqueous fluid stream. Given these considerations, it is not surprising that the effective distribution ratio found in the microreactor is lower than that found in the separation funnel.

The models show that a 100% extraction is possible if the system is designed to accommodate with a 1000 - 1500 second residence time. However, a long residence time is not all good in the interest of maintaining a selective extraction. It is desirable to maximize the distribution ratio of Te and minimize the residence time, to recover as pure as stream of Te as possible. This is because the selective extraction of Te is dependent upon a large difference in the distribution ratios between that for Te and that of Cd. A long residence time, increases the Te extracted, and also the Cd contamination (of the Te stream). The distribution ratios for Cd are reported to be quite small in Appendix K but any extraction of Cd is undesirable. This is best done by increasing the disparity between the distribution ratios of the two metals being separated thereby maintaining the shortest residence time necessary. Thus, a higher distribution ratio of Te, as compared to that of Cd, would improve the purity of the Te stream extracted.

CHAPTER 7 –CONCLUSION AND RECOMMENDED FUTURE WORK

7.1 Separation Funnel Conclusions

A unique chemistry has been tested in the separation funnel that is able to selectively extract Te from a feed solution containing dissolved Cd and Te. It was found that pure MIBK is the best solution for extracting tellurium. The distribution ratio, M, for extraction of Te with pure MIBK is found to be 0.5 for the chemistry proposed (a 1:1 volume ratio for the aqueous and organic phases).

This distribution ratio is 6 to 10-fold lower than those reported in the literature for MIBK with 6M HCl. The most effective extractions depend on large distribution ratios. There is ample room for troubleshooting and improving the distribution ratio for the present test method. However, the considered distribution ratios are theoretically sufficient to achieve a complete extraction of Te in the microchannel if the channel is long enough and/or the flow rate is low enough. It is not possible to foresee the complications which may arise due to the very low flow rates in long microchannels.

Applications for research into microchannel extraction could extend beyond the separation of Te from CdTe. Extraction of Te^{4+} into MIBK is known to very selectively leave quite a list of metals behind in the feed phase. For a 4M HCl feed phase, the metals left behind Te^{4+} include; Cu(II), Al(III), Ni(II), Co(II), Mg(II), Zn(II), Cd(II), Pb(II), Cr(III), Mn(II) [50] [36]. This leaves room for potential growth of the MIBK tests to expand into extraction of Te from a multi-metal feed

solution, broadening the scope and application of the instant research ever closer to the practical real world recycling of PV material(s).

7.2 Future Work on Chemistry

The distribution ratio of the reported chemistry needs to be improved via separation funnel experiments to reduce membrane resistance in the microreactor. It would make sense to try a spectrometric grade of MIBK rather than the ACS grade, or at least a few brands of MIBK to rule out tainted and otherwise damaged chemicals. An additive to MIBK, such as tributyl phosphate (TBP), could possibly enhance Te extraction as one publication [37] reports. The best distribution ratios reported [39], [50], [51] are in flows with 4M HCl. Based on these reports, a 4M HCl feed solution would allow more effective extraction of Te. Switching to a lower acidity in the feed would also create less wear on the membrane. There may also be a feed additive, such as nitric acid, to suppress uptake of Cd. This surmise is based on the observation that in the chemistry of MIBK extraction, small amounts of nitric acid are reported to suppress uptake of trace copper [51].

The back-extraction with 2% HCl, as presented here is quite effective. However, there are reports that water can be used to back-extract Te [50], [51]. Replacing the 2% HCl strip stream with water would reduce wear on the membrane.

In principle, the tested chemistry can also be used to selectively separate Te from metals other than cadmium. Further research can be done on extracting Te from a more complex stream of metals, that are tantamount to dissolved semiconductor material, which might contain other metals such as indium and copper.

7.3 Microreactor Conclusions

Inexpensive Teflon materials with a Celgard membrane were used to construct a microreactor capable of selectively extracting Te from a stream of mixed Cd and Te at concentrations similar to that of ground solar PV Collector materials. A reactor with a single channel fitting in the palm of a hand recovered 18.0-26.8% of the Te at the lowest flow rate tested. The simple three phase microreactor advantageously combines the extraction and back-extraction steps of a batch reactor into one continuous extraction requiring only microliters of the extractant MIBK. It is likely that recovery of Te using this technology would approach 100% if the residence time was increased by 5-7X. This might be done by increasing overall channel length, or by decreasing the flow rate, or some combination of both. There is some Cd contamination in the Te strip stream generated in the present extraction process. A 100% Te extraction might be expected to be contaminated with a small percentage of Cd due to the limitations of selectivity of the separation process.

This thesis indicated that SLM instability, delicacy and fragility are the primary drawbacks of SLM, limiting the duration of experiments to less than 6 hours. The mode of failure may be caused by molecules of extractant (MIBK) wicking out of the membrane into flow (of the aqueous feed and/or strip streams), thereby depleting the extractant available to complex with Te and transport it to release into the strip stream. There may also be small tears or perforations of the membrane caused by etching or erosion from the flow of 20% hydrochloric acid in the feed channel.

7.4 Future Work on Microreactor

Having reasonably well demonstrated the feasibility of Te extraction from a stream of CdTe at a concentration representative of that found in solar cell recycling processes, future experiments are strongly recommended. Areas of interest to investigate within the current design are the possibility of using: water for the strip solution, a 4M HCl to create the feed solution; one hydrophobic Teflon membrane or two layers of PP membrane to increase membrane endurance and retention of MIBK; lower flow rates; creating a better seal by raised features (rather than the oval gasket); longer channels, thinner channels and multilayer channels; and tests with lower feed flow rates. It is not inconceivable to place multiple microchannel reactors in parallel to improve the extraction efficiency.

Yet another alternative design for the extraction of Te with MIBK involves a three phase microchannel system, with MIBK flowing sandwiched between the aqueous streams. The results of Kuban et al. [22] support this design option, showing that MIBK forms a stable interface with a parallel aqueous stream. This approach would perpetually maintain the volume of MIBK required for continuous loop extraction rather than starting with a very small volume of it (MIBK) to be leached away by the acid. It would also prolong the time an experiment might be maintained in steady state by eliminating the issues of membrane corruption, tears, erosion, and fouling.

REFERENCES

[1] M. Marwede, W. Berger, M. Schlummer, A. Maurer and A. Reller, "Recycling paths for thin-flim chalcogenide photovoltaic waste - Current feasible processes," *Renewable Energy,* vol. 55, pp. 220-229, 2013.

[2] V. Fthenakis, "Sustainability of photovoltaics: The case for thin-film solar cells," *Renewable and Sustainable Energy Reviews,* vol. 13, pp. 2746-2750, 2009.

[3] F.-G. Simon, O. Holm and W. Berg, "Resource recovery from urban stock, the example of cadmium and tellurium from thin film module recycling," *Waste Management,* vol. 33, pp. 942-947, 2013.

[4] P. Cox, The Elements Their Origin, abundance, and distribution, New York: Oxford Univeristy Press, 1989.

[5] W. Berger, F.-G. Simon, K. Weimann and E. A. Alsema, "A novel approach for the recycling of thin film photovoltaic modules," *Resources, Conservation and Recycling,* vol. 54, pp. 711-718, 2010.

[6] V. M. Fthenakis, "Life cycle impact analysis of cadmium in CdTe PV production," *Renewable and Sustainable Energy Reviews,* vol. 8, pp. 303-334, 2004.

[7] V. M. Fthenakis and H. C. Kim, "CdTe photovoltaics: Life cycle environmental profile and comparisons," *Thin Solid Films,* vol. 515, pp. 5961-5963, 2007.

[8] V. M. Fthenakis and W. Wang, "Extraction and Separation of Cd and Te from Cadmium Telluride Photovoltaic Manufacturing Scrap," *Progress in Photovoltaics: Research and Applications,* vol. 14, pp. 363-371, 2006.

[9] S. Menezes, "Electrochemical approach for removal, separation and retrieval of CdTe and CdS films from PV module waste," *Thin Solid Films,* vol. 387, pp. 175-178, 2001.

[10] T. Maruyama, T. Kaji, T. Ohkawa, K.-i. Sotowa, H. Matsushita, F. Kubota, N. Kamiya, K. Kusakabe and M. Goto, "Intermittent partition walls promote solvent extraction of metal ions in a microfluidic device," *Analyst,* vol. 129, pp. 1008-1013, 2004.

[11] C. Priest, J. Zhou, R. Sedev, J. Ralston, A. Aota, K. Mawatari and T. Kitamori, "Microfluidic extraction of copper from particle-laden solutions," *International Journal of Mineral Processing,* vol. 98, pp. 168-173, 2011.

[12] R. Molinari, P. Argurio and T. Poerio, "Studies of various solid membrane supports to prepare stabe sandwich liquid membranes and testing copper(II) removal from aqueous media," *Separation and Purification Technology,* vol. 70, pp. 166-172, 2009.

[13] J. G. Kralj, H. R. Sahoo and K. F. Jensen, "Integrated continuous microfluidic liquid-liquid extraction," *Lab Chip,* vol. 7, pp. 256-263, 2007.

[14] H. Hisamoto, T. Horiuchi, M. Tokeshi, A. Hibara and T. Kitamori, "On-Chip Integration of Neutral Ionophore-Based Ion Pair Extraction Reaction," *Analytical Chemistry,* vol. 73, pp. 1382-1386, 2001.

[15] H. Hotokezaka, M. Tokeshi, M. Harada, T. Kitamori and Y. Ikeda, "Development of the Innovative Nuclide Separation System for High-Level Radioactive Waste Using Microchannel Chip-Extraction Behavior of Metal Ions from Aqueous Phase to Organic Phase in Microchannel," *Progress in Nuclear Energy,* vol. 47, pp. 439-447, 2005.

[16] H.-B. Kim, K. Ueno, M. Chiba, O. Kogi and N. Kitamura, "Spatially-Resolved Fluorescence Spectroscopic Study on Liquid/Liquid Extraction Processes in Polymer Microchannels," *Analytical Sciences,* vol. 16, pp. 871-876, 2000.

[17] P. Kuban, J. Berg and P. K. Dasgupta, "Vertically Stratified Flows in Microchannels. Computational Simulations and Applications to Solvent Extraction and Ion Exchange," *Analytical Chemistry,* vol. 75, pp. 3549-3556, 2003.

[18] T. Maruyama, H. Matsushita, J.-i. Uchida, F. Kubota, N. Kamiya and M. Goto, "Liquid Membrane Operations in a Microfluidic Device for Selective Separation of Metal Ions," *Analytical Chemistry,* vol. 76, pp. 4495-4500, 2004.

[19] M. Surmeian, M. N. Slyadnev, H. Hisamoto, A. Hibara, K. Uchiyama and T. Kitamori, "Three-Layer Flow Membrane System on a Microchip for Investigation of Molecular Transport," *Analytical Chemistry,* vol. 74, pp. 2014-2020, 2002.

[20] M. Tokeshi, T. Minagawa and T. Kitamori, "Integration of a Microextraction System on a Glass Chip: Ion-Pair Solvent Extraction of Fe(II) with r,7-Diphenyl-1,10-phenanthrolinedisulfonic Acid and Tri-n-octylmethylammonium Chloride," *Analytical Chemistry,* vol. 72, pp. 1171-1714, 2000.

[21] X. Wang, C. Saridara and S. Mitra, "Microfluidic supported liquid membrane extraction," *Analytica Chimica Acta,* vol. 543, pp. 92-98, 2005.

[22] P. Kuban, P. K. Dasgupta and K. A. Morris, "Microscale Continuous Ion Exchanger," *Analytical Chemistry,* vol. 74, pp. 5667-5675, 2002.

[23] Y. Ban, Y. Kikutani, M. Tokeshi and Y. Morita, "Extraction of Am(III) at the Interface of Organic-Aqueous Two-Layer Flow in a Microchannel," *Journal of Nuclear Science and Technology,* vol. 48, pp. 1313-1318, 2011.

[24] Y. Kikutani, K. Mawatari, A. Hibara and T. Kitamori, "Circulation microchannel for liquid-liquid microextraction," *Microchim Acta,* vol. 164, pp. 241-247, 2009.

[25] K. Ueno, H.-B. Kim and N. Kitamura, "Channel Shape Effects on the Solution-Flow Characteristics and the Liquid/Liquid Extraction Efficiency in Polymer Microchannel Chips," *Analytical Sciences,* vol. 19, pp. 391-394, 2003.

[26] A. Hibara, M. Tokeshi, K. Uchiyama, H. Hisamoto and T. Kitamori, "Integrated Multilayer Flow System on a Microchip," *Analytical Sciences,* vol. 17, pp. 89-93, 2001.

[27] T. Araki and H. Tsukube, Liquid Membranes: Chemical Applications, United States: CRC Press, 1990, pp. 127-128.

[28] O. Tamagawa and A. Muto, "Development of cesium ion extraction process using a slug flow microreactor," *Chemical Engineering Journal,* vol. 167, pp. 700-704, 2011.

[29] Y. Sato, Y. Akiyoshi, K. Kondo and F. Nakashio, "Extraction Kinetics of Copper with 2-

Ethylhexyl-phosphonic Acid Mono-2-ethylhexyl Ester," *Journal of Chemical Engineering of Japan,* vol. 22, pp. 182-189, 1989.

[30] F. Kubota, M. Goto and F. Nakashio, "Extraction of Rare Earth Metals with 2-Ethylhexyl Phosphonic Acid Mono-2-Ethylhexyl Ester in the Presence of Diethylenetriaminepentaacetic Acid in Aqueous Phase," *Solvent Extraction and Ion Exchange,* vol. 11, pp. 437-453, 1993.

[31] S. Glasstone, The Elements of Physical Chemistry, Seventeenth Printing ed., New York: D. Van Nostrand Company, Inc., 1958, pp. 364-365.

[32] N. A. Marine, S. A. Klein and J. D. Posner, "Partition Coefficient Measurements in Picoliter Drops Using a Segmented Flow Microfluidic Device," *Analytical Chemistry,* vol. 81, pp. 1471-1476, 2009.

[33] S. Ramprasad and K. Sharp, *Process development for separation of CdTE in a microfluidic device using liquid membranes: A pathway for efficient recycling of CdTe PV modules,* Corvallis, OR, 2010.

[34] I. Havezov and N. Jordanov, "Separation of tellurium(IV) by solvent extraction metholds," *Talanta,* vol. 21, no. 10, pp. 1013-1024, 1974.

[35] G. Knockaert, Tellurium and Tellurium Compounds, vol. 35, Weinheim: Wiley-VCH, 2012, pp. 685-695.

[36] K. Hayashi, T. Ogata and K. Bunseki, "The Separation of Tellurium from Iron and Steel by Solvent Extraction with MIBK," *Japan Analyst,* vol. 15, pp. 1120-1124, 1966.

[37] G. Venkateswarlu, A. Sahayam and S. Churasia, "Synergistic Effect of Methyl Isobutyl Ketone (MIBK) and Tributyl Phosphate (TBP) on the Extraction of Tellurium for the Determination of Trace Imputities in Tellurium," *Atomic Spectroscopy,* vol. 31, no. 6, pp. 187-189, 2010.

[38] M. Laatikainen and E. Paatero, "Gold recovery from chloride solutions with XAD-7: Competitive adsorption of Fe(III) and Te(IV)," *Hydrometallurgy,* vol. 79, pp. 154-171, 2005.

[39] I. Havezov and N. Jordanov, "Zum Mechanismus der Extraktion von Tellur(IV) aus salzsaurem Medium mit gesattigten aliphatischen Monoketonen," *Z. Anal. Chem.,* vol. 262, pp. 179-183, 1972.

[40] J. B. Milne, "Hexachlorotellurate(IV) hydrolysis equilibria in hydrochloric acid. Measurement by Raman and 125Te NMR spectroscopy and a reconsideration of earlier spectrophotometric results," *Can. J. Chem.,* vol. 69, pp. 987-992, 1991.

[41] J. Milne and M. Mehadevan, "Chlorotellurate(IV) Equilibria in Aqueous Hydrochloric Acid," *Inorganic Chemistry,* vol. 23, pp. 268-271, 1984.

[42] M. Yaftian, A. Zamini, M. Parinejad and E. Shams, "Ion-pair extraction of cadmium complex anions from hydrochloric acid media using oxonium ion-dicyclohexyl-18-crown complex," *Separation and Purification Technology,* vol. 42, no. 2, pp. 175-180, 2005.

[43] T. Sato, K. Adachi, T. Kato and T. Nakamura, "The Extraction of Divalent Manganese, Cobalt, Copper, Zinc, and Cadmium from Hydrochloric Acid Solutions by Tri-n-octylamine,"

Separation Science and Technology, vol. 17, pp. 1565-1576, 1982-83.

[44] Pub Chem Compound, "Methyl Isobutyl Ketone- Compound Summary (CID 7909)," National Center for Biotechnology Information (NCBI) U.S. National Library of Medicine, [Online]. Available: http://pubchem.ncbi.nlm.nih.gov/summary/summary.cgi?cid=7909#itabs-3d. [Accessed 19 12 2013].

[45] DOW, "Methy Isobutyl Ketone," The Dow Chemical Company, June 2002. [Online]. [Accessed 11 February 2014].

[46] P. Arora and Z. (. Zhang, "Battery Separators," *Chemical Reviews,* vol. 104, pp. 4419-4462, 2004.

[47] R. B. Bird, W. E. Stewart and E. N. Lightfoot, Transport Phenomena, New York: John Wiley & Sons, Inc., 2007, p. 678.

[48] W. Palitzsch, "Recycling of thin solar cell modules". Germany Patent DE 102008058530, 27 May 2010.

[49] R. Chakraborty and S. Datta, "Extraction of Te(IV) by liquid surfactant membrane," *Hydrometallurgy,* vol. 43, pp. 169-174, 1996.

[50] N. Jordanov and I. Havesov, "Extractionsmethode zur Trennung kleiner Tellurmengen von Begleitelementen," *Z. Anal. Chem.,* vol. 248, pp. 296-298, 1969.

[51] A. Kakumoto, "Determination of copper and lead in high purity tellurium using MIBK extraction and square-wave polarography," *Japan Analyst,* vol. 13, no. 10, pp. 1016-1023, 1964.

[52] B. Iofa, "Effect of temperature on extraction of complex metal halide acids," *Vestnik,* vol. 35, no. 6, pp. 497-501, 1994.

[53] D. Ciceri, J. M. Perera and G. W. Stevens, "A study of molecular diffusion across a water/oil interface in a Y-Y shaped microfluidic device," *Microfluid Nanofluid,* vol. 11, pp. 593-600, 2011.

[54] F. M. White, Viscous Fluid Flow Second Edition, New York: McGraw-Hill, 1991, pp. 568-569.

[55] E. Nishikata, T. Ishil and T. Ohta, "Viscosities of Aqueous Hydrochloric Acid Solutions, and Densities and Viscosities of Aqueous Hydrochloric Acid Solutions," *J. Chem. Eng. Data,* vol. 26, pp. 254-256, 1981.

[56] J. C. Slater, "Atomic Radii in Crystals," *The Journal of Chemical Physics,* vol. 41, pp. 3199-3204, 1964.

[57] E. L. Cussler, Diffusion Mass Transfer in Fluid Systems Third Edition, New York: Cambridge Univeristy Press, 2011, pp. 127, 193, 250, 407.

[58] R. K. Shah and A. L. London, Laminar Flow in Forced Convection in Ducts, New York: Academic Press, 1978, p. 52.

[59] EPA, Document 40 CFR 136. Appendix B to Part 136 - Definition and Procedure for the Determination of the Method Detection Limit - Revision 1.11.

APPENDICES

A - Material Properties

Material properties used for calculations presented are displayed in Table A-1.

Table A-1 Experimental Fluid Properties

Substance	Properties at 20 C atmospheric pressure		
	Kinematic Viscosity cSt	Dynamic Viscosity cP	Density g/cm^3
Saturated Water [54]	1.004	1.002	0.998
Aqueous HCl 2% w/w [55] [54]*	1.005	1.052	1.012
Aqueous HCl 20% w/w [55]*	1.259	1.383	1.155
Methyl Isobutyl Ketone (MIBK) [45]	.75	0.6	0.8

*Data interpolated between points.

B - Te Complex Molecular Radii

Radii for each of the Te molecules were found using the method of summing the atomic radii for each atom in the proposed molecule(s). As reported by J. C. Slater [56], this method gives a good estimation of molecular radii for ionic or covalently bonded molecules. The atomic radii for the elements H, O, Cl, and Te (indicated in Table B-1) were measured by Slater. An explanation of the radii for MIBK and the Te complex radii average follows in the next paragraphs. A calculation for the atomic radii of each Te complex (aqueous strip, aqueous feed, and organic carrier) is summarized in Table B-1.

Table B-1 Atomic Radii Calculation for Te Complex

		Radii (pm)						
		H	O	Cl	Te	MIBK	Sum	Avg.
Solute Ion Complex	Axis	25	60	100	140	186	R_0	R_0
	1			200	140		340	
Strip: $Te(OH)_2Cl_2(H_2O)_2$	2	50	120	100	140		410	375.0
	1			200	140		340	
Feed: $HTe(OH)Cl_4$	2	25	60	100	140		325	332.5
	1	100	240		140		480	
Carrier: $HTe(OH)Cl_4$ $MIBK_5$ H_2O_8	2			200	140	186	526	503.0

A 3-d model for MIBK on the NIST website displayed the molecules' dimensions as 176 pm by 196 pm by 353 pm (in the direction of the chain) [44]. For the purpose of determining the carrier molecule dimensions, the two shorter dimensions were averaged to 186 pm, to use in place of an individual atomic radius. The longer dimension of MIBK at 353 pm is less than the matching dimension of the inner Te ring, 480 pm, as indicated below; these axis for the inner and outer ring are assumed to align.

The atomic radii is found for two axes of the Te complex and averaged to yield the molecular radii used for calculation of the diffusion coefficient in the Stokes-Einstein equation. It was assumed the water molecules in the carrier Te complex outer ring stretch between the MIBK molecules, causing a negligible increase in overall molecular radius.

The atomic radii for each Te complex was found for two different axes in the molecule. The axial radii were averaged to yield the molecular radii used for calculation of the diffusion coefficient in the Stokes-Einstein equation. It was assumed the water molecules in the carrier Te complex outer ring stretch between the MIBK molecules, causing a negligible increase in overall molecular radius.

C - Diffusion Coefficient Calculation

The diffusion coefficients, denoted as D, for tellurium complex in the aqueous media as well as in the MIBK carrier were calculated according to the Stokes-Einstein diffusion model [57],

$$D = \frac{k_B T}{6\pi\mu R_o} \qquad (C.1)$$

Where the k_B is Boltzmann's constant, T is temperature, and μ is the solvent viscosity. The solute ion complex radius R_o is estimated in the proceeding material presented in Appendix B. The diffusion constant in the membrane was adjusted to correct for the ratio of solvent to membrane pore size using the Hindered model [57].

$$D = D_0 \left[1 + \frac{9}{8}\lambda \ln\lambda - 1.54\lambda + O(\lambda^2)\right] \qquad (C.2)$$

The parameter λ is defined to be the ratio of the diameter of the solute to diameter of the pore. A summary of the diffusion coefficient calculation may be seen in Table C-1. Fluid properties are found in Appendix A.

Table C-1 Calculation of Te Complex Diffusion Coefficient

	Stokes-Einstein $D = k_B T/(6\pi\mu R_0)$					Hindered Pore D		Te
Solvent	k_B $\frac{g\ cm^2}{s^2\ K}$	T K	Solvent μ cP	Solute R_0 m	Solute D cm^2/s	λ	Solute D cm^2/s	Complex D cm^2/s
Strip	1.38E-16	293.15	1.052	3.75E-10	5.44E-06	N/a	N/a	5.44E-06
Feed	1.38E-16	293.15	1.383	3.33E-10	4.67E-06	N/a	N/a	4.67E-06
SLM	1.38E-16	293.15	0.600	5.03E-10	7.11E-06	0.023	6.152E-06	6.15E-06

D – An Analysis of Diffusion Mass Transfer
In Separation of Te from Cd in a Microchannel Reactor

Murty Kanury and Heather Johnson Liburdy

Presented in this Appendix is a theoretical model of diffusion of tellurium complex from the feed flow to the feed-side surface of a Supported Liquid Membrane (SLM). The model is intended to be: (a) a predictive tool; (b) a rational basis to interpret the measured data; and also (c) a diagnosis tool to identify and appraise the performance of individual components of the reactor.

§1. The Problem/Estimates of Some Parameters

Sketched in Fig. D-1 is the considered arrangement of feed and strip (counter) flow microchannels separated by the SLM. The membrane chemistry mechanism stipulates that the tellurium complex (termed *Te-complex*, in this Appendix) transported to the strip side surface of the SLM undergoes an abrupt irreversible transformation which will be carried away in the strip flow. The channels are of square cross section of side $a = 0.05\ cm$. The membrane thickness is 25 μm. The present analysis considers transport processes in the feed flow and across the membrane.

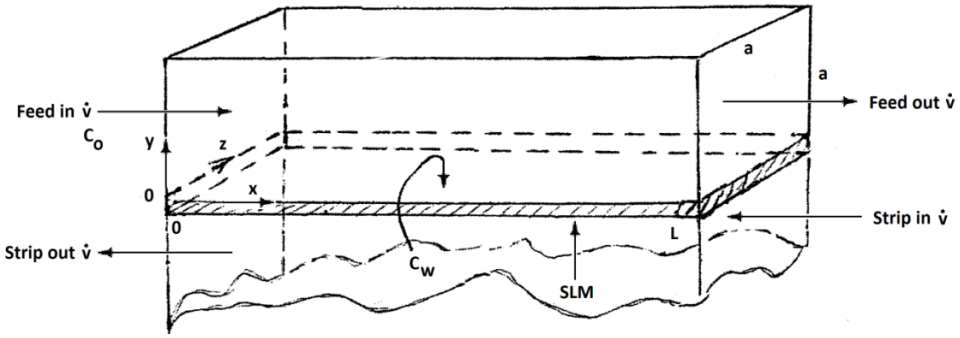

Fig. D-1 Layout of the Feed Channel, SLM, and the Counterflow Strip Channel

The flow is in the x-direction, with inlet at $x = 0$ and exit at $x = L$. Diffusion of the Te-complex occurs in y-direction from the flow to the membrane surface located at $y = 0$. The top of the channel is at $y = a$. The uniform channel width in the z-direction is a (cm). Both the top and the sides are impervious. Known at the channel inlet are the feed flow rate $\dot{V}$ cm^3/s as well as the tellurium concentration C_o g/cm^3. The inlet flow velocity u_o cm/s is simply the volumetric flow rate divided by the cross sectional area of the channel, $\dot{V}/a^2$.

Experiments are conducted at three different flow rates: 0.01, 0.02 and 0.03 cm3/min which correspond to flow speeds u_o of 0.067, 0.133, and 0.200 cm/s

respectively. Two channel lengths are tested in the layouts of "straight" for the short (3.4 cm) ones and "serpentine" for the long (12.9 cm) ones. In the feed flow at the inlet, two Te-complex concentrations C_o = 1149 ppm and 2300 ppm are tested. The flow problem will be simplified by assuming it to be a plug-flow. Effects of temperature and gravity are ignored. The flow is assumed to be steady with constant physical and chemical properties.

The kinematic viscosity of the feed solution $\nu = 1.26 \text{ x } 10^{-2}$ cm^2/s. Diffusivity of the Te-complex in the feed solution is $D = 4.67 \text{ x } 10^{-6}$ cm^2/s so that the Schmidt number $Sc \equiv \nu/D$ is about 2,700. With these momentum and species diffusivities and the three different inlet feed volume flow rates mentioned above, a number of useful channel flow conditions can be calculated and tabulated as done below, (in units of cm and sec), for $a = 0.05\ cm$ and channel lengths 3.4 cm and 12.9 cm.

Table D-1 Estimates of Some Relevant Parameters

				$Pe_L = Re_L\, Sc = \frac{Lu_o}{D}$		$Flow\ Time = \frac{L}{u_o} sec$	
$\dot{V}$ cm^3/s	u_o cm/s	Re_a	Pe_a	$L = 3.4$ cm	$L = 12.9$ cm	$L = 3.4$ cm	$L = 12.9$ cm
1.667x10^{-04}	0.067	0.265	715	48,620	184,470	51	192
3.333x10^{-04}	0.133	0.530	1,424	96,832	367,392	26	97
5.000x10^{-04}	0.200	0.794	2,141	145,588	552,378	17	64

It is evident that the small channel dimensions and volumetric flow rates coupled with a relatively large kinematic viscosity make both the inlet flow speed and the Reynolds number small. The species diffusivity being order of magnitude smaller than the kinematic viscosity, the Schmidt and Peclet numbers are large. Residence times are less than about one minute in the short channel and about three minutes in the long channel.

Because the side walls of the channel are impervious, it would appear reasonable to assume that the concentration is uniform in the (width-wise) z-coordinate. The Te-complex species conservation equation for spatial concentration distribution in the 2-dimensional, steady, constant property channel flow, is described by

$$u\frac{\partial C}{\partial x} + v\frac{\partial C}{\partial x} = D\frac{\partial^2 C}{\partial y^2} \tag{1}$$

Where C is the Te-complex concentration. Denoting the feed fluid density by ρ, the y-component velocity $v \approx -\left(\frac{D}{\rho}\right)\frac{\partial C}{\partial y} \approx O\left(\frac{D}{a}\right) \approx 10^{-4}\ cm/s$. This is two to three orders of magnitude smaller than even the smallest of the x-component velocities indicated in

Table D-1. On this basis, it appears reasonable to apply the *Oseen approximation* to Eq.(1) to drop the y-directional convection terms in Eq. (1), thus simplifying it to

$$u\frac{\partial C}{\partial x} = D\frac{\partial^2 C}{\partial y^2} \tag{2}$$

Finally, the plug flow assumption is made for the flow in the channel. This assumption makes the velocity distribution $u(x, y)$ is equal to the constant and uniform inlet velocity $u_o$at all values of x and y within the rector channel. Literature contains numerous examples indicating that the plug flow approximation leads to useful engineering solutions. This is especially to be appreciated when studying the processes in microchannels, in which measurement of velocity distributions are at best tedious and at worst impossible. The final form of conservation equation thus is

$$\frac{\partial C}{\partial (x/u_o)} = D\frac{\partial^2 C}{\partial y^2} \tag{3}$$

which is one of the most important equations in engineering applications (e.g. Conduction of Heat [Carslaw and Jaeger], Mass Diffusion [Crank]) of applied mathematics.

Two boundary layer conditions in the y direction, and one in x, are required to solve Eq. (3) for the $C(x, y)$ distribution of the Te-complex concentration. These are:

Inlet	$x = 0$	$C(0, y) = C_o$	uniform over all values of y.
Surface	$y = 0$	$C(x, 0) = C_w$	uniform over all values of x.
Stream	$y \to a$	$C(x, a) \to C_o$	uniform over all values of x.

The y boundary conditions will be further discussed later.

The contents of the Appendix follow in this order: A heuristic solution of the subject problem composed of separation, transport and extraction of Te^{4+} complex will first be presented in §2. A well-known general solution of Eq. (3) with the given boundary conditions will be high-lighted in §3. This parent solution will be adapted to the problem at hand from a *boundary layer* point of view in §4. Some comments on continued analysis in the future are made in §5. These comments pertain to adaptation of the solution of the parent equation to the present problem from a *developing pipe flow* point of view; coupling of diffusion in the feed fluid flow with diffusion across the SLM and a membrane chemistry mechanism. The heuristic solution in §2 and boundary layer solution in §4 complement one another by reinforcing some conclusions while each also standing alone to bring an improved understanding of the problem studied.

§2. Some Heuristic Deductions:

Looking at each term in Eq. (3) and the dimensions (or units) of each part of it, there is much to learn. Note for example, the independent coordinate x, when dividend by the constant u_o, gets linearly transformed to (x/u_o) which is a time-variable. It is called the "flow time" by some in the literature and "residence time" by others. (See the last two columns of Table D-1). This transformation makes Eq. (3) a transient one-dimensional diffusion equation.

The flow enters the channel at $x = 0$, bearing a uniform Te-complex concentration C_0. It feels the presence of the membrane, the surface of which is at a constant and uniform concentration of the complex C_w. This surface concentration is smaller than C_0. Only at the inlet is it equal to C_0, the largest value in the system. The region of y in which C decreases from C_0in the stream to C_w at the membrane surface is called, the *diffusion layer*. Its thickness $\delta(x)$ monotonically increases with x, from 0 at $x = 0$. The difference $(C_0 - C_w)$ is the potential which drives the mass transfer of the complex by diffusion from the stream to the membrane surface.

The ratio of the magnitudes of the two equally important terms of Eq.(1) has to be of the order of unity; put in terms of order-of magnitude, $\frac{y^2/D}{x/u_o} = O(1)$ from which one obtains

$$\frac{u_o\delta^2}{xD} \approx 1 \qquad or \qquad \frac{\delta}{x} \approx \left(\frac{D}{xu_o}\right)^{1/2} \tag{4}$$

so that $\delta(x) \approx \left(\frac{xD}{u_o}\right)^{\frac{1}{2}}$. The diffusion layer thickness $\delta(L)$ at the exit of the channel $x = L$ can now be estimated from this result.

$$\frac{\delta(L)}{L} \approx \left[\frac{D}{Lu_o}\right]^{\frac{1}{2}} = \left[\frac{1}{Pe_L}\right]^{\frac{1}{2}} \qquad or \qquad \frac{\delta(L)}{a} \approx \left[\frac{L}{a}\cdot\frac{D}{au_o}\right]^{\frac{1}{2}} = \left[\frac{L}{a}\cdot\frac{1}{Pe_a}\right]^{\frac{1}{2}} \tag{5}$$

The Peclet numbers for the short and long channels and for the three flow rates are available in Table D-1. The $\delta(L)/a$ values calculated for the six cases are presented below.

Table D-2 Diffusion Layer Thickness as a Fraction of Channel Depth, $\frac{\delta(L)}{a}$

L, cm	u_o, cm/s		
	0.067	0.133	0.222
3.4	0.308	0.218	0.178
12.9	0.601	0.426	0.347

It is clear that longer channels and smaller flow rates make the diffusion layer at the exit thicker. Both these observations are not only consistent with intuition but also hold important implications in the design of a reactor. The small magnitude of species diffusivity causes a very large Schmidt number, which in turn leads to a diffusion layer that develops in its thickness rather slowly with increasing x. An important and consequential conclusion that can thus be reached is that the flow in the channel is far from being fully developed. The solution of Eq.(3), therefore, can be sought through boundary layer type analysis.

§3. Solution of Equation (3):

The observation that the diffusion layer at the exit of the channel is sufficiently far from reaching the top surface $y = a$ leads one to approach it as a problem of diffusion from a semi-infinite fluids bounded by the membrane flat plate surface at $y = 0$. For convenience in viewing the steps of the argument, this equation is placed here again.

$$\frac{\partial C}{\partial (x/u_o)} = D \frac{\partial^2 C}{\partial y^2}$$

The variables $x, y, u_o$and D conviently group together into a nondimensional form as $\left(\frac{y^2}{D}\ \frac{u_o}{x}\right)$, a ratio of diffusion time in y direction to the flow time in x direction. This ratio has been interpreted and used in the literature in a number of revealing ways, in a variety of momentum, heat and mass transfer problems. Considered here is the square root of the ratio to arrive at a composite independent variable, (also widely known as the *similarity variable*), denoted by η and defined as follows.

$$\eta \equiv \frac{y}{2}\sqrt{\frac{u_o}{xD}} = \frac{y}{2x}\sqrt{\frac{xu_o}{D}} = \frac{y}{2x}\sqrt{Re_x Sc} = \frac{y}{2x}\sqrt{Pe_x}$$

Substitution of η turns Eq.(3) into

$$\frac{\partial^2 C}{\partial \eta^2} = -2\eta \frac{\partial C}{\partial \eta}$$

in which all the independent variables and parameters namely $x, y, u_o$and D are absorbed into the definition of η. If the boundary conditions permit, concentration C of the transported Te-complex shall be a function of η only. Recalling that C_o, concentration at the inlet of the feed, and C_w, concentration at the "wall" which is the feed side surface of the membrane are both assumed to be constant and uniform make this permission. The constancy and uniformity of the boundary concentration is an essential requirement in obtaining the error function solution. One of the factors of

concern here is the extent to which this requirement is met in the reactor for transport and separation of Te-complex. With constant C_o and C_w, the concentration C pf the Te-complex can be normalized and nondimensionalized as $\emptyset \equiv \left(\frac{C_o - C}{C_o - C_w}\right)$. The value of $\emptyset$, at the membrane surface is unity and, in the stream, it is zero. Finally, the governing equation and its boundary condition are:

$$\frac{\partial^2 \phi}{\partial \eta^2} = -2\eta \frac{\partial \phi}{\partial \eta} \tag{6}$$

$$\text{Boundary conditions:} \quad \phi(0) = 1 \qquad \phi(\eta \to \infty) = 0$$

The solution of this problem can be obtained with a few straight forward integration steps along with the application of two boundary conditions.

$$\phi(\eta) = 1 - \text{erf}(\eta) \tag{6a}$$

Here, $\text{erf}(\eta)$ is the *error function* which is available tabulated as a function of its argument η, shown in the first panel of Fig. D-2 below. The error function is zero when η is zero and unity when η exceeds about 2. Its slope at an η of zero is $2/\sqrt{\pi} = 1.1284$.

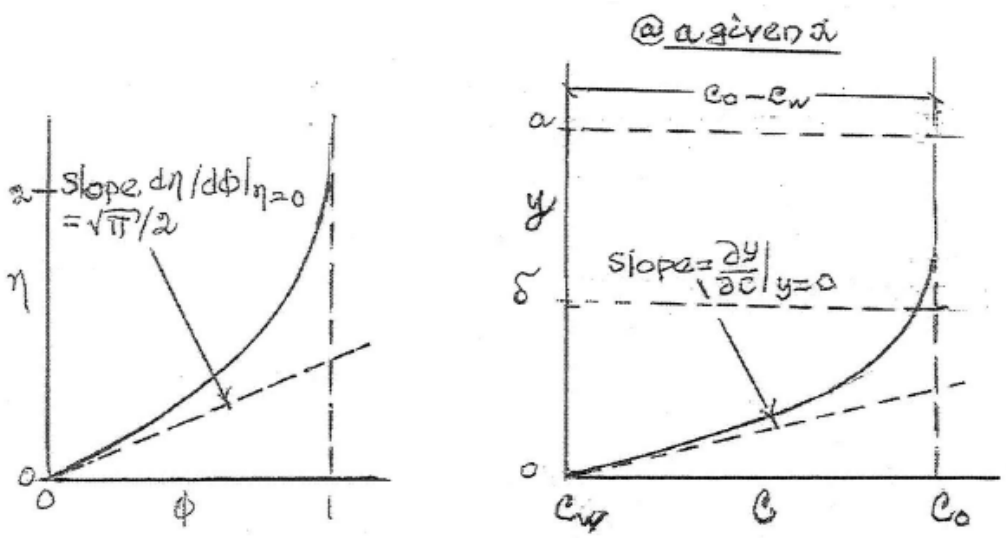

Fig. D-2: (a) The Error Function Solution and (b) the same in Physical Terms.

§4. Diffusion Boundary Layer Over the Membrane Plate Under Plug-Flow Feed:

Two view points are possible in applying the solution given in §3. The first view point is described in this section. The diffusion layer is visualized to develop a 2-d boundary layer flow over a flat plate that the membrane surface. In this model, the effects of the side walls and the ceiling are ignored. The second view point is based on a

diffusion boundary layer developing near the entrance section of a pipe of square cross section (see comments in §5).

This flat plate boundary layer analysis in the present situation is a variant of the Blasius problem of flow and transport over a 2-d flat plate. The membrane surface represents the plate to which diffusive transport of the Te-complex occurs from the feed fluid stream. First, the fluid in the channel is not of infinite extent in the y-direction normal to the membrane surface. This is not a serious issue for two reasons resulting from the very large value of the Schmidt number of the feed fluid: the flow in the channel is already highly simplified by the plug flow assumption; and, as well, the heuristic arguments convincingly indicate that the diffusion layer is not anywhere close to becoming fully developed. The second difference calls attention to the presence and possible effects of sidewalls in applying the notion of flow over a flat plate to 'channel' configuration. The issue too is rendered moot by the absence of fluid friction implied yet again in the plug flow assumption.

The mechanism of transport visualized is that the concentration of Te-complex in the layer above the diffusion layer, i.e., in the region between $y = \delta$ and $y = a$, remains the same as at the inlet, C_o, constant and uniform with respect to y. The diffusion layer is yet to penetrate into this layer. (See the second panel of Fig. D-2). The concentrations at the channel inlet and at the membrane surface are respectively $C_o \; and \; C_w$, both being constant in this analysis. The constant difference $(C_o - C_w)$ is the driving force for mass transfer from the stream and the membrane surface. Putting together the diffusion in the feed flow with diffusion across the membrane to the strip side, and adopting a hypothetical mechanism for membrane chemistry, C_w can be determined.

The error function solution from §3 is useful towards determining this rate of mass transfer. The $\phi(\eta)$ relation given by Eq.(6a) can be differentiated to obtain the slope of concentration at the surface $(y = 0)$ at any x lying between the inlet a $x = 0$ and exit at $x = L$ where L is the length of the channel. According to Fick's law of diffusion, the local mass flux (over-dot is for 'per unit time' and each prime is for per unit length) $\dot{m}"(x)$ $(g/[cm^2 s])$ is the product of this gradient and the diffusivity D of the diffused substance, Te-complex, through the feed fluid. Thus, the mass flux at any x along the membrane, $\dot{m}"(x)$ is determined to be

$$\dot{m}"(x)|_{y=0} \equiv -D \left.\frac{\partial C}{\partial y}\right|_0 = D(C_o - C_w)\sqrt{\frac{u_o}{\pi D x}} = \frac{u_o(C_o - C_w)}{\sqrt{\pi}}\sqrt{\frac{D}{x u_o}}$$

Put more succinctly,

$$\frac{\dot{m}"(x)}{u_o(C_o - C_w)} = \frac{1}{\sqrt{\pi}} \frac{1}{\sqrt{Pe_x}} = 0.5642 \cdot Pe_x^{-1/2} \tag{7}$$

Where $Pe_x = xu_o/D$ is the Peclet number based on length dimension x. This result is in excellent agreement with those available in existing literature. $(C_o - C_w)$ appears to be a natural and correct choice for driving potential.

§4a. Analogy: The analogy between transfers of heat and mass deserve a short comment here. Following the definition of heat transfer coefficient as the ratio of heat flux to the driving potential, namely the temperature difference, $h \equiv \dot{q}"/(T_o - T_w)$, the ratio of mass flux of the transferred species to the driving potential, i.e., the concentration difference, $\dot{m}(x)"/(C_o - C_w)$ on the left side of Eq.(7) can be identified as the mass transfer coefficient denoted by h_D (or k_F in chemical engineering literature) so that the left side becomes h_D/u_o. This ratio is a nondimensional quantity called the Stanton number for mass transfer, St_D which is analogous to the heat transfer Stanton number $St \equiv h/(\rho u_o c_p)$, where $c_p$is the heat capacity of the flowing fluid.

The Stanton number in heat transfer is the ratio of the Nusselt number Nu to the product of Reynolds and Prandtl numbers. Analogously, St_Din mass transfer is the ratio of Sherwood number and the product of Reynolds and Schmidt numbers. The product of Re and Pr or Re and Sc are, of course, the Peclet numbers for transfer of heat Pe and mass Pe_D respectively. The analogy is complete: just as $Nu_l = St \cdot Pe = hl/K$ in heat transfer, Sherwood number $Sh = h_D l/D$ in mass transfer. In both heat and mass transfer, l is a characteristic length, a, x, L or d as appropriate in the context of concern.

It should be obvious from Eq.(8) and understandable that the Sherwood number, Sh^o, based on x, is

$$Sh_x^o \equiv \frac{h_D^o x}{L} = \frac{Pe_x^{1/2}}{\sqrt{\pi}} = 0.5642 \cdot Pe_x^{1/2} \tag{8}$$

The form and content of this result is consistent with intuition and also the abundantly available literature in the fields of heat and mass transfer (e.g. Bird, Stewart and Lightfoot). The superscript o on the Sherwood number, on the mass transfer coefficient $h_D^o$and some other parameters is meant to associate them with the flat plate boundary layer approach to the problem at hand.

§4b. $\dot{m}$ Over the total length $x = 0$ to L of the channel: In order to calculate the efficancy of capturing the Te-complex at the SLM surface, the total mass rate diffused to the surface is of interest. To determine this $\dot{m}$, Eq.(8) is first rewritten as follows.

$$\dot{m}"(x) = \frac{u_o}{\sqrt{\pi P e_x}}(C_o - C_w) = \left(\sqrt{\frac{u_o D}{\pi}}\right)(C_o - C_w)x^{-1/2}$$

The differential mass $d\dot{m}$ reaching the surface over a differential length dx along the flow direction is this mass flux multiplied by the differential membrane surface are $dA = a \cdot dx$. Recall that a is the width of the channel. Thus, $d\dot{m} = \dot{m}"a \cdot dx$. Integrating the result with respect to x from $x = 0$ to L, the following result is reached. With $A = aL$ denoting the total surface area of the membrane,

$$\frac{\dot{m}_{w,total}}{2A_w u_o(C_o - C_w)} = \frac{1}{\sqrt{\pi P e_L}} \tag{9}$$

§4c. Capture Efficacy F^o: The input rate of Te-complex into the channel at the inlet is the product of the feed volumetric inflow rate $\dot{V}$ (cm^3/s) and the uniform concentration C_o (g/cm^3) at the inlet. Of this, $\dot{m}_{w,total}$ (g/s) given by Eq.(10) has been transported to the SLM surface. The efficacy F^o of transport therefore can be defined as the ratio of transport to the infeed rates. Thus,

$$F^o = 2\left(\frac{L}{a}\right)\left(\frac{C_o - C_w}{C_o}\right)\left(\frac{D}{\pi L u_o}\right)^{1/2} \tag{10}$$

Eq.(10) can be verified by comparison with the experimental measurement(s). Such comparisons are useful in diagnosing the strengths and/or weaknesses of the analysis and/or experiment(s).

§4d. Use of the Foregoing Results: Whereas the results obtained above are in nondimensional form in order to facilitate ease and accuracy of the model development, they are also useful for use in comparing the measurable with the predictions. Consider, for illustration, Eq.(9) and forego the nondimensionality by resolving it for $\dot{m}_{w,total}$, or simply $\dot{m}_w$ in the form,

$$\dot{m}_w = \frac{2}{\sqrt{\pi}}(C_o - C_w)\sqrt{\mathrm{DL}\dot{\mathrm{V}}} \tag{11}$$

All the variables on the right side of the equation are either measureable in an experiment or specified. The mass rate $\dot{m}_w$, of the total transferred substance, Te-complex, is not easily and accurately measurable. However, it is equal to $\sqrt{\dot{\mathrm{V}}}(C_o - C_L)$, where C_L is the concentration at the exit of the channel, (i.e. the concentration in the 'raffinate', a measurable quantity). Equation (11) now takes the form

$$\frac{C_o - C_L}{C_o - C_w} = \frac{2}{\sqrt{\pi}}\sqrt{\frac{\mathrm{DL}}{\dot{\mathrm{V}}}} \tag{12}$$

All the quantities in this equation are known or measurable (except for $C_w$which may be obtained as described in §6). Measurements satisifying this equation fall along a straight line with a slope of unity on a linear graph.

§5. Diffusion in the Entrance Region of a Pipe-flow Boundary Layer:

Use of a flat plate boundary layer mechanism for transport of Te^{4+} in the preceding Section leads to a simple prediction. In this Section, an internal flow approach is examined, as mentioned at the end of §2, the diffusion layer near the entrance of the channel develops into the plug flow of the aqueous feed.

Most of the simplifying assumptions of the earlier sections shall be retained in this section. These assumptions include: the Oseen approximation; the plug flow assumption; ignorable fluid friction in the flow; ignorable effects of gravity, temperature, pressure, and the ceiling/side wall effects; and z-directional effects are absent.

The problem of development of a diffusion boundary into a plug flow in a channel near the entrance is a variant of the Graetz problem in heat transfer (see Kakaç and Yener). The membrane surface represents only a part of the periphery, one of the four sides of the square channel of width a. The other three sides are impervious. Solving diffusion problems with peripherally nonuniform boundary conditions is not unusual (see Shaw and London). The present slow flows into which diffusion is greatly slower permit some useful and reasonable approximations.

The plug flow assumption greatly simplifies the flow in the channel. As shown in Table D-2, the Schmidt number indicates the *entrance length* to be quite large i.e., the diffusion layer is far from fully developed. The absence of fluid friction implied yet again in the plug flow assumption render the possible effects of sidewalls on the diffusion layer growth negligible. In a similar spirit the pressure drop in the channel flow is assumed to be negligible.

As Fig. D-2 shows, the internal flow mechanism suggests that the concentration of the Te-complex in the layer $\delta \leq y \leq a$ above the diffusion layer remains the same as at the inlet. Recall that C_o and C_w are respectively the concentrations at the channel inlet and at the membrane surface. Both are assumed to be constant. The constant difference $(C_o - C_w)$ is nominally the driving force for mass transfer from the stream to the membrane surface. Putting together the diffusion in the feed flow with diffusion across the membrane to the strip side, and adopting a hypothetical mechanism for the

chemistry, C_w can be determined as described below in §6. The constancy of the boundary concentrations is an essential requirement for obtaining and using the error function solution given by Eq. (6a).

§5a. Bulk Concentration in the Channel Flow: The error function solution for the distribution of the Te-comlex concentration will be used in the channel flow problem as well. Repeating Eq. (6a), for convenience,

$$\phi(\eta) = \frac{C_o - C}{C_o - C_w} = 1 - \text{erf}(\eta) \equiv \ erfc\left(\frac{y}{2x}\right)\sqrt{Pe_x}$$

Where $Pe_x = u_o x/D \ and \ u_o = \dot{V}/a^2$ is the feed inlet velocity.

Starting with Eq. (6a) which given the normalized concentration as a function of the composite variable η, the bulk (or mixed mean) concentration $C_B(x)$ is obtained by integrating the $C(y)$ from $y = 0$ to $y = a$ and width normal to the paper a at any x and dividing by the area $u_o a^2$. At the inlet, $C_B(x = 0) = C_o$. The result of this averaging is

$$C_B = \frac{\int_0^a C(y)u(y)(ady)}{u_o a^2} \qquad so \ that \qquad \frac{C_o - C_B}{C_o - C_w} = \frac{1}{\eta_a}\int_0^{\eta_a} erfc(\eta)\ d\eta$$

Here, η_a is η with y set equal to a. The integral can be written as the difference between two integrals, the first one with limits of zero to infinity and the second one with limits of η_a to infinity.

$$\int_0^{\eta_a} erfc(\eta)\ d\eta = \int_0^{\infty} erfc(\eta)\ d\eta - \int_{\eta_a}^{\infty} erfc(\eta)\ d\eta \equiv ierfc(0)\ - ierfc(\eta_a)$$

The second equality in this equation is meant to convey that the first integral of $erfc$ is denoted as $ierfc$, which is tabulated as a function (see Carslaw and Jaeger, pp. 482-485). The argument of $ierfc$ is the lower limit of integration while the upper limit is always infinity. Tables give $ierfc(0) = 1/\sqrt{\pi}$. It is clear that the nondimensional/normalized bulk concentration at any x in the channel length (as embodied within the definition of η_a) is given by

$$\frac{C_o - C_B(x)}{C_o - C_w} = \frac{1}{\eta_a}\left[\frac{1}{\sqrt{\pi}} - ierfc(\eta_a)\right]$$

The equation is more useful in the following slightly modified form which is central to subsequent development.

$$\frac{C_B(x) - C_w}{C_o - C_w} = 1 - \frac{1}{\eta_a}\left[\frac{1}{\sqrt{\pi}} - ierfc(\eta_a)\right] \equiv \{1 - [B(\eta_a) - A(\eta_a)]\} \qquad (13)$$

where, A and B are abbreviations introduced for convenience. The x-dependency of concentration is embedded in η_a. The definitions of these three quantities are as presented below.

$$A(\eta_a) \equiv \frac{ierfc(\eta_a)}{\eta_a}, \qquad B(\eta_a) \equiv \frac{1}{\eta_a\sqrt{\pi}}, \qquad \eta \equiv \frac{a}{2x}\sqrt{\frac{xu_o}{D}}$$

§5b. Total Te^{4+} Mass Transfer Rate $\dot{m}$ Over the Total Length of the Channel: Over a differential length dx along the channel, the Te^{4+} mass flow rate $d\dot{m}$ carried away by the feed flow decreases by $d\dot{m} = \dot{V}dC = a^2u_o dC_B$. Integrating between stations $x = 0$ and $x = L$, $(\dot{m}_o - \dot{m}_L) = a^2u_o[C_B(0) - C_B(L)]$. Denote $(\dot{m}_o - \dot{m}_L)$ by $\dot{m}_{(0-L)}$. This decrease is delivered to the membrane surface at $y = 0$ the area of which is $(aL)\ cm^2$. With the concentration difference from Eq.(13),

$$\frac{\dot{m}_{(0-L)}}{a^2u_o(C_o - C_w)} = [B(\eta_a(L)) - A(\eta_a(L))] \qquad (14)$$

Where A and B are defined above and $\eta_a(L)$ is η_a in which x is set equal to L, i.e., $\eta_a(L) \equiv \frac{a}{2L}\sqrt{\frac{Lu_o}{D}}$.

§5c. Capture Efficacy F: The input rate of Te-complex into the channel at the inlet as in Section §4c is $a^2u_oC_o$ g/s. As before the capture efficiency F can be defined as the ratio of rate of Te4+ mass delivery to the membrane divided by the rate mass input into the feed flow at $x = 0$: $\dot{m}_{(0-L)}/a^2u_oC_o$. Thus,

$$F = \frac{\dot{m}_{(0-L)}}{a^2u_oC_o} = \frac{(C_o - C_w)}{C_o}[B(\eta_a(L)) - A(\eta_a(L))] \qquad (15)$$

If A is very much smaller than B, this result is identical to the F^o in Eq.(10) in §4c, so that the appearance of A represents the difference between diffusion in the channel entry flow and diffusion across the flat plate boundary layer.

The implications of this observation are of considerable interest. At $\eta_a(L) = 1$, ignoring A in comparison to B will cause a 10.3% error in $[1 - B + A]$. At $\eta_a(L) \geq 1.4$, the error will be $\leq 1\%$. Based on these calculations, it appears acceptable to ignore A in Eq.(15) when $\eta_a(L) \geq 1.4$. This means, when channel size a and feed flow speed u_o are large while diffusivity D and channel length L are small, then $A \ll B$ and the predictions of diffusion rate and efficacy of transport to the membrane are identical in the external and internal boundary layer models.

§5d. Mass Flux to the Membrane Surface, $\dot{m}"(x)$, $(g/cm^2\ s)$: The mass flux of Te^{4+} reaching the membrane surface as a function of x, the location in the flow direction, is

needed in the determination of local mass transfer coefficient, h_D. As will be shown in §6, this coefficient in its own turn is required to obtain the concentration C_w of Te^{4+} at the membrane surface.

The Te^{4+} mass content in the bulk feed flow decreases with x in the feed stream. Over a differential increase of x by dx, the differential change in the bulk concentration is $dC_B(x)$. The corresponding differential Te-complex mass transfer to the membrane surface is $-d\dot{m}(x) = \dot{V}dC_B(x)$. Dividing both sides of this result by the differential membrane surface area $a \cdot dx$ receiving this diffused mass and recalling that $\dot{V}$ is a^2u_o, the mass balance equation takes the form $d\dot{m}''(x) = au_oC_B(x)/dx$. The symbol $\dot{m}''(x)$ stands for the local mass flux. Using Eq. (13) to arrive at $dC_B(x)/dx$ and A and B as defined for Eq.(13), the surface mass flux distribution is obtained. This result can be written in four different forms, each convenient in different contexts of its use.

$$\frac{\dot{m}''(x)}{u_o(C_o - C_w)}\frac{x}{a}\frac{2}{\eta_a} = \frac{d}{d\eta_a}(1 - [B(\eta_a) - A(\eta_a)]) \tag{16}$$

Upon differentiation of the right hand side,

$$\frac{\dot{m}''(x)}{u_o(C_o - C_w)}\frac{2x}{a} = [B(\eta_a) - A(\eta_a)] - erfc(\eta_a) \tag{17}$$

Equation (17) can now be written in two forms: first, multiplying and diving the right had side by η_a and multiplying both side of the result by $a/2x$, one obtains

$$\frac{\dot{m}''(x)}{u_o(C_o - C_w)} = \frac{1}{\sqrt{Pe_x}}\left(\left[\frac{1}{\sqrt{\pi}} - ierfc(\eta_a)\right] - \eta_a erfc(\eta_a)\right) \tag{18}$$

where the definition of the Peclet number Pe_x is defined as xu_o/D. The two terms related to the error function in this result become close to zero when $\eta_a \geq 1.4$. This result is precisely the same as Eq. (8). The second manipulation of Eq. (17) calls for a replacement of $[B(\eta_a) - A(\eta_a)]$ by the concentration ratio according to Eq. (13),

$$\frac{\dot{m}''(x)}{u_o(C_o - C_w)}\frac{2x}{a} = 1 - \frac{C_B(x) - C_w}{C_o - C_w} - erfc(\eta_a) = erfc(\eta_a) - \frac{C_B(x) - C_w}{C_o - C_w} \tag{19}$$

§5e. Local Mass Transfer Coefficient $h_D(x)$ and the Sherwood Number $Sh_a(x)$: Let the local mass transfer coefficient $h_D(x)$ be defined as the local species mass flux $\dot{m}''(x)$ (from the preceding subsection) divided by the difference (see Eq. (13)) between the local bulk concentration $C_B(x)$ and constant concentration C_w at the membrane surface $y = 0$.

$$h_D(x) \equiv \frac{\dot{m}''(x)}{C_B(x) - C_w} \tag{20}$$

The units of $h_D(x)$ are cm/s. Multiplying and dividing the left side of Eq. (19) by $(C_B(x) - C_w)$, eliminating the mass flux from the result by substituting this definition of mass transfer coefficient, and writing out the ratio of concentration differences in terms of η_a by invoking Eq. (13), the following result is reached.

$$\frac{h_D(x)}{u_o} = \frac{a}{2x}\left\{-1 + \frac{\text{erf}(\eta_a)}{1 - \frac{1}{\eta_a}\left[\frac{1}{\sqrt{\pi}} - ierfc(\eta_a)\right]}\right\} \tag{21}$$

The ratio h_D/u_o on the left side of Eq. (21) is nondimensional and it can be called the local mass transfer Stanton number, $St_D(x)$. Equation (21) can be integrated with respect to x to determine the mass transfer coefficient averaged over the length of the surface. This matter will be further discussed in §6.

The local Sherwood number is defined as $Sh_a(x) \equiv ah_D/D$. Here, the subscript a is to indicate that the hydraulic diameter a of the channel is the characteristic length. The x in parenthesis indicates that h_D is local. Equation (21) adapted to the Sherwood number is

$$Sh_a(x) = \frac{au_o}{D}\left(\frac{a}{2x}\right)\left\{-1 + \frac{\text{erf}(\eta_a)}{1 - \frac{1}{\eta_a}\left[\frac{1}{\sqrt{\pi}} - ierfc(\eta_a)\right]}\right\} \tag{22}$$

Clearly, the Stanton number is a ratio of the Sherwood number to Peclet number.

$$St \equiv \frac{Sh}{Pe} = \frac{\frac{h_D a}{D}}{\frac{au_o}{D}} = \frac{h_D}{u_o}$$

These relationships between the Sherwood, Peclet and Stanton numbers have been used extensively in correlations of experimental data in the fields of heat and mass transfer.

§6. Coupling of Diffusion in the Feed with Diffusion Across the SLM: The error function solution is central to the analysis described in this Appendix. There are two very important requirements which have to be met for the existence of an error function solution to be steady as well as unsteady, heat and mass transfer problems in very thick media. Both these requirements relate to the boundary conditions.

First, diffusion occurs from the bounding surface, $y = 0$, of the medium which is stationary or steadily flowing. The extent (or thickness) of the medium in the y direction has to be infinite, i.e., a semiinfinite medium has only one boundary at $y = 0$). There is a large Schmidt number, as estimated in §2 of this Appendix, implying a slow growth of the diffusion layer thickness (in the flow direction) so that the layer thickness is substantially smaller than the channel height $y = a$ even in the microchannel. It is safe to assume that the medium is *semiinfinite* when the magnitude of the Schmidt number is in the hundreds or thousands, as is the case with diffusion in the aqueous phase.

Even a more important requirement for the validity of applying the error function solution in description of species (or heat) diffusion into a semiinfinite medium is the uniformity and constancy of concentration at the boundary $y = 0$ (the error function solution is not as simple as Eq. (6a) if the surface boundary condition involves a time-dependent concentration or a constant or time-dependent but uniform concentration gradient boundary condition). The concentration C_w at the membrane surface throughout the analysis here has been assumed to be constant and uniform. Prior to further dealing with this requirement, it is appropriate to recall the resistance analogy of the overall transport process.

§6. Resistance Analog: There are two diffusive resistances and one membrane chemistry hypothesis that are of concern. These pertain to: (i) diffusion of the Te-complex across the feed fluid boundary layer under the driving potential difference of $(C_\infty - C_w)$ and with resistance equal to the inverse of mass transfer coefficient, h_D, a function of x from Eq. (8) for diffusion according to the flat plate boundary layer analysis presented in §4 and from Eq. (21) for diffusion according to the analysis of plug-flow in a channel presented in §5. The subscript ∞ stands for the inlet (subscript o), (a constant with respect to x) in the boundary layer diffusion. It stands for the bulk concentration C_B, (a function of x as given by Eq. (13)) in the channel flow diffusion. By the conclusion of this article, it will be evident that C_w is directly proportional to C_∞ so that the driving potential in the boundary layer analysis $(C_o - C_w)$ is independent of x. In contrast, in the channel flow analysis, it is proportional to $C_B(x)$ and so varies decreasingly with x. The concentration C_w is an unknown at this point, but assumed all along to be lower than C_∞ and a uniform constant.

The diffusive flux arriving at the feed side surface of the membrane is, hence,

$$\dot{m}'' = h_D(x)(C_\infty - C_w(x)) \tag{23}$$

(ii) The second resistance of concern pertains to the feed side surface of the membrane. As the tetrachloro-Te^{4+} reaches the feed side surface of the SLM it encounters two phases of the membrane, the organic phase methyl isobutyl ketone (MIBK) (which is the carrier diffusing across the membrane) and the aqueous phase.

The proportions of the Te-complex taken up by the membrane is determined by thermodynamic equilibrium in which the chemical potential of all the phases is the same. A membrane parameter known as the Distribution Constant, denoted by M, modifies the constant coefficient of diffusion k_M (the subscript M identifies that rate constant k is that of the membrane) of the carrier by multiplication. Thus, with C_{ws} denoting the strip side concentration, (subscript s is for strip side and subscript w is for the surface), the diffusive flux across the membrane is

$$\dot{m}'' = Mk_M(C_w(x) - C_{ws})$$

k_M is given by D_M/b where D_M is the diffusivity of the Te-complex in MIBK and b is the membrane thickness.

(iii) The third concern relates to a membrane chemistry hypothesis. Upon diffusing to the strip side surface the carrier MIBK releases its cargo, the tetrachloro Te-complex into the certified blank, strip aqueous phase. The pH of the strip phase flow makes the tetrachloro complex undergo an instantaneous and irreversible transformation to a dichloro Te-complex, which cannot be taken up by MIBK in the membrane to transport it to the feed side. The dicholoro Te-complex is carries away in the strip flow. This has two consequences: first, diffusion on the strip side of the tetrachloro Te-complex is not a rate controlling step, and second $C_{ws} \approx 0$. The foregoing equation is thus simplified to

$$\dot{m}'' = Mk_M C_w(x)/b \tag{24}$$

Combining Eqs.(23) and (24) to eliminate the mass flux, and rearranging, one obtains C_w the feed side surface concentrations as

$$C_w(x) = \frac{H}{1+H} C_B(x) \quad where \quad H = \frac{bh_D}{MD_M} \tag{25}$$

where H is the ratio of the membrane resistance to the feed phase diffusion resistance. Whereas the former is a constant, the later is dependent on x through $h_D(x)$.

One approach to solving this problem is to consider averaging $C_w(x)$ from Eq. (25) over the membrane length. Another approximation is to average h_D and C_B over the membrane length. Let their averages be denoted by $\bar{h}_D$ and $\bar{C}_B$. With these values, Eq. (25) yields an average value $\bar{C}_w$ for use in the results [Eq. (7), (9), (10), and (12)] of the boundary layer analysis and [Eq. (13)-(15) and (17)-(22)] of the flow analysis. There are enough uncertain aspects of the properties and the processes of separation, diffusion, and recovery of tellurium that this averaging is not unreasonable. Only comparison of the experimental measurements with the predictions of this analytical approach will validate the models, as well as the experiments, to reveal insight for future research.

E - Dimensionless Number Definitions

The dimensionless numbers used in fluid and diffusion analysis are defined in Table E-1. The Reynolds number in the duct or channel Re_d, is consistent with usage in Shaw and London [58].

Table E-1 Dimensionless Numbers Defined

Dimensionless Number	Equation
Sherwood Number	$\mathrm{Sh} = \frac{kl}{\mathrm{D}}$
Schmidt Number	$\mathrm{Sc} = \frac{\nu}{\mathrm{D}}$
Reynolds Number for Plate	$Re_L = \frac{vl}{\nu}$
Reynolds Number for Duct	$\mathrm{Re}_d = \frac{vd_h}{\nu} = \frac{v\,4A_c}{\nu\,\mathrm{P}}$
Peclet Number	$Pe_L = Re_L \mathrm{Sc} = \frac{vl}{\mathrm{D}}$
The equation variables follow; k is the mass transfer coefficient, l is length, D is the diffusion coefficient, ν is kinematic viscosity, v is velocity. The hydraulic diameter $d_h = 4A_c/P$ for a cross sectional area of the duct A_c and its wetted perimeter P [58], $d_h = a$ for the square cross section duct used in experiments.	

F - Dimensionless Number Calculations

The value of the Schmidt, Reynolds, and Peclet numbers for various experimental flow rates and media are shown in Table F-1 and Table F-2.

Table F-1 Schmidt, Reynolds, and Peclet Numbers for Straight Channel

Solvent	Solute D cm^2/s	Solvent v cm^2/s	Sc Number v/D	Channel a cm	Flow Rate ml/min	Velocity v cm/s	Re_a Number a*v/v	Channel L cm	Re_L Number L*v/v	Pe_L Number L*v/D
					Flow Rate 1					
Strip	5.44E-06	0.0101	1847	0.05	0.01	0.067	0.332	3.7	24.5	45341
Feed	4.67E-06	0.0126	2698	0.05	0.01	0.067	0.265	3.7	19.6	52851
SLM	6.15E-06	0.0075	1219	0.05	0.00	0.000	0.000	3.7	0.00	
					Flow Rate 2					
Strip	5.44E-06	0.0101	1847	0.05	0.02	0.133	0.663	3.7	49.1	90682
Feed	4.67E-06	0.0126	2698	0.05	0.02	0.133	0.530	3.7	39.2	105703
SLM	6.15E-06	0.0075	1219	0.05	0.00	0.000	0.000	3.7	0.00	
					Flow Rate 3					
Strip	5.44E-06	0.0101	1847	0.05	0.03	0.200	0.995	3.7	73.6	136022
Feed	4.67E-06	0.0126	2698	0.05	0.03	0.200	0.794	3.7	58.8	158554
SLM	6.15E-06	0.0075	1219	0.05	0.00	0.000	0.000	3.7	0.00	

Table F-2 Schmidt, Reynolds, and Peclet Numbers for Serpentine Channel

Solvent	Solute D cm^2/s	Solvent v cm^2/s	Sc Number v/D	Channel a cm	Flow Rate ml/min	Velocity v cm/s	Re_a Number a*v/v	Channel L cm	Re_L Number L*v/v	Pe_L Number L*v/D
					Flow Rate 1					
Strip	5.44E-06	0.0101	1847	0.05	0.01	0.067	0.332	12.9	85.6	158080
Feed	4.67E-06	0.0126	2698	0.05	0.01	0.067	0.265	12.9	68.3	184266
SLM	6.15E-06	0.0075	1219	0.05	0.00	0.000	0.000	12.9	0.00	
					Flow Rate 2					
Strip	5.44E-06	0.0101	1847	0.05	0.02	0.133	0.663	12.9	171.1	316160
Feed	4.67E-06	0.0126	2698	0.05	0.02	0.133	0.530	12.9	136.6	368531
SLM	6.15E-06	0.0075	1219	0.05	0.00	0.000	0.000	12.9	0.00	
					Flow Rate 3					
Strip	5.44E-06	0.0101	1847	0.05	0.03	0.200	0.995	12.9	256.7	474240
Feed	4.67E-06	0.0126	2698	0.05	0.03	0.200	0.794	12.9	204.9	552797
SLM	6.15E-06	0.0075	1219	0.05	0.00	0.000	0.000	12.9	0.00	

G - Inductively Coupled Plasma (ICP) Methods

A. The intensity of the wavelengths for Tellurium State I line 225.902 nm, Cadmium State I line 228.802 nm, and Indium State I line 325.609 nm are measured on the ICP. Other wavelengths are not measured. The exact locations of these wavelengths are verified by linear correlations between the standards and ICP intensity measurements in accordance with Beer's Law. For example, given the element In in Fig. G-1, the peak in the spectrum shrinks with decreasing concentration of In, while surrounding noise peaks remain static. The screen shot Fig. G-1 shows the In λ=325.609 nm peak changes with intensity at the wavelength λ=325.576 nm. The surrounding peaks are noise.

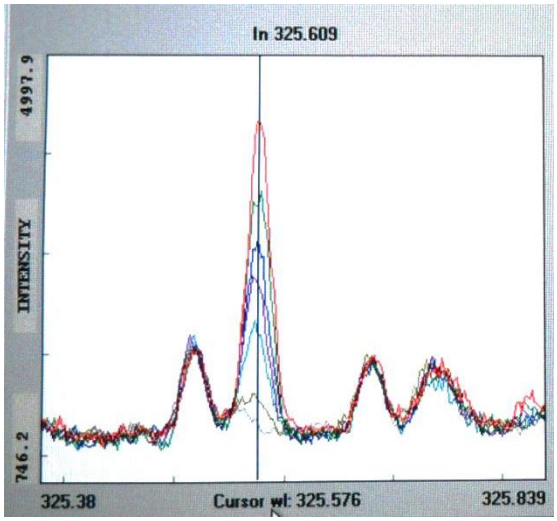

Fig. G-1 Indium 325.609 nm scan varies with concentration at 325.576 nm.

B. Each vial of ICP sample solution (calibration or experimental test dilution) is shook by hand with five brief up and down motions prior to aspiration of fluid by

the ICP. This was done to prevent sample stratification and improve the average and standard deviation.

C. The ICP method is set to sample each solution vial 10 times and report an average intensity reading for the sample vial. This uses about 5 ml of standard solution for each intensity measurement.

D. The Eppendorf pipette set and eptips are used all small volume measurements. The scale is used for large volume measurements (for example ACS acid flush solution dilutions).

E. A certified High Purity Standard HCl 2% blank solution is used for matrix when diluting standard solutions and for blanks.

F. Routine flushing is done between samples and batches.

    a. An ACS grade 2% HCl matrix (diluted in the PNNL lab) is used to wash the ICP peristaltic tubing between samples.

    b. An ACS grade 2% nitric acid matrix is used to wash the ICP peristaltic tubing at the beginning and end of each batch of samples.

G. The routine calibration points for Cd and Te are 0, 400, 600, 800, 1000, 1500, 2000, and 3000 ppb. The calibration solutions were prepared from stock solutions (dilutions of the ordered standards). A peak search standard with 6000 ppb Cd/Te/In was prepared to find peaks when creating the method in the ICP. There is some variation in test points between experiments and not all points

were required for every calibration. The formula for mixing test solutions for calibration points is shown in Table G-1.

Table G-1 Calibration Solution Preparation Volume

Calibration Series Preparation	End Concentration Cd/Te µg/l (ppb)	HPS* 2% HCL Blank (ml)	Internal Standard (IS) End Concentration Indium µg/l (ppb)	IS Stock Soln (ml)	Suplemental Solution Source	Suplemental Solution Volume (ml)	Total Mixed Volume (ml)
Te/Cd Stock Soln	100000	2	0	0	**Std Soln Cd & Te	0.25	2.5
IS Stock Soln	100000	4.5	0	0	HPS In Std Soln	0.5	5
Standard PS***	6000	4.4	6000	0.3	Te/Cd Stock Soln	0.3	5
Standard 1	6000	4.6	2000	0.1	Te/Cd Stock Soln	0.3	5
Standard 2	3000	4.75	2000	0.1	Te/Cd Stock Soln	0.15	5
Standard 3	2000	9.6	2000	0.2	Te/Cd Stock Soln	0.2	10
Standard 4	1500	9.65	2000	0.2	Te/Cd Stock Soln	0.15	10
Standard 5	1000	4.85	2000	0.1	Te/Cd Stock Soln	0.05	5
Standard 6	800	4.86	2000	0.1	Te/Cd Stock Soln	0.04	5
Standard 7	600	9.74	2000	0.2	Te/Cd Stock Soln	0.06	10
Standard 8	400	4.88	2000	0.1	Te/Cd Stock Soln	0.02	5
Standard 9	0	4.9	2000	0.1	Te/Cd Stock Soln	0	5
Blank	0	10	0	0	Te/Cd Stock Soln	0	10
Abbreviations: *HPS - High Purity Standards, **Std Soln - Standard Solution (Ordered), *** PS - peak search							

H. Internal standard methodology is used for ICP experimental work.

   a. All test solutions are uniformly spiked with a 2000 ppb of In during preparation of samples and calibration solutions.

   b. A blank with an In spike of 2000 ppb was also prepared (for a zero point in the intensity ratio calibration plot).

I. ICP solution test order is varied to prevent order dependence in results.

   a. The calibration solutions are tested in a random order which varies from experiment to experiment.

b. The experimental samples are tested in a random order inside small batches as the batch is completed.

c. A calibration test solution is run with each batch of experimental samples to monitor drift during ICP operation. This test solution is included in the calibration points for the regression prepared for the day's results.

J. Test solutions were diluted to prevent oversaturation of the ICP that might lead to high readings in subsequent tests. Dilutions were aimed to test for concentration over the ICP's most reliable range (between 400 ppb and 2500 ppb). The dilutions factor, referred to as d, is the amount the sample is diluted from the original experimental material. For example, a dilution factor of 333, means that the preparation was diluted to 333 times the original experimental concentration. Often, the correct dilution was not known for a sample, so several dilutions were prepared and tested in the ICP. The dilution factors commonly used in experiments were 10, 50, 100, and 333. A table showing the volumes of solutions used to create dilutions is shown in Table G-2.

Table G-2 Experimental Sample Dilution Test Solution Volume

Experimental Sample Dilution	Final Dilution Factor	HPS Blank ml	Internal Standard Concentration µg/l (ppb)	In Stock ml	Sample Volume ml	Total Volume ml
Feed Tests - 333x	333	4.88	2002	0.1	0.015	4.995
Raffinate Tests -333x	333	4.88	2002	0.1	0.015	4.995
Strip Tests - 100x	100	4.85	2000	0.1	0.05	5
Strip Tests - 50x	50	4.8	2000	0.1	0.1	5
Strip Tests - 10x	10	4.4	2000	0.1	0.5	5

K. ICP test solution average intensity measurement and standard deviation is reported by the ICP and recorded by the operator in the lab notebook in ink. The ICP software was not used for data manipulation to prevent loss of information (critical digits). The intensity average and standard deviation of each measurement was entered into a spreadsheet in Excel manually.

L. The data is managed in Excel software to yield regressions.

   a. The data is used to calculate the intensity ratio of Te:In and Cd:In at each calibration point.

   b. The intensity ratio is scaled (to prevent loss of digits) via multiplication (of the ratio) by the integer 10,000.

   c. The data is plotted with the analyte (Cd or Te) concentration as prepared from the standards on the x axis. The scaled intensity ratio (from ICP intensity data) is plotted on the y axis.

   d. A linear regression of the plot is generated in Excel. The y-intercept of the regression is set manually as the lowest data point (created by the blank solution).

   e. The general linear equation y=mx+b created by the regression, is interpreted as; $Intensity_{Te}/Intensity_{In} = m \cdot Concentration_{Te} + b$. This regression is used to find unknown concentrations of Te where both the $Intensity_{Te}$ and $Intensity_{In}$ are known from reported intensity measurements taken on the ICP.

M. The data is managed in Excel software to calculate experimental concentration values. Experimental analyte concentration results are calculated in Excel software from the regression equation expression G.1 where $I_{Te}$is the sample measured Te intensity, I_{In} is the sample measured In intensity, 10,000 is the scaling factor, b is the regression intercept, and m is the regression slope, and d is the dilution factor of the sample.

$$C_{Te} = \left[\frac{\frac{I_{Te}}{I_{In}} \cdot 10{,}000 - b}{m}\right] \cdot d \qquad (G.1)$$

N. The data is managed in Excel software to yield uncertainty.

   a. Error intervals for each data point are reported using a one sided confidence interval t-table function in Excel. The function *confidence.T(c, s, n-1)* was called upon to calculate an error interval for each sample's average measurement (from 10 sample measurements made upon a single vial) as reported by the ICP with the corresponding standard deviation. The chosen confidence interval was c=0.01 to report the 99% confidence interval. The standard deviation, s, for each average intensity measurement is reported by the ICP software. The number of intensity samples measured by the ICP is programmed to n=10 in the ICP operation software. In the t-table function, n-1 = 9 is used to calculate the confidence interval. T-table confidence interval calculation for both

calibration points and experimental samples are handled in the same fashion.

b. Error bars were added to the calculated internal standard ratio calibration plots using expression G.2, where RCI is the regression confidence interval (for the calculated value), u_1 is the t table uncertainty interval of the analyte (Te or Cd) signal, u_2 is the t table uncertainty of the internal standard (In) signal, p is the average intensity of the analyte (Te or Cd) signal, and q is the average intensity of the internal standard (In) signal.

$$RCI = \pm\sqrt{\left[\left(\frac{u_1}{p}\right)^2 + \left(\frac{u_2}{q}\right)^2\right]} \qquad (G.2)$$

c. Overall regression error, UR, in the analyte calculated regression concentration, $Y_{Regression}$, is addressed by accounting for the cumulative error resulting from the ratio of analyte to internal standard as a percentage of the calculated regression value. This permits determination of relative error for extrapolated points in the regression. Thus expressed as G.3, the overall regression confidence interval regression is,

$$UR = \pm\frac{RCI}{Y_{Regression}} \cdot 100\% \qquad (G.3)$$

d. The overall confidence interval for experimental data, U, was expressed as a function of both the regression error and as a function of the

standard deviation corresponding to the individual data point. This permitted reporting of error bars for each experimental data point according to expression G.4, where U is the calculated experimental data concentration confidence interval, u_1 is the t table uncertainty interval of the analyte (Te or Cd) signal, u_2 is the t table uncertainty of the internal standard (In) signal, p is the average intensity of the analyte (Te or Cd) signal, and q is the average intensity of the internal standard (In) signal.

$$U = \pm\sqrt{\left[\left(\frac{u_1}{p}\right)^2 + \left(\frac{u_2}{q}\right)^2 + (UR)^2\right]} \qquad (G.4)$$

O. The ICP method detection limit (MOD) is defined by the EPA to be the "minimum concentration of a substance that can be measured and reported with 99% confidence that the analyte concentration is greater than zero and is determined from analysis of a sample in a given matrix containing analyte" [59]. The same EPA report specifies that the MOD may be estimated as the calculated concentration at the intensity three standard deviations above the intensity of a blank signal. Using this method, for the day 08/27/2012 the MOD is estimated to be 10 ppb for the element Cd. On the same day, the MOD for Te is estimated to be 92 ppb. The standard deviation of the blank on this day is fairly representative of typical results. Concentration results below the MOD for a given element fall outside the 99% confidence interval, and may be less reliable

than those at or above the MOD. However, Dilutions were aimed to test for concentration over the ICP's most reliable range (from 400 ppb and 2500 ppb)

P. An example of calibration data, regression plots, and experimental data made for the day August 27, 2012 is put forth here for review in the sequence generated. A calibration data table demonstrating preliminary calculations for regression is shown in Table G-3. A calibration regression plot for Cd is shown in Fig. G-2. The same calibration regression methodology, as applied to Te, is shown in the regression plot of Te found in Fig. G-3. An experimental data table demonstrating a sample of data recorded and the subsequent concentration calculation is shown in Table G-4.

Table G-3 Calibration Data/Preliminary Calculations 08/27/2012

Concentration		Intensity ($\bar{y}$) & Standard Deviation (S)						99% Confidence			Intensity Ratio (IR)			
Analyte	In	Cdλ=228.802		Teλ=225.902		Inλ=325.609		Cd	Te	In	Analyte/IS*10000		99% Confidence	
ppb	ppb	$\bar{y}$	S	$\bar{y}$	S	$\bar{y}$	S	error t table			Cd/In	Te/In	Cd/In	Te/In
1000	2000	4726	238	968.2	25.1	6936	283	266	28	317	6814	1396	493.94	2.040
3000	2000	12370	502	1629	19	9342	89	561	21	100	13241	1744	617.35	0.247
400	2000	2157	15	664.3	12.7	8468	76	17	14	85	2547	784	32.35	0.219
800	2000	3845	54	826.4	12.4	8597	59	60	14	66	4472	961	78.19	0.164
0	2000	497.1	13	540.7	10.9	8468	67	15	12	75	587	639	17.94	0.187
6000	2000	25170	391	2665	26	8968	49	437	29	55	28066	2972	516.93	0.232
800	2000	3549	40	792.8	15.4	8326	76	45	17	85	4263	952	69.15	0.274
400	2000	1975	33	661.4	13.4	8287	67	37	15	75	2383	798	49.48	0.238
1000	2000	3635	32	814	17.8	8889	52	36	20	58	4089	916	48.34	0.293

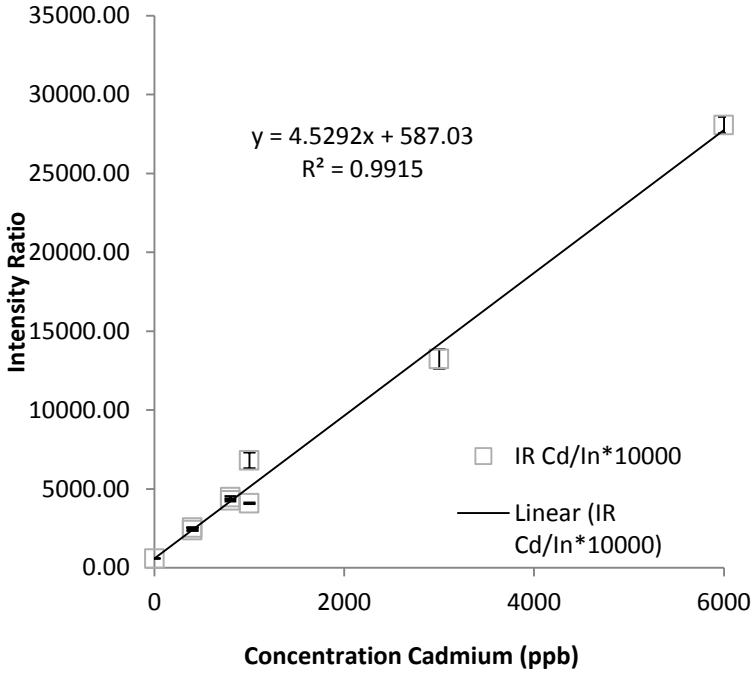

Fig. G-2 Calibration regression plot for Cd ratio to In on 08/27/2012 data

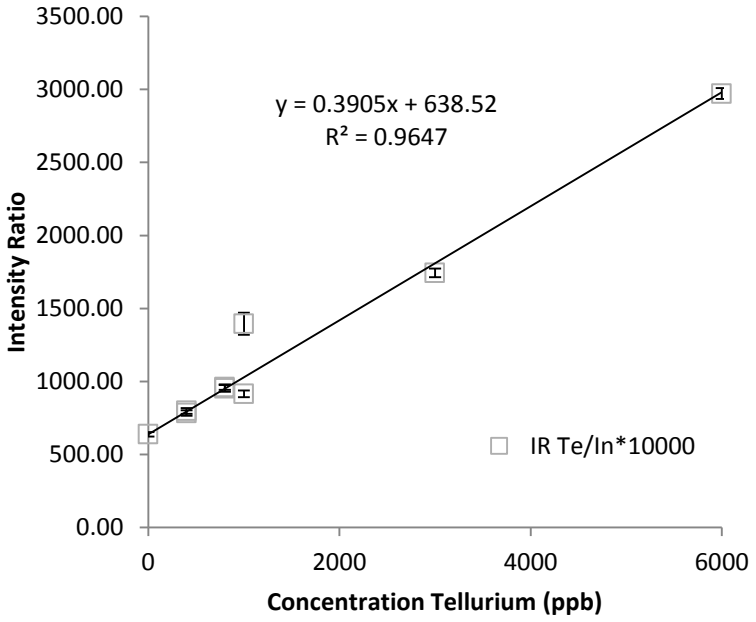

Fig. G-3 Calibration regression plot for Te ratio to In on 08/27/2012 data

Table G-4 Sample Data/Concentration Calculations 08/27/2012

Sample Name	Intensity of Signal (ȳ) and STD (S)							99% Confidence Interval			Concentration with IS Methodology			
	Cdλ=228.802		Teλ=225.902		Inλ=325.609		Dilution	Cd	Te	In	Regression		Final (*Dilution)	
	ȳ	S	ȳ	S	ȳ	S	Factor	conf_t	conf_t	conf_t	Cd (ppb)	Te (ppb)	Cd (ppb)	Te (ppb)
TF2200-333x	10080	76	1466	15	8564	80	333	85.00	16.78	89.48	2469	2749	822219	915257
TF2200-333x	12140	91	1681	19	8501	36	333	101.78	21.25	40.26	3023	3429	1006797	1141746
T11F2200-333x	10760	105	1546	10	8415	61	333	117.44	11.18	68.23	2694	3070	896955	1022174
T11F2200-333x	12290	94	1700	22	8285	70	333	105.14	24.61	78.29	3146	3619	1047482	1205265
T11Raf-333x	24750	186	2845	28	8513	57	333	208.03	31.32	63.75	6289	6923	2094385	2305356
T11Raf-333x	12310	110	1715	16	8245	71	333	123.03	17.90	79.41	3167	3691	1054556	1229268
T11Raf-333x	10520	67	1547	10	8207	67	333	74.94	11.18	74.94	2701	3192	899281	1062919
T11Strip-50x	3364	44	811.3	15.6	7982	78	50	49.21	17.45	87.24	801	968	40045	48386
T11Strip-10x	13690	118	1840	13	7302	80	10	131.98	14.54	89.48	4010	4818	40098	48178

In Table G-4, an explanation of the sample names is; TF2200 stands for test feed 2154 (2200 designates the approximate concentration of Te plus Cd); T11F stands for Test Feed 11; T11Raf stands for Test 11 Raffinate; T11Strip stands for Test 11 Strip. The number after the dash on the sample name indicates the dilution factor.

H - ICP Standard Operating Procedure

1) For questions not addressed in Standard Operating Procedure please refer to loose leaf manual stored on top shelf of ICP cart (located on East wall of Fab Lab) titled AtomScan 16/25 Spectrometers Operator's Manual Part Number 127183-02 Copyright 1991 by Thermo Jarrell Ash Corporation.
2) Turn on ICP 24 hours prior to measurements to insure the optic system is steady state.
    a. Turn on power supply (standing behind the computer monitor) – toggle red bar switch to up position.
    b. Turn on ICP (inside door at ICP right end). Press red power switch up to on position. Toggle five metal dip switches to up position. Small red light on the front of ICP should light up if ICP is on.
3) Ignite torch plasma 15-30 minutes prior to measurements to insure steady state.
    a. Open Argon gas feed line
        i. Confirm Argon tank indicator is full, not empty. If needle reads empty, gently jar tank to get needle to move. If tank still reads empty email Neill for a replacement.
        ii. Open green knob on top of big Argon tank until it won't turn anymore
        iii. Open valve below dial until gauge reads 60 psi.

b. Open Nitrogen gas line on piped building supply source behind the ICP. If the arrow is pointing down the N2 line is open. If the arrow is pointing to the left, the N2 line is closed.

c. Prepare fluid to flush through peristaltic pump and nebulizer.

    i. Dilute an ACS grade nitric acid to 2% with UHP water.

    ii. Place the diluted nitric acid flush solution in a clean LDPE or HDPE 125 ml bottle with a small hole punched in the cap.

    iii. Thread the rigid amber peristaltic feed tube through the hole in the bottle's cap.

    iv. Set the feed solution in the ICP hood taking care to insure the bottle will not tip over causing a spill during operation.

    v. Place the peristaltic pump exit tube in an empty beaker to contain waste.

    vi. Cover the waste beaker with paraffin or place inside ICP hood. Follow lines to confirm all liquid will be contained. Used secondary containment if needed.

d. Strike an arc in torch.

    i. Double click on the desktop icon titled *Atomscan 16 ICP Start Batch File* to open the ICP control panel (if not already open on desktop).

ii. A warning usually comes up on monitor “Some or all the lines in the method have not yet been peak searched. Peak search now?” Click the button “No”. A peak search is not possible at this time as the ICP torch is not burning.

iii. Click the flame symbol on the action shortcut bar to open the Plasma Control Panel.

iv. If ICP control panel “Establishing Communication Bar” readings are “Controller ready” and “RF supplies are on” both in blue letters then the ICP is ready to ignite. However, if the Plasma Status is “Argon pressure error” in red letters then the Argon supply needs to be corrected prior to igniting the ICP.

v. Click the flame picture button “Ignite” on the Plasma Control Panel. A window opens up in the bottom right of the screen “Ignite Plasma”. The following default settings are generally acceptable;

    1. PF Power 1150 watts (pump power)
    2. Auxiliary Flow 0.5 1/min
    3. Nebulizer Flow 0.6 1/min
    4. Pump Rate 100 rpm
    5. Purge time 90 sec (after first purge it’s ok to purge for 10s)

vi. Click the “Ok” button to accept default settings or the settings of your preference.

vii. The peristaltic pump starts a 90 second purge. Thereafter the torch strikes an arc for ignition. Generally the first time the torch is lit in a given day, it immediately extinguishes itself. If this occurs, permit the torch to cool a few minutes before repeating the ignition steps v.-vii. The second time a torch is lit it seems to be quite steady unless the peristaltic tubing is not emptying correctly (an accumulation of fluid in the nebulizer chamber can cause a splashing of liquid up into the torch that will prevent the torch from burning for days thereafter if not addressed).

e. Let plasma burn for 15 minutes to warm up. Visually check torch periodically to confirm it is on and burning steady.

f. Close the “Plasma Control Window”.

4) Prepare ICP calibration solutions during down time while torch is warming.

a. Draw up a calibration plan. Expect to use 5ml-15ml of calibration solution for each calibration point. Calibration solutions should be less than 10 ppm to avoid saturation of the equipment. Prepare 10-20ml of high standard in the range of 3-6 ppm for a peak search to identify the correct spectral peak for element if it has not recently been peak searched.

b. Label each centrifuge vial or clean HDPE/LDPE bottle with calibration solution concentrations and a number. For example; “Standard 1 – 500 ppb Cd/Te” and “Blank – 0 ppb”.

c. Pull needed clean items out of drawers before putting on dirty acid gloves that might contribute contamination.

d. Don safety equipment; lab coat, apron, nitrile gloves, acid gloves, and goggles over glasses. Lay down clean bench paper on work surface to avoid contamination of materials.

e. Carefully pour 50 ml of Certified HCl 2% Blank Matrix into a clean HDPE/LDPE bottle for pipetting. Replace caps on both bottles.

f. Carefully pour 3-5ml of each needed certified standard solution into a new disposable 25 ml beaker. Replace caps on all bottles.

g. Use the large electric pipette with a new tip to draw and transfer needed volumes of Certified HCl 2% Blank Matrix from pipetting bottle to centrifuge vials. Do not lay the electric pipette down on the counter between jobs. Expel the tip into a waste bag and return to pipette stand.

h. Use the small electric pipette with a new tip to draw and transfer needed volumes of Certified Standard Solutions from disposable 25 ml beaker to centrifuge vial. Do not dip the tip into the matrix in the centrifuge vial. Change the tip between each different elemental Standard Solution.

i. For an internal standard, add spike to centrifuge vials (including the blank) last. Carefully keep track of which vial the last spike went into for the purpose of avoiding mistakes.

j. Dilute an ACS grade HCl acid to 2% to run between samples as a flush.

k. Pour 50 ml UHP grade water into a small clean bottle for flushing out the peristaltic pump lines.

l. Pour excess poured solutions into bottle labeled “Acid Working Solution”.

m. Place calibration solutions/tray in secondary containment to walk to wet lab.

n. There is no need to filter calibration solutions as they are certified materials. However, keep in mind that unknown samples must be filtered with a 0.2 micron filter prior measurement on the ICP to avoid occluding the tiny nebulizer nozzle.

5) Return to ICP and Review Method

a. Click on “Method” then “Open” to use a previously created method or “New” to create a new method.

b. Click on “Setup” and “Elements” to add elemental wavelength lines to the method. For example, to add tellurium, double-click on Te in the elemental table until it turns cyan. Then double click each desired wavelength to add a check beside the wavelength. After all needed wavelengths are added, click “OK”. A warning message “All new lines in a

method should be peak searched prior to standardization or analysis" will appear on screen after changes are made – click "OK".

c. Click on "Setup" and "Standards" to add calibration solutions to method. Add standard labels from highest calibration concentration (Standard 1) to lowest calibration concentration (Blank). Click on each standard to confirm the concentration and lines are correct. Edit as needed then click "Ok".

d. Click on "Setup" and "Internal Standards" to add an internal standard correction. Click on the button "Sel. Int Stds" to select the internal standard element and wavelength – double click the desired element until it turns cyan and then double click the desired wavelength – before clicking "Ok". Now click on the element wavelength line added under "None". Select the elements to reference to the internal standard. Click "Ok".

6) Correctly identify elemental spectral peaks with Peak Search.

a. Open the vial containing the high standard or peak search solution and place amber tube in sample beaker.

b. Click on "Setup" and "Peak Search". Click on "Standard 1" to highlight and then the "Run" button. [Note: Remember to close "Plasma Controller Panel" window before you start peak search to avoid error message].

c. The pump will flush for 30 seconds.

d. A peak should be found for each elemental wavelength without error. Note: If multiple peaks are found in scan range and you are uncertain which peak is the correct elemental spectral peak - stop. Take time to do a scan with multiple concentrations of the element on the same screen (found under “Instrument” and “Wavelength scans”. The correct peak will vary in intensity with changes in concentration.

e. After peak search is completed, move the amber feed tube back 2% HCl ACS flush and cap centrifuge vial.

7) Measure calibration solutions.

a. Click “Run” then “Standards”. The “Standardization” window should come up on screen.

b. Uncap “Standard 2” and place amber needle in solution.

c. Highlight “Standard 2” on the window and then click “Run”.

d. After intensity readings are completed move amber needle back to ACS HCl 2% acid flush and cap centrifuge vial.

e. Note intensity readings in open screen on monitor in lab notebook.

f. Repeat steps a-e for remaining standards and blank.

g. Review calibration data to evaluate regressions. Click “Method” then “Standardization Report”. The “Standardization Report” window opens on screen. Click on “Plot” and “Readback” for each elemental line

measured. Results should be linear and regressions should be of positive slope. If acceptable, move on to next step.

8) Run an unknown sample.
    a. Samples must be filtered with a 0.2 micron filter prior measurement on the ICP to avoid occluding the tiny nebulizer nozzle.
    b. A sample volume in the range of 5ml-15ml is needed for measurement.
    c. Samples should be diluted, if needed, with certified 2% HCl acid blank matrix and spiked with internal standard (if using internal standard methodology).
    d. Put the unknown solution under the hood and place amber tube in sample beaker.
    e. Click “Run” and then “Unknown”. Enter the sample name, enter correction factor for dilution/concentration, and click “Run”.
    f. The pump will flush for 30 seconds with the torch on.
    g. A peak should be found without error.
    h. A window should appear on screen with intensity measurements and statistics.
    i. Move amber needle back to 2% ACS HCl flush.
    j. Note intensity measurements and statistics in lab notebook before proceeding to close window.
9) Shut down ICP.

a. After last measurement is done move the amber needle to UHP water to flush the ICP for 3-5 minutes and empty peristaltic tubing of corrosive acids.
b. Click on “Method” and “Save”. Give the method a name and enter in lab notebook to save time if method is to be used again.
c. Click the flame button on the shortcut bar to open the “Plasma Control Panel”.
d. Click “Extinguish” to turn off the torch. Let the torch cool off a minute.
e. Close software window if desired.
f. Turn off the Argon gas line.
g. Turn off the Nitrogen gas line.
h. Turn off the ICP and power supply if it won’t be used indefinitely.
i. Leave the ICP computer controller on.
j. Record discarded calibration and sample solutions volume and content in lab notebook and ICP Hazard Waste log. Transfer discarded solutions to designated waste container wearing eye glasses and goggles with other PPE. Make sure the ICP hood is empty removed remaining containers/materials in secondary containment.

I - Straight Channel Shim Drawing

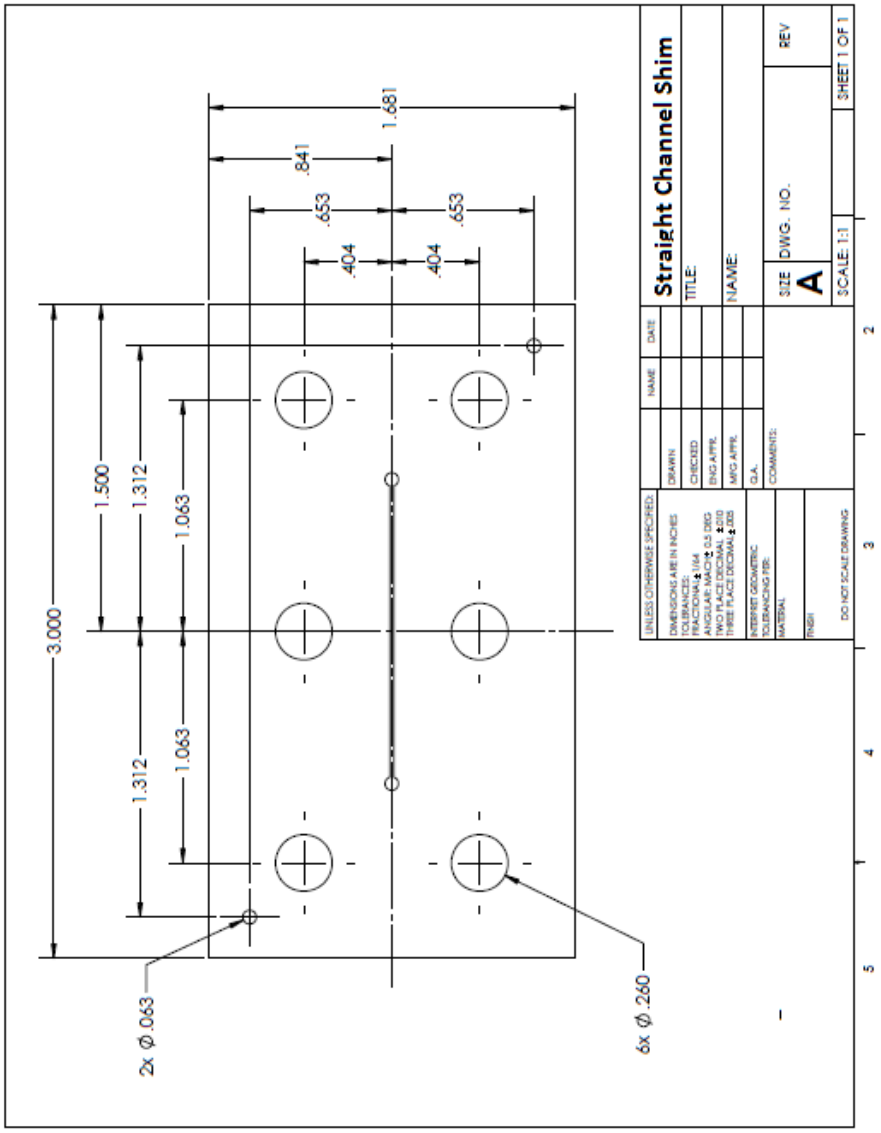

J - Serpentine Channel Shim Drawing

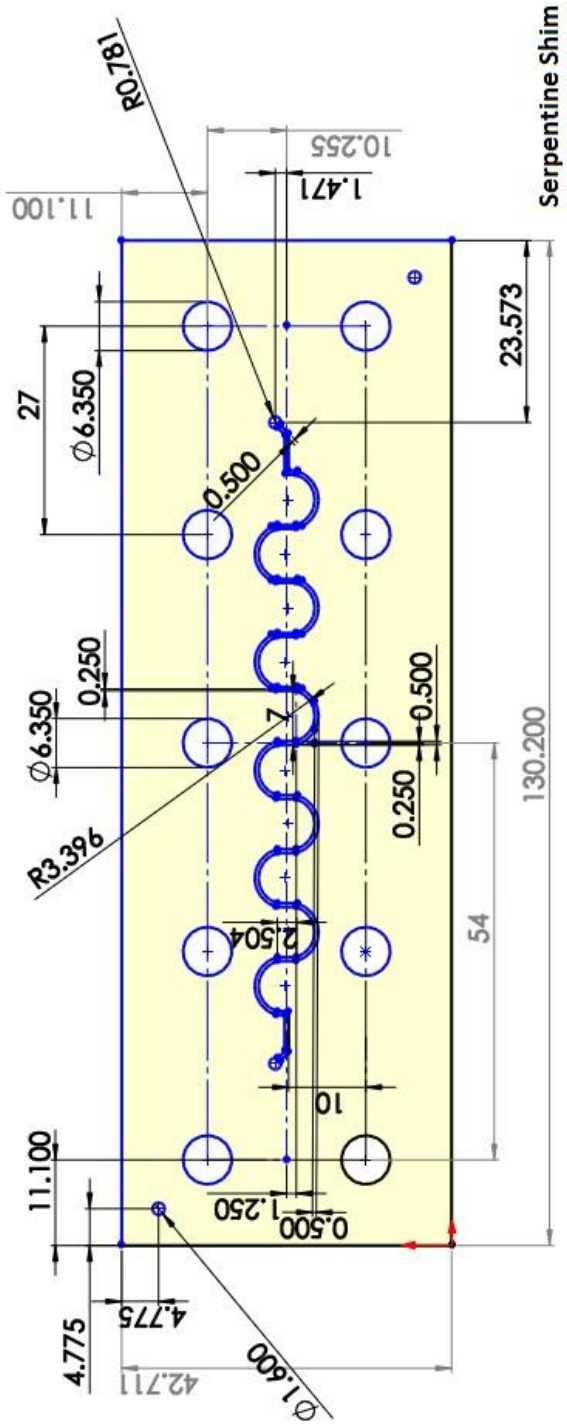

K - Separation Funnel Data and Calculations

Table K-1 Separation Funnel Experimental Data

	Test Variables					Experimental Data with Calculated Error															
						Concentration (ppm)															
2012	Contact	Volume				Feed		Error Feed		Raffinate		Error Raffinate		Strip 1		Error Strip 1		Strip 2		Error Strip 2	
Test	Time	MIBK	Feed	OP	Strip																
Date	hrs	ml	ml	ml	ml	Cd	Te	Cd	Te	Cd	Te	Cd	Te	Cd	Te	Cd	Te	Cd	Te	Cd	Te
8/28	0.17	0.05	10	10	10	1168	1401	23	39	1142	1377	25	41	54	71	1	2	4	6	0	0
9/5	0.17	10.00	10	10	10	914	1088	18	20	971	729	19	16	26	382	1	7				
9/7	24.00	10.00	10	10	10	988	1173	18	45	933	722	19	19	21	355	0	8				
9/6	2.00	10.00	10	10	10	994	1179	20	32	985	763	19	19	15	326	0	8				
9/7	24.00	10.00	10	10	10	991	1187	18	26	988	701	19	16	27	389	1	9				
9/7	0.17	30.00	10	30	10	963	1133	18	24	946	330	17	9	30	639	1	14	2	30	0	1
9/10	0.17	45.00	5	45	10	944	1150	23	31	976	56	22	2	48	475	1	13	2	16	0	1
9/10	0.17	7.50	10	10	10	960	1145	22	30	948	1098	21	27	17	73	0	2				
9/14	0.17	45.00	3	45	6	966	1136	20	32	948	18	21	1	121	467	3	13	5	33	0	1
Abbreviations; OP = organic phase, D = distribution ratio, E = Extraction, R = Recovery																					

Table K-2 Separation Funnel Calculations

	Test Variables					Calculations											
						Distribution Ratio			Extraction			Back-Exraction(s)					
2012	Contact	Volume				D		Error			Error			Error			Error
Test	Time	MIBK	Feed	OP	Strip	OP:Feed		D	E%		E%	R1%		R1%	R2%		R2%
Date	hrs	ml	ml	ml	ml	Cd	Te	Te	Cd	Te	Te	Cd	Te	Te	Cd	Te	Te
8/28	0.17	0.05	10	10	10	0.023	0.02	0.001	2	2	0.1	5	5	0.2	5	5	0.3
9/5	0.17	10.00	10	10	10	-0.059	0.49	0.018	-6	33	1.1	3	35	0.9			
9/7	24.00	10.00	10	10	10	0.059	0.63	0.034	6	38	2.3	2	30	1.3			
9/6	2.00	10.00	10	10	10	0.009	0.55	0.024	1	35	1.6	2	28	1.0			
9/7	24.00	10.00	10	10	10	0.003	0.69	0.027	0	41	1.6	3	33	1.0			
9/7	0.17	30.00	10	30	10	0.006	0.81	0.034	2	71	2.8	3	56	1.7	3	59	2.4
9/10	0.17	45.00	5	45	10	-0.004	2.17	0.124	-3	95	5.0	10	83	3.2	11	85	4.2
9/10	0.17	7.50	10	10	10	0.013	0.04	0.002	1	4	0.2	2	6	0.2			
9/14	0.17	45.00	3	45	6	0.001	4.14	0.226	2	98	5.1	25	82	3.3	26	88	4.7
OP = organic phase, D = distribution ratio, E = Extraction, R = Recovery																	